Impact of beryllium reflector ageing on Safari-1 Reactor core parameters

L.E. Moloko
20239858

Mini-dissertation submitted in partial fulfilment of the requirements for the degree of Master of Science in Engineering at the Potchefstroom campus of the North–West University

Supervisor: Prof E. Mulder
Co-supervisors: Mr. S. Korochinsky, Mr. T.J. van Rooyen

September 2011

Abstract

The build-up of ^{6}Li and ^{3}He, that is, the strong thermal neutron absorbers or the so called "neutron poisons", in the beryllium reflector changes the physical characteristics of the reactor, such as reactivity, neutron spectra, neutron flux level, power distribution, etc.; furthermore,gaseous isotopes such as ^{3}H and ^{4}He induce swelling and embrittlement of the reflector.

The SAFARI-1 research reactor, operated by Necsa at Pelindaba in South Africa, uses a beryllium reflector on three sides of the core, consisting of 19 beryllium reflector elements in total. This MTR went critical in 1965, and the original beryllium reflectors are still used. The individual neutron irradiation history of each beryllium reflector element, as well as the impact of beryllium poisoning on reactor parameters, were never well known nor investigated before. Furthermore, in the OSCAR–3 code system used in predictive neutronic calculations for SAFARI-1, beryllium reflector burn-up is not accounted for; OSCAR models the beryllium reflector as a non-burnable, 100% pure material. As a result, the poisoning phenomenon is not accounted for. Furthermore, the criteria and hence the optimum replacement time of the reflector has never been developed.

This study presents detailed calculations, using MCNP, FISPACT and the OSCAR–3 code system, to quantify the influence of impurities that were originally present in the fresh beryllium reflector, the beryllium reflector poisoning phenomenon, and further goes on to propose the reflector's replacement criteria based on the calculated fluence and predicted swelling. Comparisons to experimental low power flux measurements and effects of safety parameters are also established.

The study concludes that, to improve the accuracy and reliability of the predictive OSCAR code calculations, beryllium reflector burn-up should undoubtedly be incorporated in the next releases of OSCAR. Based on this study, the inclusion of the beryllium reflector burn-up chains is planned for implementation in the currently tested OSCAR–4 code system. In addition to beryllium reflector poisoning, the replacement criteria of the reflector is developed. It is however crucial that experimental measurements on the contents of ^{3}H and ^{4}He be conducted and thus swelling of the reflector be quantified. In this way the calculated results could be verified and a sound replacement criteria be developed.

In the absence of experimental measurements on the beryllium reflector, the analysis and quantification of the calculated results is reserved for future studies.

Keywords: neutron poisons, reactivity, SAFARI-1 research reactor, beryllium reflector, swelling, embrittlement, OSCAR–3, MCNP, FISPACT

Dedication

“Kgaka-kgolo ga ke na mebala, mebala e dikgakaneng”
To my son
KUTLWANO
I dedicate this work
PULA !!

Acknowledgements

Firstly I would like to thank GOD ALMIGHTY for giving me the strength and courage to complete this work despite all the challenges. It would not have been possible to complete this work without His grace.

A special note of thanks goes to my co-supervisors Sergio Korochinsky and Johann van Rooyen who have continually supported, guided and encouraged me throughout this work. Thank you for contributing so immensely to my professional career growth.

I would also like to thank Professor Eben Mulder for showing interest in this work and his willingness to supervise it.

Many thanks to all my colleagues of the Radiation and Reactor Theory group at Necsa for their support. Special thanks goes to Bessie Makgopa and Mohamed Belal for their valuable inputs in sharpening my skills as an MCNP user, and Rian Prinsloo for his assistance during the initial phase of this work. I would also like to thank Hantie Labuschagne for editing and proof reading of this thesis as well as ensuring consistency in the layout and format.

My exceptional thanks to my family for their endless love, support and sacrifices that they have made and continue to make throughout my career endeavours and other aspects of my life. My sincere thanks are extended to all my friends who somehow touched my life.

Finally, I would like to thank Necsa management and gratefully acknowledge the financial support they provided me with in completing this work.

Contents

List of Figures

List of Tables

Nomenclature and Acronyms

This is a list of nomenclature used in this mini-dissertation listed in alphabetical order

AEC	Atomic Energy Corporation
appm	atomic parts per million
ATR	Advanced Test Reactor
BOC	Beginning Of Cycle
BR2	Belgian Reactor 2
EOL	End-Of-Life
HEADE	Heterogeneous Assembly Depletion
HFIR	High Flux Isotope Reactor
HEU	Highly Enriched Uranium
IAEA	International Atomic Energy Agency
IAE	Institute of Atomic Energy
IEA	International Energy Agency
INEEL	Idaho National Engineering and Environmental Laboratory
ITER	International Thermonuclear Experimental Reactor
JAERI	Japan Atomic Energy Research Institute
JMTR	Japan Materials Testing Reactor
LEU	Low Enriched Uranium
MEU	Medium Enriched Uranium
MGRAC	Multi-Group Reactor Analysis Code
MTR	Material Testing Reactor
MURR	Missouri Research Reactor
MWd	MegaWatts days
MW	Mega Watts
NASA	National Aeronautics and Space Administration
Necsa	South African Nuclear Energy Corporation
ORNL	Oak Ridge National Laboratory
ORR	Oak Ridge Research Reactor
OSCAR–3/4	Overall System for the CAlculation of Reactors version 3 and 4

OSMINT	OSCAR MCNP INTerface
ppm	parts per million (mg/kg)
SAFARI–1	South African Fundamental Atomic Research Installation 1
SAR	Safety Analysis Report

Chapter 1

Introduction

1.1 Overview and background

Beryllium naturally occurs as a ^{9}Be isotope, with a natural abundance of 100%; it is a metal of low mass–density, with exceptional properties that make it very attractive for specific nuclear and non–nuclear applications. The properties that make it ideal for specific nuclear applications, include: (1) the lowest absorption cross section σ_a for thermal neutrons of all metals, (2) a large scattering cross section σ_s, (3) readiness to part with one of its own neutrons in (n,2n) reactions, and (4) a high melting point. This makes it an excellent structural, as well as neutron moderator and neutron reflector material, where its prime function is to, via scattering, reflect many leakage neutrons back to the reactor core.

In nuclear applications, it is a combination of the above properties that make beryllium a very attractive material for use in both fusion and fission nuclear reactors [1], [2].

Beryllium metal is currently used as a neutron multiplier in breeder applications and "oxygen getter" for plasma–facing surfaces in fusion test reactors, e.g. the ITER Reactor – the International Thermonuclear Experimental Reactor. Beryllium is also widely used as a structural and neutron reflector and moderator material in Materials Testing Reactors (MTRs) such as, the Advanced Test Reactor (ATR) at the Idaho National Engineering and Environmental Laboratory (INEEL) in the USA, the JMTR (Japan Materials Testing Reactor) of JAERI in Japan, the BR2 Belgian Engineering Reactor in Mol, Belgium, the MARIA reactor of the IAE in Poland, the High Flux Isotope Reactor (HFIR) at the Oak Ridge National Laboratory in the USA, and the University of Missouri Research Reactor (MURR) in Columbia, Missouri, USA [1], [2].

The Oak Ridge Research Reactor (ORR), which was based in Oak Ridge, USA, used beryllium metal as a reflector before it was permanently shut down in March 1987 [3]. The SAFARI–1 research reactor of the South African Nuclear Energy Corporation (Necsa) at Pelindaba near Pretoria, South

Africa, is very similar in design to the Oak Ridge Research Reactor and also uses beryllium metal as a reflector material.

Beryllium metal is used at several other research reactors and experimental facilities.

A minor application of metallic beryllium is to use it as a source of photo–neutrons to control start–up of certain reactors [4]. The binding energy of the outer neutron in the ^{9}Be nucleus has a very low binding energy of only circa 1.67 MeV, so that (α,n) and (γ,n) reactions have low energy thresholds. This makes beryllium ideal for use in radioisotope–based neutron sources.

Notwithstanding these many admirable qualities, there are a number of issues associated with the use of beryllium, when it is subject to intense neutron irradiation over a long period of time. Factors that strongly influence the useful lifetime of beryllium in nuclear reactors include fast neutron irradiation damage, irradiation temperature, fabrication methods and materials purity – high purity is desirable to minimize the induced radioactivity and to increase the effectiveness of the reflector. Pure beryllium has a very high ratio $\frac{\sigma_s}{\sigma_a}$ and any impurities will lower this $\frac{\sigma_s}{\sigma_a}$ ratio. Any impurities in the beryllium metal will increase σ_a, which will lead to a loss of neutrons via neutron absorption reactions. Such neutron absorption reactions by impurities will also produce undesired radionuclides. The more impurities present in the beryllium, the more radioactive it will be when removed from the reactor core at EOL (end–of–life) and the bigger its health hazard and radioactive waste disposal burden will be after the removal from the core at EOL. Some of the impurities that may be present in beryllium metal have high absorption cross sections for thermal neutrons, which can strongly decrease the reflector's efficiency [5], [6] – instead of reflecting neutrons back into the core via scattering, neutrons are now absorbed in the reflector and thus lost.

Prolonged fast neutron irradiation of beryllium induces swelling and embrittlement caused by gas formation and gas build–up in the beryllium metal; specifically the gases ^{3}H (tritium), ^{3}He and ^{4}He (helium 3 and helium 4) are formed. Furthermore, some of the isotopes that are formed in beryllium by nuclear reactions, especially ^{3}He and ^{6}Li, act as strong neutron absorbers (the so–called "neutron poisons" or simply "poisons") for thermal neutrons, as a result of their large absorption cross sections. The formation and build–up of these neutron poisons will consequently perturb and impact negatively on some reactor core parameters such as reactivity, core power and neutron flux distribution and others [7].

It is the combination of these undesirable factors that limit the lifespan of beryllium and consequently, call for its periodic replacement in nuclear reactors. Non–nuclear technical factors affecting the use of beryllium are, that it is chemically highly toxic and also a very expensive material; despite all these drawbacks, its use for nuclear applications remain critical.

1.1.1 Experiences with beryllium metal use in research reactors

Experiences with beryllium reflected reactors, including some that were shut–down, are briefly discussed in subsequent paragraphs. This section provides sound reasons as to why the reactor management and calculational support teams of beryllium reflected reactors should understand the behaviour of the metal under fast fluence irradiation.

The above–mentioned problems associated with the use of beryllium as a neutron reflector in nuclear reactors, demand that reactor management and calculational support teams develop various methods and criteria to evaluate the impact that the beryllium reflector have on key reactor parameters over its operational lifetime. These methods and criteria have made it possible to assess the reflector performance and physical condition with the eye to schedule beryllium reflector element replacement at the optimal time.

As an example, a thermal expansion analogy to predict swelling and concomitant stresses is one of the methods that have been applied successfully at the ATR (Advanced Test Reactor) at INEEL (Idaho National Engineering and Environmental Laboratory) in the USA – see reference [7] for details of the methodology. A brief summary of some nuclear reactors that have successfully replaced their beryllium reflector before, and continue to do so, is given in subsequent paragraphs. Table 1.1 summarises the reactor criteria for the replacement of the beryllium reflector obtained from references [6], [7], [8], [9], [10], [11], [12].

Table 1.1: Some of the high fluence beryllium reflected test reactors, operating in 2010

Reactor	**Location**	**Rated Power (MW_{th})**	**Maximum Flux ($\times 10^{14}$n/cm^{2}s)**			**Date on-line**	**Replacements Criterion Fast Fluence (10^{22}n/cm^2)**	**Average Time between Replacement (years)**	**Number of Replacements**
			Thermal	**Fast**	**Ratio**[a]				
ATR	**INEEL, ID, USA**	110–120	5.3	14.0	2.64	**Jul**–67	0.80	10	6
BR-2	**Mol, Belgium**	100	10.0	7.0	0.70	**Jun**–61	6.40	17–19	3
MIR	**Dimitrovgrad, Russia**	100	5.0	3.0	0.60	**Dec**–66	6.00	7	6
HFIR	**ORNL, TN, USA**	80	1.5	13.0	8.67	**Aug**–65	**No fluence limit**	**RB**[b] 2.7	16
								SPB[c] 5.4	8
								PB[d] 9.0	4
JMTR	**JAERI, Japan**	50	4.0	4.0	1.00	**Mar**–68	1.10	6–7	7
SAFARI-1	**Necsa, Pretoria, South Africa**	20	2.4	2.8	1.17	**Mar**–65	**Not defined**	**No replacement**	**None**
MURR	**Missouri University, USA**	10	6.0	1.0	0.17	**Oct**–66	2.52	8	4

[a] $\frac{\text{Fast}}{\text{Thermal}}$
[b] Removable beryllium
[c] Semi–permanent beryllium
[d] Permanent beryllium

It is important to note that the position of the beryllium reflector in the core and hence, the intensity of the fast neutron fluence rate in the reflector, plays a major role in determining the magnitude of poisoning by ^{3}He and ^{6}Li isotopes, as well as their build-up rate in the reflector. The beryllium reflector elements in the high neutron fluence vicinity will exhibit higher concentrations of these neutron–poison isotopes, while the beryllium reflector elements in the lowest fluence vicinity will exhibit low isotopic concentrations of neutron poisons. Therefore, the rate at which the beryllium reflector element is damaged, as well as its lifespan, is a function of the intensity of the neutron flux and the energy spectrum of the neutron flux, all of which are a function of the beryllium reflector element's position in the reactor core.

Therefore this phenomenon, that is beryllium reflector poisoning, swelling and embrittlement, is dependent on the reactor configuration and consequently will be different for different reactors designs.

At INEEL it was determined that beryllium must be replaced at nominally 10 year intervals for the ATR. The method used to determine the time for replacement is made by visual observation using a periscope to examine the beryllium surface for cracking and swelling. This method has been successfully used for five generations of beryllium replacement, during the core internal change–outs of 1970, 1977, 1986, 1994 and 2004. Including the original reflector, five sets of beryllium reflectors have been removed from the ATR; the installation of the sixth beryllium reflector was completed in 2007 and a seventh reflector is currently in the process of being procured for an envisaged core internal change–out in 2014 [9].

The first beryllium reflector replacement with the second new one in the BR2 (Belgian Reactor 2) took place during 1979–80, after about 19 years of operation. The second replacement by the third reflector was executed about 17 years later, in 1997. Similar to the ATR, visual inspection is one of the techniques used to monitor the status of the reflector for possible replacement, in addition to this, the maximum allowable fast fluence criterion is used – limited to $6.4 \times 10^{22} \ \frac{n(>1 \text{ MeV})}{\text{cm}^2}$. An agreement has been reached with the National Safety Authority concerning this value. Consequently, this maximum admissible fast fluence value has been used for the second and the third beryllium surveillance programmes [10].

At JMTR, the beryllium reflector is replaced by new ones every 6 or 7 years; the reactor has undergone six generations of beryllium reflector replacements between 1966 and 2007; the 7th generation beryllium reflector has now been manufactured and was scheduled for replacement installation early in 2010 [11].

The HFIR beryllium reflector consists of three annuli, the innermost removable beryllium reflector (RB), the middle semi–permanent beryllium reflector (SBP) and the outer, which is the permanent beryllium reflector (PB). The HFIR does not have fluence limits on the beryllium reflectors, they use the reactor operator's judgment for replacement. The replacement is done when operators experience difficulties in inserting or removing irradiated specimens from the reflectors – such

difficulty is a sign of beryllium reflector swelling, caused by fast–neutron damage and swelling. The typical lifetime values of the HFIR reflectors obtained from reference [12] are given in Table 1.1.

The analytical technique, that is the numerical solution of systems of coupled differential equations describing the transmutation of beryllium under neutron irradiation, has been one of the most successful methods used to estimate the build–up and concentration of important, undesired isotopes in the beryllium reflector, namely ^{6}Li, ^{3}He, ^{4}He and ^{3}H. This analytical technique is used by, amongst others, the reactor management team of the MARIA reactor. In the MARIA reactor, the agreement of the anticipated behaviour of the reactor with measurements, has been more than satisfactory when the evolution of the isotopic concentrations of ^{6}Li, ^{3}He and ^{3}H (estimated by using this analytical approach), is applied to the standard fuel management calculations [13].

The reactor core management teams of most of the beryllium reflected reactors discussed above, have developed and implemented methods to account for the effects associated with using beryllium as a neutron reflector and moderator.

The results of beryllium reflector burn–up was investigated for the 30–MW Oak Ridge Research Reactor (i.e. similar in design to the SAFARI–1 reactor) before it was permanently shut down in 1987. The build–up and burnout of ^{6}Li and ^{3}He in all the beryllium regions in the reactor were taken into account in the REBUS burn–up calculations, further details can be found in reference [3].

It is evident that the poisoning and ageing (i.e. swelling and embrittlement) of beryllium reflectors are an important topic in the management of all the beryllium reflected reactors and that it must be accounted for in reactor core calculations.

1.2 Motivation

The SAFARI–1 research reactor core layout employs two different beryllium reflector types placed at the core periphery, that is the hollow and solid beryllium reflector elements. The elements are used on three sides of the reactor. The reactor has been operating with beryllium as a reflector since it went critical in 1965 – it has been in operation for at least 45 years as at 18 March 2010. The placement of the beryllium reflectors in the SAFARI–1 reactor core is shown in Figure 1.1.

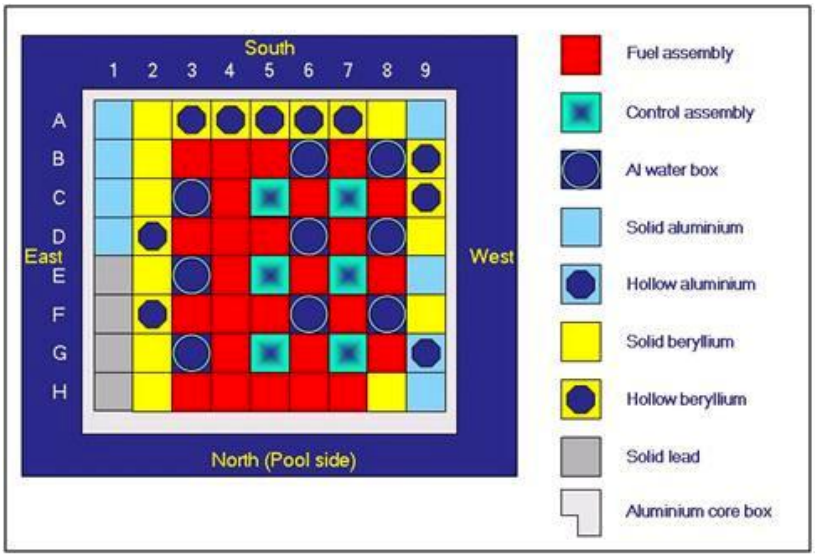

Figure 1.1: Placement of the beryllium reflectors in SAFARI-1 reactor core

Experience with other reactors using beryllium as a neutron reflector and moderator, has shown that it is very important to understand how the element behaves under neutron irradiation over the entire operational history of the reactor. This plays a vital role in evaluating the effectiveness of the reflector element, the impact that the reflector has on the reactor core parameters, determining its lifespan and thus the optimal replacement intervals of the beryllium reflector in a specific reactor.

The calculation of fuel depletion burn–up and core safety parameters such as power peaking, control rod worth, cycle length, etc. for the SAFARI–1 reactor are routinely performed using the OSCAR code system. OSCAR is an acronym for "**O**verall **S**ystem for the **CA**lculation of **R**eactors".

The results of routine reactor experiments such as control–rod calibration, copper–wire activation flux measurements, foil activation flux measurement, etc. are constantly used to benchmark the OSCAR code. This feedback and refinement process contributes to the accuracy of the reactor parameters calculated using the OSCAR code. It is important to ensure that all the phenomena, considered neutronically important, are accounted for in reactor code systems such as OSCAR, as well as in fuel and reflector isotopic composition data, if the desired accuracy is to be achieved.

The origin and neutron irradiation history of the beryllium reflector element, as well as the

performance implications it has on the SAFARI–1 reactor core parameters, are not well known nor has it been investigated before. Furthermore, the isotopic transmutation of an irradiated beryllium reflector has not been accounted for in the cross–section data prepared by other OSCAR modules for the code that performs the nodal diffusion calculations of the SAFARI–1 reactor. In other words, the neutron fluence induced isotopic evolution of beryllium is not implemented at all in either OSCAR–3 or OSCAR–4. The neutron–poison isotopes that build–up in the beryllium reflector will have a negative effect on the ability of the reflector to reflect neutrons.

The international practice is that reactor core management codes should model the isotopic evolution of the beryllium reflector accurately. It is therefore necessary to: (1) quantify the isotopic evolution of the neutron poisons in the beryllium reflector, (2) quantify its impact on reactor parameters such as power distribution, neutron flux, neutron energy spectrum, reflector savings, reactivity and more, (3) quantify the service-life of beryllium and (4) initiate steps to implement this in OSCAR as well as in special and time dependence of the beryllium reflector isotopic composition data that will be passed from OSCAR to OSMINT (OSCAR–MCNP INTerface), to the OSMINT–generated MCNP (Monte Carlo N–Particle) model of the SAFARI-1 reactor core, which serves as a reference benchmark for the verification of results computed with the OSCAR code system.

Based on the literature survey and the facts discussed above, it is clearly imperative that a rigorous study of the quantitative nature and the important consequences of the build–up of neutron–poison isotopes in the beryllium reflector elements around the SAFARI–1 research reactor should be performed as a matter of urgency. Accurate quantification of these phenomena is internationally the best practice, and Necsa should follow suit.

1.3 Research objective and scope

The primary objective of this study is to investigate the importance of the isotopic evolution of the beryllium reflector for a typical SAFARI–1 reactor neutron spectrum, taking into account the entire operational history of the reactor. Furthermore, the effects of the reflector burn–up on core parameters, on the beryllium reflector itself and on the day–to–day SAFARI–1 reactor core calculations, will be investigated and quantified.

The scope of the research is as follows:

1. Calculate the present isotopic composition in:
    i. Each beryllium reflector element using the element–specific neutron fluence–rate and energy spectrum;
    ii. The whole–core beryllium elements – using the averaged neutron fluence–rate and energy

spectrum over all the beryllium reflector elements.

Conclusions will be drawn based on these two approaches, that is whether to use the element–specific spectrum or a core–averaged neutron spectrum over all the elements, to account for beryllium reflector burn–up calculations.

2. Develop a suitable way of accounting for the beryllium reflector burn–up effects in the OSCAR code system and thus, in the MCNP model generated from OSCAR's results via the OSMINT code which interfaces MCNP with OSCAR. This will make it possible to determine the following:

   i. The time step intervals required to update the isotopic content in OSCAR;

   ii. The impact of the isotopic contents of the beryllium reflector on the important core parameters.

3. Finally, well–founded criteria to determine when the beryllium reflector must be replaced will be developed based on the expression used to estimate swelling and the experimental data published in the literature.

At each of the above steps, the isotopic concentration in the reflector as well as the accompanying effects the isotopes have on core parameters will be quantified. In this way the behaviour and the influence of the beryllium reflector burn–up on the SAFARI–1 reactor core parameters will be well understood and accounted for in the code systems. Finally, the calculated parameters, that is, calculated when the poison effect is taken into account, will be compared with experimental data such as copper–wire activation flux measurement.

1.4 Thesis layout

Including the introductory section, this thesis is divided into 6 chapters. The literature is discussed in **Chapter 2**. The chapter include a description of the SAFARI–1 research reactor and more details on beryllium use as a reflector material in the SAFARI–1 reactor. The behaviour of the reflector under fast neutron irradiation and its impact on reactor core parameters from previous studies is also discussed here in detail.

Chapter 3 gives a brief summary of the numerical methods of interest. The actual models that were set–up for each code are discussed in **CHAPTER 4**, that is the model employed in both OSCAR and MCNP, the burn–up calculations model in FISPACT and the BERYL program as well as the nuclear data input required for each code, specific to this study.

CHAPTER 5 is dedicated to the analysis and discussion of the calculated results and a comparison of the calculated results to the copper-wire activation flux measurement experimental data.

Conclusions and findings of this research are summarised in **CHAPTER 6**. This chapter also suggests areas of future work.

Chapter 2

Literature study

2.1 Introduction

The SAFARI–1 research reactor and its operational history, with special emphasis on the beryllium reflector are described in this chapter. Some of the results and experience obtain from other beryllium reflected reactors are also discussed here.

Section 2.2 describes the SAFARI–1 reactor and the reactor's operational history. Subsections 2.2.2 covers a description of the SAFARI–1 reactor beryllium reflector element, the nuclear properties of beryllium, its reaction with neutrons and a solution to a system of differential equations involving beryllium chain reactions. The chapter is concluded with a brief discussion on swelling of the SAFARI–1 reactor beryllium reflector.

2.2 SAFARI–1 research reactor description

The SAFARI–1 research reactor, an acronym for the **S**outh **A**frican **F**undamental **A**tomic **R**esearch **I**nstallation–1, was commissioned in 1965 by AEC, the **A**tomic **E**nergy **C**orporation in South Africa. It is a tank–in–pool MTR type reactor (**M**aterial **T**esting **R**eactor) similar in design to the Oak Ridge Research Reactor. The reactor is currently operated at 20 MW, the coolant and moderator is light water and cooling occurs via the primary and secondary heat exchange systems. SAFARI–1 has an 8×9 core lattice, housing 26 fuel elements, 5 control rods, 1 regulating rod, a number of solid lead shield elements, solid and hollow aluminium filler elements as well as solid and hollow beryllium reflector elements [14].

All the reflector elements, filler elements, water boxes and special devices have the same overall dimensions as a fuel element and differ only in their internal detail. This allows for the core layout changes, mainly to accommodate client requirements. The three possible core designs, with cores

containing 26, 28 and 31 fuel elements have been evaluated in Chapter 16 of the SAR (**S**afety **A**nalysis **R**eport) document [14]. The SAFARI–1 reactor vessel is shown in Figure 2.1.

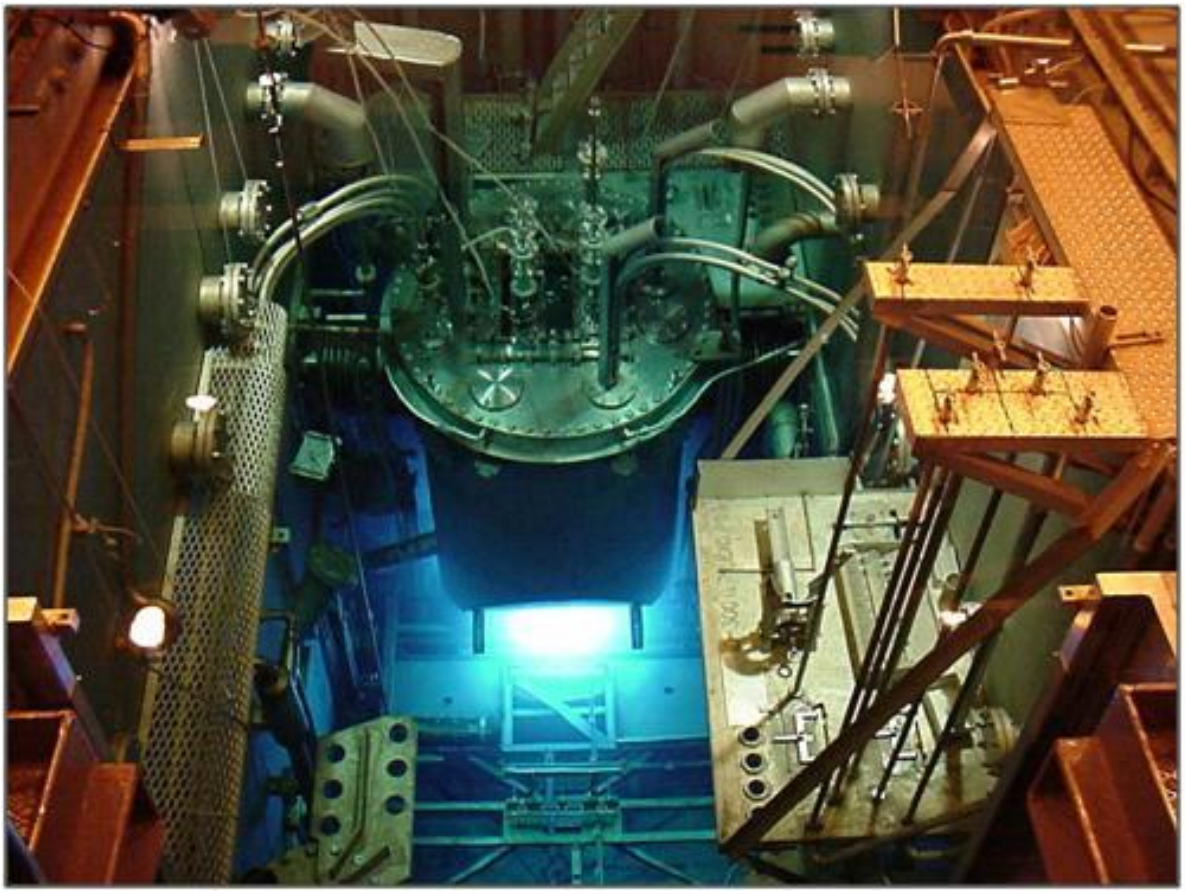

Figure 2.1: SAFARI-1 reactor vessel immersed in pool water

The reactor vessel is cylindrical in shape, except for one flattened side, which is also the wall of the rectangular core box adjacent to the poolside facility (north side). The large ex–core poolside facility allows irradiations to be performed in relatively high neutron fluxes since it is directly adjacent to the fuel elements. The reactor is also equipped with a number of beam tubes, which are used for neutron radiography, neutron scattering (e.g. Small Angle Neutron Scattering, Powder Neutron Diffraction and Residual Strain Scanning), and prompt gamma neutron activation facilities, while hydraulic and pneumatic rabbit facilities provide for the irradiation of various samples [14]. Some of the routine reactor experiments include control–rod calibration, copper–wire activation flux measurements, foil activation flux measurements, etc.

The reactor is a major producer of medical and industrial isotopes for both domestic and international markets.

The core is fuelled with 19 plate MTR–type fuel elements and the control rods are comprised of a 15 plate fuel follower section beneath a hollow rectangular cadmium absorber section. The fuel

element and the control rod with the fuel follower sections are shown in Figure 2.2 and Figure 2.3 respectively.

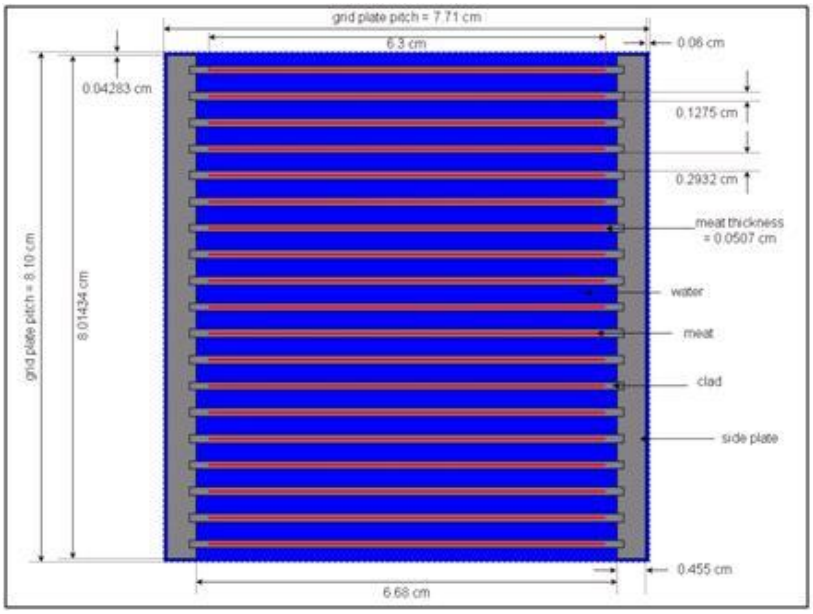

Figure 2.2: Radial view of the fuel assembly

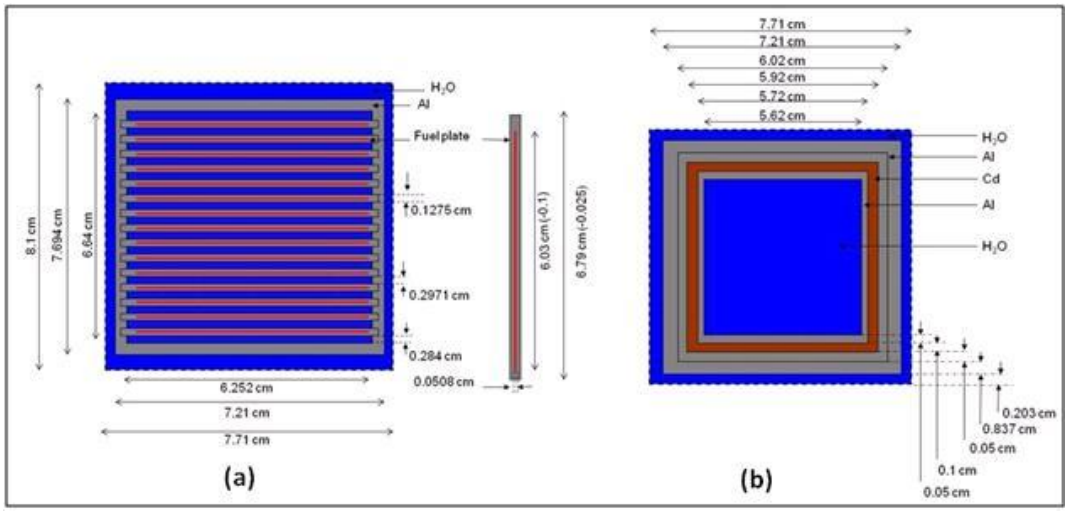

Figure 2.3: Radial view of the fuel follower (a) and the control rod assembly (b)

The reactor was originally fuelled with 90 wt% enriched U–Al alloy fuel (HEU) but was converted to 45 wt% U–Al alloy (MEU) fuel during the early 1980s. Due to the higher rejection rate in the manufacturing process of the MEU fuel and the availability of HEU in South Africa, it was later decided to resume the manufacture and use of HEU fuel assemblies for economic reasons.

The reactor is currently operated with fully low enriched fuel (LEU); the conversion from HEU to LEU fuel was completed in 2009. Some of the key parameters for the different cores are presented in Table 2.1 [14].

Table 2.1: Some key parameters of the SAFARI–1 research reactor for different cores

Parameters	**HEU CORE**	**MEU CORE**	**LEU CORE**
Number of control rods	6	6	6
Fuel type	**U-Al Alloy**	**U-Al Alloy**	**U_3Si_2-Al**
Enrichment wt%	90.00	45.8	19.75
Uranium density (g.cm^{-3})	0.61–0.92	1.35	3.13–4.76
Number of fuel plates per assembly	19	19	19
Number of fuel plates per follower assembly	15	15	15
Total Uranium in alloy (mass %)	19	37	74–79
U^{235} per fuel plate(g)	300 ± 4.0	225 ± 3.30	340 ± 6.65
U^{235} per follower plate (g)	202 ± 3.0	152 ± 2.3	230 ± 5.25
Fuel meat thickness (cm)	0.0508	0.0508	0.0508
Fuel cladding thickness (cm)	0.0384	0.0384	0.0384
Follower meat thickness (cm)	0.0507	0.0507	0.0507
Follower cladding thickness (cm)	0.0384	0.0384	0.0384
Inlet temperature (°C)	40	40	40
Outlet temperature (°C)	47.2	47.2	47.2

2.2.1 SAFARI–1 reactor operational history

The SAFARI–1 reactor power history is depicted in Figure 2.4.

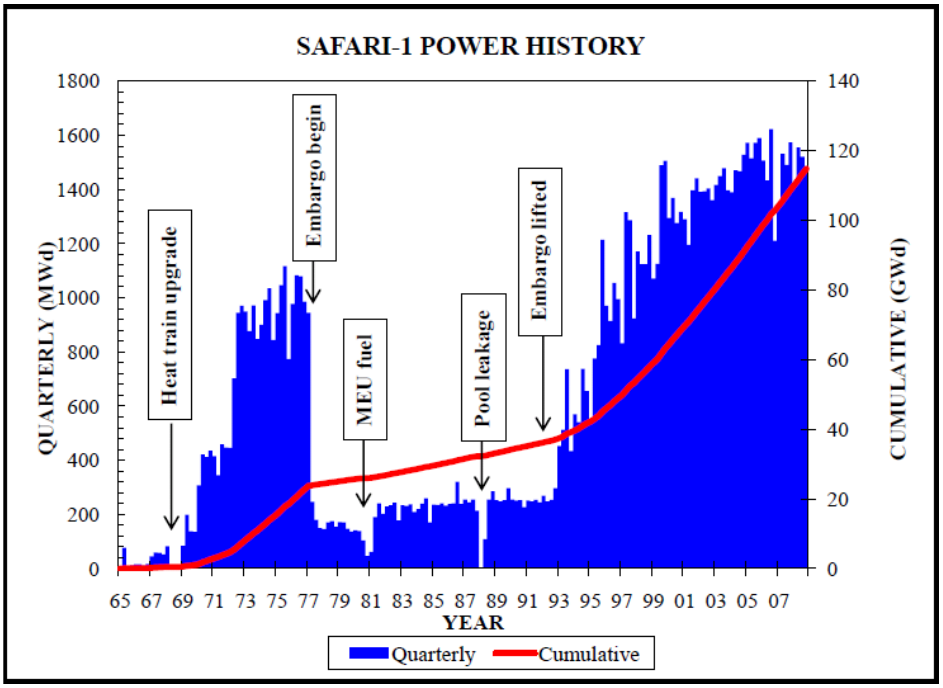

Figure 2.4: The SAFARI-1 reactor power history

Initially the reactor was operated at a thermal power of 6.67 MW. In 1968 the reactor was shut–down for approximately 9 months to upgrade a heat removal train to allow the maximum operation power of 20 MW. The reactor operated at a power level of between 5–10 MW and occasionally at 20 MW, until 1976 when an embargo was placed on the supply of fuel to SAFARI–1. The operating power was reduced to 5 MW and operating hours greatly shortened (in some instances for four days per week) in order to conserve the fuel stocks while the local enrichment and fuel manufacturing capability was developed. In 1981 the first locally produced MEU fuel assemblies became available and the reactor continued to be operated at 5 MW for five days a week until 1993 [14], [15]. During the first half of 1988, the reactor was shut–down for 6 months to repair a pool leak.

In 1993/94, when the embargo against supplying reactor fuel to South Africa was lifted, the power was increased to 10 MW to accommodate commercial applications. The nominal power level was initially increased to 10 MW, with gradually more frequent operations at 20 MW for the development and implementation of commercial programmes [14], [15].

Since 1996 the reactor power levels were progressively increased from an average of 16 MW to 20 MW continuously and it was operated for the last nine years approximately for 305 days per year at 20 MW. Currently the reactor is operated for about 30 days, interrupted by a 4–5 day refuelling

shut–down period and one extended 12 days refuelling and maintenance shut–down per annum. The full operational SAFARI–1 reactor history can be found in Appendix A.

2.2.2 SAFARI–1 beryllium reflector element

The reflector elements of the SAFARI–1 reactor are made of beryllium, either hollow or solid. The two types are identical except that a hollow element has a 52 mm diameter hole bored along its axial centre line. Each hollow reflector element contains a perforated aluminium basket into which an isotope stringer 44.4 mm diameter sample, or ten solid beryllium plugs can be inserted. With the plugs fitted, the hollow element is neutronically identical to the solid element. The hollow beryllium element in position A4, see Figure 1.1, is usually fitted with a cadmium ring mainly for fast neutron flux sample irradiation. The beryllium reflector is used on three sides of the reactor as depicted in Figure 1.1 and the schematic figure of the element is shown in Figure 2.5.

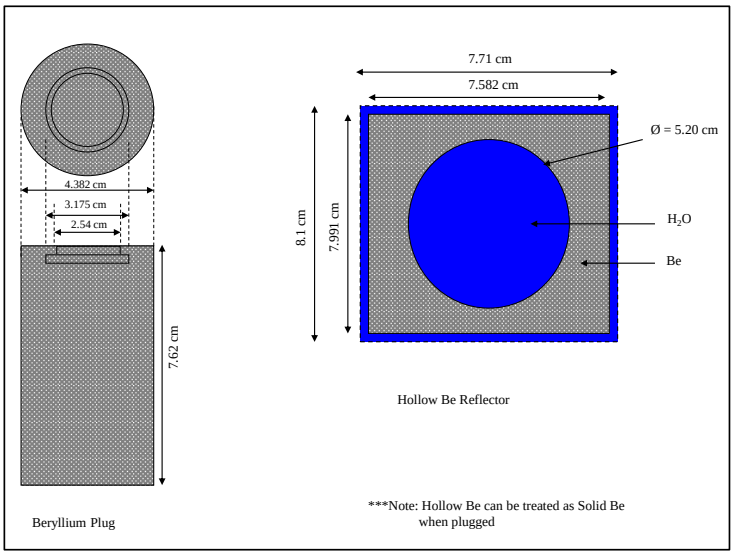

Figure 2.5: Radial view of the beryllium reflector element and beryllium plug

The irradiation history of each SAFARI–1 reactor beryllium reflector element is neither documented nor well–known. The reflectors do not have any unique numbers or engraving for identification and tracking purposes. Therefore it is not known if the reflectors have ever been repositioned in the core. It is therefore assumed that the elements were never repositioned or rotated since the reactor started operation [16].

The beryllium reflector technical specification of the nuclear grade, N–50–A is also assumed [16]. The technical specifications, as found in reference [17], are given in Table 2.2.

Table 2.2: Chemical compositions for nuclear grade hot pressed beryllium

Elemental Impurity	**Analysis of N-50-A lot 413 (ppm)**	**σ_a at E = 0.0253 eV neutrons (barns)**	**Boron Equivalent (ppm)**
Aluminum	400	0.24	0.0502
Boron	1	766	1.0000
Cadmium	0.7	2450.0	0.2153
Carbon	400	0.0035	0.0016
Cobalt	1	37.0	0.0089
Iron	360	2.73	0.2484
Lithium	1	71	0.1444
Magnesium	90	0.07	0.0037
Manganese	50	13.2	0.1696
Nickel	95	4.8	0.1097
Silicon	45	0.16	0.0036
Total Boron Equivalent in Beryllium (ppm)			**1.9553**

Impurities such as Cd, B, Li, Co and Mn are the main contributors in increasing the beryllium absorption cross section due to their high absorption cross sections for thermal neutron. Nevertheless, these strong absorbers are expected to burn–out within the first few years of operation. Even a small amount of impurities, i.e., less than 10 ppm, can increase the absorption cross section of beryllium considerably. At a maximum, the impurities in beryllium can increase the absorption cross section by up to 30 times [18], [19], [20]. These impurities decrease the efficiency of the reflector strongly; high purity is therefore desirable to minimize the neutron absorption in beryllium as well as the induced radioactivity.

2.3 Nuclear properties of beryllium

The principal isotopes of beryllium that have been identified are: ^{6}Be, ^{7}Be, ^{8}Be, ^{9}Be and ^{10}Be. ^{9}Be is the only stable beryllium isotope and ^{10}Be is a semi–stable beryllium isotope with a very long half–life. Beryllium is used as a neutron reflector in many MTRs as already indicated and discussed in CHAPTER 1. In Table 2.3 the properties of commonly used moderators are compared to those of beryllium [19].

Table 2.3: Properties of potential moderators at 20°C

Parameters	**Potential Moderators**				
	H_2O	**D_2O**	**Graphite**	**BeO**	**Be**
Atomic weight	18	20	12	25	9
Density (ρ), g·cm^{-3}	1.00	1.10	1.60	3.025	1.85
Thermal neutron nuclear properties (0.0253 eV)					
Scattering cross section (Σ_s), cm^{-1}	1.47	0.35	0.38	0.72	0.76
Thermal absorption cross section (Σ_a), cm^{-1}	0.0220	0.000036	0.00036	0.00066	0.0011
Diffusion coefficient (D), cm	0.16	0.85	0.86	0.59	0.54
Epithermal neutron nuclear properties					
Logarithmic Energy decrement (ξ) $\xi=1+\frac{(A-1)^2}{2A}\ ln\left(\frac{A-1}{A+1}\right)$	0.925	0.504	0.158	0.173	0.206
Diffusion length (L) $\left(L=\sqrt{\frac{D}{\Sigma_a}}\right)$, **cm**	2.70	154	49	30	22
Moderating ratio, $\frac{\xi\cdot\Sigma_s}{\Sigma_a}$	62	5,000	165	190	145
Slowing down power ($\xi\Sigma_s$)	1.36	0.18	0.060	0.12	0.16

For a good moderator, it is necessary that the values of ξ are large, to ensure that fission neutron are slowed down to thermal energies in few collisions, the scattering cross section (Σ_s) is as large as possible, so that the distance between collisions is small and the absorption cross section (Σ_a) is as small as possible so that few neutrons are lost during moderation. The collective properties of beryllium make it a valuable moderator.

The total, absorption, scattering and non–elastic cross sections of beryllium as a function of neutron energy are shown in Figure 2.6 [21].

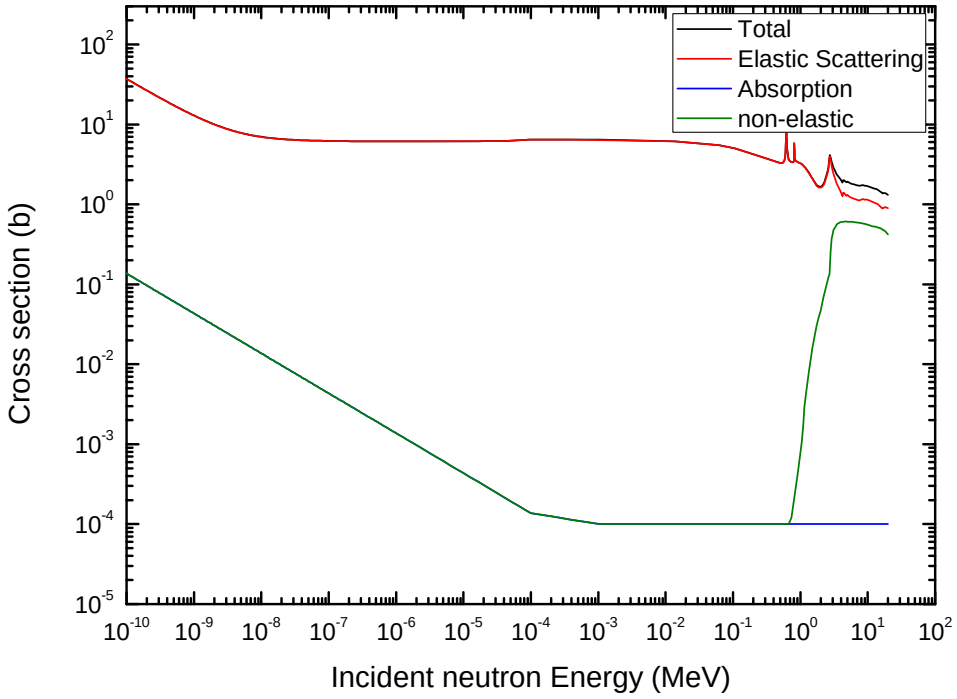

Figure 2.6: Total, absorption, scattering and non–elastic cross section of beryllium (ENDF/B VII.0, T=300°K)

The absorption cross section is very small, as seen in the Figure 2.6, this results in a small difference between the scattering and total cross sections. The non–elastic cross section is similar to the absorption cross section; it only rises rapidly at about 1 MeV.

The use of beryllium in an MTR has a number of important advantages, such as an increase in neutron economy and reactivity reserve, fuel cycle length, as well as fuel economy; these advantages translate to savings in fuel cost [22], [23]. The neutron reflection back into the fuel region via elastic scattering and (n,2n) in the fast energy range (see Figure 2.6) by the beryllium reflector is responsible for these phenomena. The use of beryllium reflector elements will therefore also flatten the power distribution throughout the core, by increasing the fission rate at the edges of the fuel region through neutron multiplication and neutron reflection.

Irradiation effects on a beryllium reflector are discussed in detail in Section 2.4.

2.4 Reactions of beryllium with neutrons

The pronounced radiation effects on beryllium, as a structural reflector material, by fast neutron, that is in the energy range of 0.7 to 20 MeV over a long period, are dimensional instability, helium embrittlement and swelling [24], [25].

In a beryllium reflected reactor the fast neutron flux will be greater on one side of the beryllium block than on the other side, thus the side nearest to high flux will swell more than the opposite side. This results in beryllium being curved or bowed on the side experiencing high flux, thus causing beryllium to be dimensionally unstable. It is therefore important to note that in the beryllium reflector design and service life prediction, the most likely failure mechanisms will be associated with dimensional instability, irradiation swelling and helium embrittlement.

The above–mentioned effects are as a result of the transmutation of beryllium upon fast neutron irradiation. The beryllium transmutation occurs via (n,α) and (n,2n) reactions, which result in the formation of ^{6}Li, ^{3}H, ^{3}He and ^{4}He isotopes. The isotopes ^{6}Li and ^{3}He have large thermal neutron absorption cross sections (i.e., $\sigma^{^{6}\mathrm{Li}} = 950$ b and $\sigma^{^{3}\mathrm{He}} = 5327$ b) and their presence and build–up in the beryllium reflector will result in negative effects on the power distribution, reactivity, neutron fluxes and spectrum in the core. The accumulation of ^{3}H, ^{3}He and ^{4}He causes swelling and embrittlement in beryllium.

The formation of ^{6}Li, ^{3}H, ^{3}He and ^{4}He isotopes via the nuclear reaction chains of beryllium is shown in more detail in Figure 2.7 [7], [26]. The important chains in this study are that of Chain 2, that is the highlighted chains of Figure 2.7.

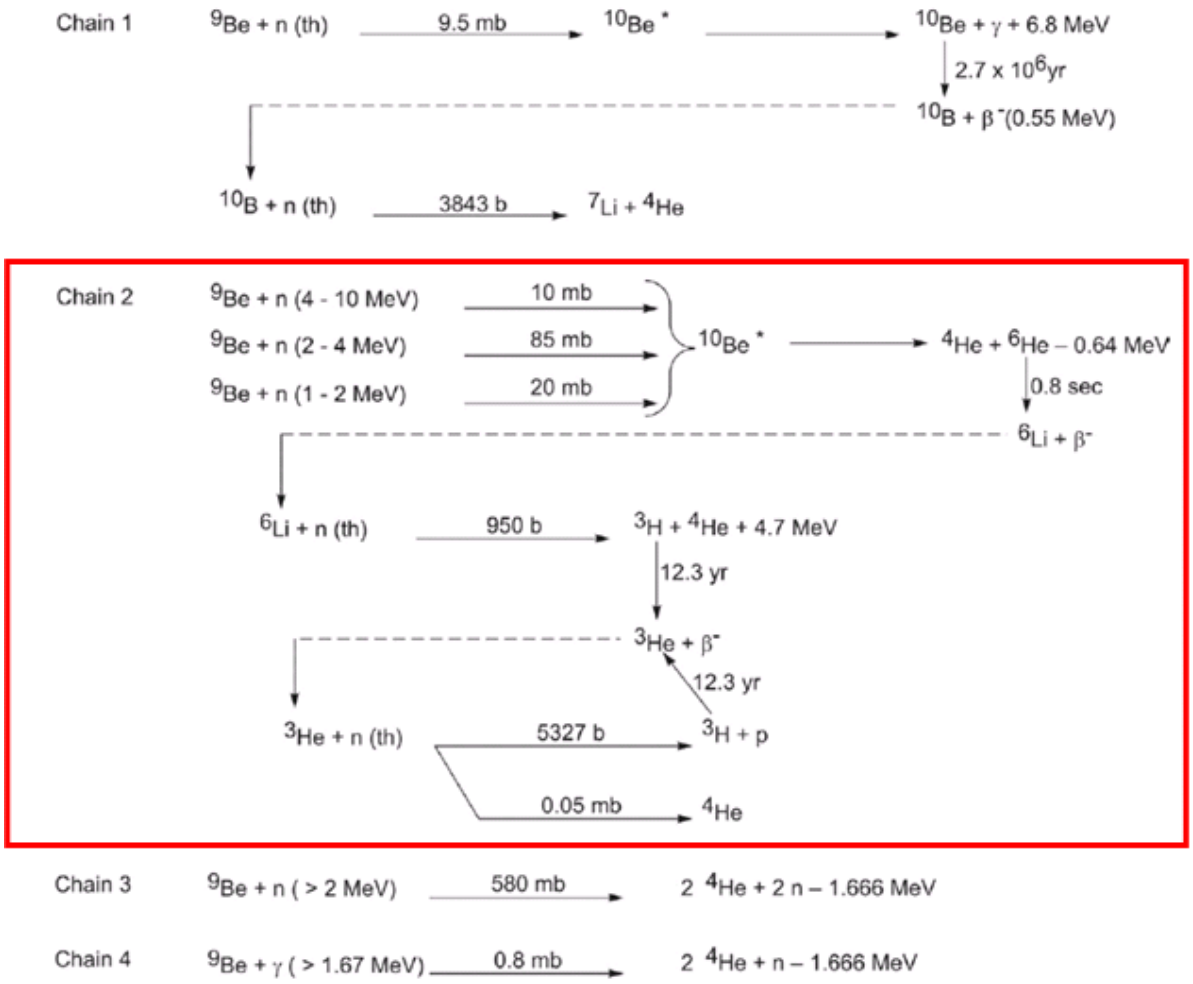

Figure 2.7: Beryllium nuclear reaction chains

In Figure 2.7, the reactions types, (n,γ), (n,α), (n,2n) and (γ,n) are represented by Chains 1, 2, 3 and 4 respectively.

The amount of ^{10}B formed, that is Chain 1, is small in practice in a reactor because of the low (n,γ) cross section of ^{9}Be and the long half–life of ^{10}Be (i.e., 2.7 $\times$ 10^6 yr), which is fortunate in view of the large absorption cross section of ^{10}B.

Reaction chains 2, 3 and 4 are responsible for the gradual build–up of ^{4}He in beryllium, which may become significant after long–term exposure. The ^{4}He build–up is associated with swelling and embrittlement of beryllium. Chain 2 has one of the significant reaction products, tritium (^{3}H), a radioisotope of concern in nuclear reactor waste streams. The other important reaction products of Chain 2 are ^{6}Li and ^{3}He, as mentioned before. The reaction shown in Chain 3, that is (n,2n), indicates the mechanism by which beryllium can act as a neutron multiplier.

Chain 4, that is (γ,n), can be utilized to produce a neutron source by subjecting beryllium atoms to

high energy gamma rays from a radioactive material (e.g. radioactive Antimony). This technique has been used to produce neutron sources to assist in the start–up of nuclear reactors.

The nuclear reaction equations of interest in Chain 2 of Figure 2.7 are summarised and discussed in details below.

$$^{9}_{4}\mathrm{Be}(n,\alpha) \longrightarrow {}^{6}_{2}\mathrm{He} \tag{2.1}$$

$$^{6}_{2}\mathrm{He} \xrightarrow{\beta^-} {}^{6}_{3}\mathrm{Li};\ T_{1/2} = 0.8 \text{ sec} \tag{2.2}$$

$$^{6}_{3}\mathrm{Li}(n,\alpha) \xrightarrow{950 \text{ barns}} {}^{3}_{1}\mathrm{H} \tag{2.3}$$

$$^{3}_{1}\mathrm{H} \xrightarrow{\beta^-} {}^{3}_{2}\mathrm{He};\ T_{1/2} = 12.3 \text{ years} \tag{2.4}$$

$$^{3}_{2}\mathrm{He}(n,p) \xrightarrow{5\,327 \text{ barns}} {}^{3}_{1}\mathrm{H} \tag{2.5}$$

The nuclear reactions in Equation (2.1) to (2.5) are further simplified by assuming the following:

(a) The beryllium number density is assumed constant, since beryllium losses due to (n,2n) and (n,α) are negligibly small.

This has been shown in the MARIA reactor with the beryllium density changing by about 0.11% over a period of about 10 – 12 years, that is, 0.08% and 0.03% due to (n,2n) and (n,α) reactions respectively [27]. In this case the (n,α) reaction is considered since it initiates important reactions in Equations (2.2) to (2.5).

(b) Eliminating Equation (2.2) from the chain since the half–life of ^{6}He is very short, that is ^{6}He is immediately transformed to ^{6}Li (i.e. 0.8 seconds).

(c) ^{3}H and ^{3}He remains (if they do not diffuse) in the beryllium reflector throughout the reactor operational history due to the long half–life of ^{3}H, i.e. $T_{1/2}$=12.3 years.

(d) The (n,γ) capture rates are totally negligible relative to the (n,α) and (n,p) processes, therefore the reaction is not considered here.

The orders of magnitude of important cross sections of the neutron irradiated beryllium are shown in Figure 2.8 [21].

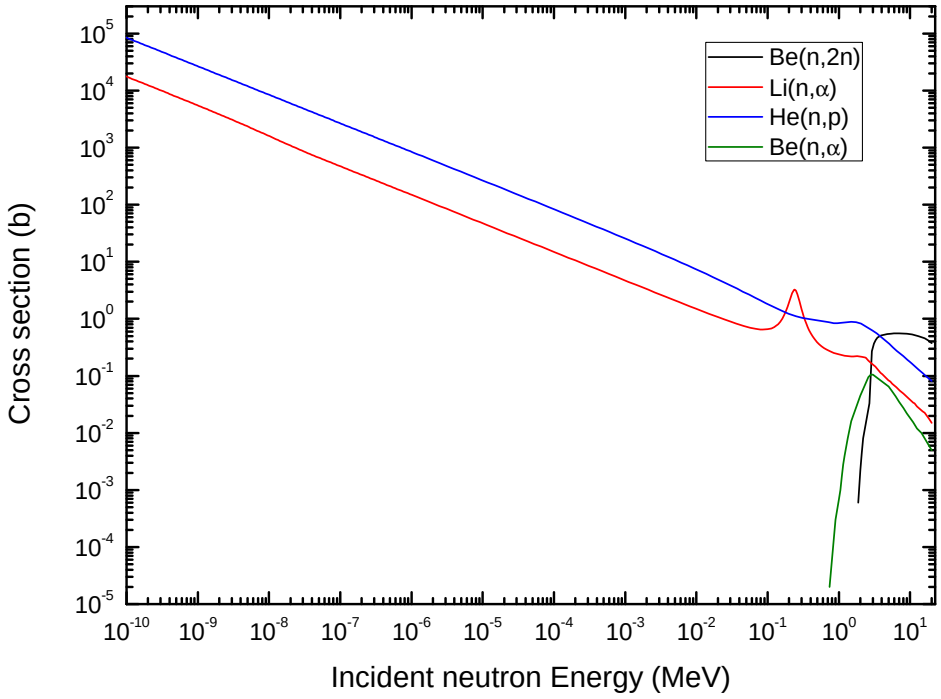

Figure 2.8: Beryllium reaction cross sections, ^{9}Be(n,2n), ^{9}Be(n,α), ^{6}Li(n,α) and ^{3}He(n,p), (ENDF/B VII.0, T=300°K)

In this case, a system of differential equations describing the isotopic transformation as a result of the beryllium irradiation becomes [28] [29]:

$$\frac{\mathrm{d}N_{Be}}{\mathrm{d}t} = -N_{Be}(r) \int \phi_f(r,E,t)\sigma^{Be}_{(n,\alpha)}(E)\mathrm{d}E = 0 \tag{2.6}$$

(Equation (2.6) is based on assumption (a)).

$$\frac{\mathrm{d}N_{Li}(r,t)}{\mathrm{d}t} = N_{Be}(r) \int \phi_f(r,E,t)\sigma^{Be}_{(n,\alpha)}(E)\mathrm{d}E - N_{Li}(r,t) \int \phi_{th}(r,E,t)\sigma^{Li}_{(n,\alpha)}(E)\mathrm{d}E \tag{2.7}$$

(Equation (2.7) is based on assumption (b)).

$$\frac{\mathrm{d}N_H(r,t)}{\mathrm{d}t} = N_{Li}(r,t)\int \phi_{th}(r,E,t)\sigma^{Li}_{(n,\alpha)}(E)\mathrm{d}(E) + N_{He}(r,t)\int \phi_{th}(r,E,t)\sigma^{He}_{(n,p)}(E)\mathrm{d}E - \lambda_H N_H(r,t) \tag{2.8}$$

$$\frac{\mathrm{d}N_{He}(r,t)}{\mathrm{d}t} = -N_{He}(r,t)\int \phi_{th}(r,E,t)\sigma^{He}_{(n,p)}(E)\mathrm{d}E + \lambda_H N_H(r,t) \tag{2.9}$$

where N_{Li}, N_H, N_{He} and N_{Be} are atomic concentrations of ^{6}Li, ^{3}H, ^{3}He and ^{9}Be respectively, $\sigma^k_{(n,x)}$ is the microscopic cross section of nuclide k for reaction *(n,x)*, $\phi_{th}(r,E,t)$ and $\phi_f(r,E,t)$ are the thermal and fast neutron flux densities as a function of the beryllium reflector position in the core, neutron energy and time and λ_H is the tritium decay constant, that is $\lambda_H = 1.78 \times 10^{-9}\mathrm{s}^{-1}$. The variable r is a general spatial variable.

The reaction rates, $RR_{k,(n,x)}$, as a function of beryllium reflector position in the core and the irradiation time for nuclide k and reaction type *(n,x)* can be written as:

$$RR_{k,(n,x)} = \int_{E_{min}}^{E_{max}} N_k \phi_{(th,f)}(r,E,t)\sigma^k_{(n,x)}(E)\mathrm{d}E \tag{2.10}$$

where (E_{min}, E_{max},) is the entire energy range of interest and $\phi_{th,f}(r,E,t)$ is either a thermal or fast flux density. It should be noted that Equations (2.6) to (2.9) are nonlinear because the equation coefficients are dependent on the reaction rates of ^{3}He and ^{6}Li. The reactions are spectrum dependent and the spectrum in turn depends on the poison concentrations. In the MARIA reactor, the nonlinearity problem has been overcome by an assumption of constant reaction rates within specific periods. The assumption is valid as long as the change in the spectrum and hence the poison concentration is not pronounced within a specified period, otherwise the actual variation of reaction rates with time is not negligible and should be accounted for [29], [30].

The general solutions, as found in reference [3], for the atomic densities of Equations (2.7) to (2.9) are:

$$N_{Li}(r,t) = N_{Li}(0)e^{-\phi_{th}(r)\sigma^{Li}_{(n,\alpha)}\cdot t} + N_{Be}(r)\cdot\frac{\phi_f(r)\sigma^{Be}_{(n,\alpha)}}{\phi_{th}(r)\sigma^{Li}_{(n,\alpha)}}\cdot\left(1 - e^{-\phi_{th}(r)\sigma^{Li}_{(n,\alpha)}\cdot t}\right) \tag{2.11}$$

$$N_H(r,t) = a_1 + a_2\cdot e^{-(\lambda_H + C)\cdot t} + \frac{AC}{(\lambda_H + C)} + \frac{(C-B)\cdot[N_{Li}(0) - \frac{A}{B}]}{B - (\lambda_H + C)}e^{-\phi_{th}(r)\sigma^{Li}_{(n,\alpha)}\cdot t} \tag{2.12}$$

$$N_{He}(r,t) = \frac{\lambda_H}{C}\cdot a_1 - a_2 \cdot e^{-(\lambda_H + C)\cdot t} + \frac{\lambda_H A}{(\lambda_H + C)}\left(t - \frac{1}{C}\right) + \frac{\lambda_H \cdot [N_{Li}(0) - \frac{A}{B}]}{B - (\lambda_H + C)} e^{-\phi_{th}(r)\sigma^{Li}_{(n,\alpha)}\cdot t} \quad (2.13)$$

where the constants are defined as:

$$A = N_{Be}(r)\phi_f(r)\sigma^{Be}_{(n,\alpha)} \quad (2.14)$$

$$B = \phi_{th}\sigma^{Li}_{(n,\alpha)} \quad (2.15)$$

$$C = \phi_{th}\sigma^{He}_{(n,p)} \quad (2.16)$$

and the integration constants a_1 and a_2, follows from initial conditions:

$$a_1 = \left[N_{Li}(0) + N_{He}(0) - \frac{A}{B} + \frac{\frac{\lambda_H A}{C}}{\lambda_H + C}\right] \cdot \left(\frac{1}{1 + \frac{\lambda_H}{C}}\right) \quad (2.17)$$

$$a_2 = \left[\frac{B}{B - (\lambda_H + C)} \cdot N_{\mathrm{Li}}(0) - \frac{A}{B} + N_H(0) - \frac{C}{\lambda_H} \cdot N_{He}(0) - \frac{A}{(\lambda_H + C)}\right] \cdot \frac{1}{1 + \frac{\lambda_H}{C}} \quad (2.18)$$

These general solutions have been applied to the Oak Ridge Research reactor beryllium reflector, amongst other reactors, and the poisoning effect has been quantified – refer to reference [3].

The equilibrium level of ^{6}Li is determined by formation in a fast neutron spectrum, that is the reaction in Equation (2.1) and its burn–up in the thermal energy range, that is the reaction in Equation (2.3). Its concentration saturates after some time of reactor operation and the duration of saturation in different beryllium reflector elements depend on their position in the core. That is, the ^{6}Li saturation will be quicker in the thermal flux region but at a lower level than in the fast flux region, since its concentration will vary according to Equation (2.11).

All of the SAFARI–1 reactor beryllium reflectors are placed in unique different surrounding environments, see Figure 1.1, thus it is expected that they will differ in ^{6}Li content, as well as in the contents of other isotopes, that is ^{3}He, ^{4}He and ^{3}H.

Lithium–6 is a stable isotope; it does not decay or burn–out during shut–down periods, therefore operational breaks do not influence the build–up of ^{6}Li and the asymptotic value of the ^{6}Li number density is reached. However, when the spectral changes are considered, the ^{6}Li concentration might increase. In general, the asymptotic value of ^{6}Li depends on the ratio of fast to thermal neutron

flux, that is on the neutron spectrum in the beryllium reflector – refer to the general solution in Equation (2.11).

The generation and depletion of helium–3 (^{3}He) during reactor operation, is depicted in Chain 2 of Figure 2.7, by the reactions in Equations (2.4) and (2.5), and Equations (2.8) and (2.9). The relative amount of tritium and helium in the reactor depend on the magnitude of the thermal flux and the reactor operating conditions (i.e. duration of shut–downs). The depletion of ^{3}He ceases during reactor shut–down periods (e.g. long shut–down periods), it is during this time that highly irradiated beryllium reflectors can experience a significant increase in ^{3}He concentrations due to the radioactive decay of ^{3}H to ^{3}He. During shut–down, that is $\phi(r, E, t) \approx 0$, Equations (2.8) and (2.9) take the form of Equations (2.19)and (2.20):

$$\frac{\mathrm{d}N_H(r,t)}{\mathrm{d}t} = -\lambda_H N_H(r,t) \tag{2.19}$$

$$\frac{\mathrm{d}N_{He}(r,t)}{\mathrm{d}t} = \lambda_H N_H(r,t) \tag{2.20}$$

thus explaining the decay of ^{3}H and build–up of ^{3}He during shut–down periods. In some rare cases, the ^{3}He concentration in an individual beryllium reflector continues to increase during operation. This is explained by the fact that the power delivered by the fuel assemblies in the region of these reflectors is minimal; therefore the ^{3}He build–up rate becomes higher than the burn–up rate.

The SAFARI–1 reactor experienced long shut–down periods as depicted in Figure 2.4 of Subsection 2.2.1, during its operational history. It is expected that the ^{3}He concentration will increase (see Figure 5.7 on page 67) during these periods, thus resulting in a major impact on core parameters and the beryllium reflector itself.

The formation of ^{6}Li, ^{3}He and ^{3}H isotopes in beryllium reflectors has been accounted for by the solution of Equations (2.11) to (2.13) during operation and Equations (2.19) to (2.20) during shut–down periods, for isotopic concentrations. This approach has been used by many reactors including some of Table 1.1. Details on the approaches used in solving these equations at various reactors can be found in references [26] to [31]. Computing the isotopic concentration in any beryllium reflected reactor using the general solution above requires knowledge of:

(a) The few–group microscopic cross sections dependent on the spectrum in the beryllium reflector for each reaction type,

(b) The neutron flux and neutron spectrum in individual reflector elements; as well as

(c) The reactor operational history, that is operation (irradiation) and shut–down times (cooling).

Based on the general solution of Equations (2.12) to (2.13), different numerical programs have been

developed and successfully used in calculating the isotopic concentration of ^{6}Li, ^{3}He and ^{3}H.

For example, a FORTRAN program, BERYL has been extensively used for the MARIA reactor beryllium poisoning effects [30], while the MCU and BERCLI programs are used for the MIR reactor [31]. At the Plum Brook reactor which was operated by NASA in Ohio, USA, before it was shut down in January 1973, Equations (2.6) to (2.9) were solved by using the Laplace transform and the complex inversion integral, then a FORTRAN program was written based on these solutions to compute the poison build–up for cyclic reactor operation. The associated change in reactivity was calculated using the perturbation theory [32]. For the BR2 reactor, the beryllium poisoning was accounted for by using MCNP–4C to calculate reaction rates, that is Equation (2.10), and solving Equations (2.6) to (2.9) for ^{6}Li, ^{3}He and ^{3}H concentrations [33].

As stated before, this is not accounted for in the OSCAR code system.

A brief summary on the analysis, results and conclusions of the beryllium reflector poisoning effects in different reactors, is given in the next few paragraphs:

In the MARIA reactor, the WIMS–ANL program was used to generate the 7–group microscopic cross sections for reactions, (n,α) on ^{9}Be, (n,α) on ^{6}Li and (n,p) on ^{3}He; the calculations were based on the ENDF/B–VI neutron cross section library. The 7–group flux values were calculated using the REBUS–3 code and the reaction rates were calculated in accordance with Equation (2.10). The initial conditions applied to the first period of operation were that the initial number densities of ^{6}Li, ^{3}He and ^{3}H were zero and that of beryllium correspond to the manufacturers technical specification. This information, together with the reactor operational history, is then transferred to the BERYL program, for computing the isotopic concentrations [29], [30].

This calculation showed that simplification of the reactor operational schedule and hence the neutron spectrum, that is no neutron spectrum updating during reactor operation and no operational breaks (i.e. lumped operation and shut–down hours), in modelling the isotopic transmutations in the beryllium reflector introduced large errors in the results. When the simplified case was compared to the explicit case, spectrum updating and detailed operational history, differences of 14% in the ^{6}Li number density with an underestimation of 5% and 11% in ^{3}H and ^{3}He number densities were observed, respectively. The differences in the case of ^{6}Li were mainly due to a quick saturation of number densities in the simplified case, as compared to the explicit case. The effect of simplifying the shut–down and operation periods, is clearly seen in the errors associated with the number densities of ^{3}H and ^{3}He [29], [30].

It was therefore concluded that the computation must be performed with detail modelling of: (1) the operating conditions (i.e. core configurations), (2) updated spectrum at each step and (3) operation and shut–down times.

Moreover, it was shown that for the MARIA reactor, the time steps for updating the neutron spectrum and hence the poison concentrations should be 50 to 100 days [29]. Further findings at

the MIR reactor showed that during a run (cycle) of average length, that is about three weeks, the concentration of poisons changed negligibly [31].

The SAFARI–1 reactor average cycle length is about 4 weeks and these findings might be important when determining the time step for the neutron spectrum updating.

Further analysis showed that the actual power distribution has a strong influence on the ^{6}Li, ^{3}H and ^{3}He content, through the different flux levels in the beryllium reflector. This implies that the flux level in the beryllium reflector adjacent to particular fuel channels differs strongly and so does the content of ^{6}Li and ^{3}He. The fuel burn–up process is weakly influenced by the poisoning of beryllium since the poison density build–up process has a time–scale of years while the fuel element burn–up is accomplished within a few months. Comparisons of the influence of fresh and burned fuel spectra on poison formation showed important effects, that is poison formation is sensitive to changes in the neutron spectrum. It is therefore important to perform a detailed analysis for individual beryllium reflector elements in a given core configuration, in order to quantify and accurately account for the poison distribution and build–up in the reflectors [29] to [31].

The dependence of neutron fluxes and hence the reaction rates across the thickness of the beryllium reflector from the fuel channel edge have been conducted and it was verified that both parameters decrease exponentially with the distance from the first beryllium layer adjacent to the fuel channel. In some cases, this could provide the possibility of re–positioning or rotating of the beryllium reflector element so that the less poisoned side faces the core (i.e. the side that experienced lower neutron fluence over the reactor's operational history) [30], [34].

The paragraph above forms part of the aims of this study, that is to verify the possibility of rotating the SAFARI–1 reactor beryllium reflector.

The losses in reactivity significantly limit the maximum available excess reactivity as well as the shut–down times. The maximum possible fuel load in the core and hence the excess reactivity as well as the loss in reactivity through poison formation should be known – if not, it might be impossible to start–up the reactor after shut–down unless major core changes are made.

It was calculated that over a period of 20 years of the MIR reactor operation, the total reactivity decrease was about 8% due to the accumulation of ^{6}Li and ^{3}He [31]. In the Plum Brook reactor, after a shut–down of approximately 100 days, the critical rod bank height at restart was about 0.8 inch (2 cm) higher than normal [32] and this is attributed to beryllium poisoning. The reactivity loss caused by the presence of ^{6}Li and ^{3}He, in the MARIA reactor was estimated to be in the order of 4 – 9% with a stable value of 6% for more regular reactor operations [35].

Similar conclusions have been reached in other reactors when the beryllium reflector poisoning effects were considered [36]. As a result, the phenomenon is well understood and has been accounted for in reactor core calculations.

Most of the beryllium reflected reactors have implemented the isotopic transmutation in irradiated beryllium in their day–to–day in–core fuel management codes, for example, the REBUS–3 code system used in the MARIA reactor, thus accounting for the beryllium poisoning effects. This increases the reliability of predictive calculations and improves on experimental planning and operational safety of the reactor.

It is therefore of undeniable and urgent importance to include explicit models of beryllium reflectors under fast neutron irradiation in the fuel management calculation and depletion codes, that is the OSCAR code system, in this instance.

However, knowledge of the poisoning phenomena alone is not enough to quantify the service life of the reflector; it only account for the perturbation in reactor core parameters. In this case additional analyses have been conducted in order to relate the formation of gas atoms or concentration, in particular, helium, to swelling and embrittlement, thus effectively determining the service life of the reflector. Correlation between the gas formation, fluence and temperature has been extensively studied so as to quantify swelling and hence the service life of the beryllium reflector.

It has been observed that gas formation is nearly a linear function of the fast fluence. At fast neutron fluence higher than 6.4 $\times 10^{22}$ $\frac{n(>1\text{ MeV})}{\text{cm}^2}$, accelerated swelling and dimensional changes were observed in the beryllium reflector of the BR2 reactor; the tritium concentration in the primary water also started to increase at this value – indicating the diffusion of the gas atoms from the reflector. As a consequence, this value was adopted as the maximum admissible fast fluence for the lifespan of the reflector. It was further observed that at a lower operating temperature ($\sim$50 °C), gas atoms nearly do not diffuse, it is at higher temperatures and a higher fast fluence where the diffusion seems to be accelerated [37], [38]. Equation (2.21) below is recommended to estimate swelling at low temperatures [39], that is 40 °C to 50 °C, (these are typical SAFARI–1 reactor operating temperatures):

$$\frac{\Delta V}{V} \approx (0.58 \pm 0.3) \times 10^{-25}\phi t \tag{2.21}$$

where ϕt is the fast fluence in $\frac{n(>1\text{ MeV})}{\text{cm}^2}$.

Beeston [40] uses Equation (2.22) to estimate the volumetric change and Equation (2.23) to estimate the change in length, for beryllium irradiated at a temperature of 100°C:

$$\frac{\Delta V}{V} = 0.00549(\phi t)^{1.035} \tag{2.22}$$

$$\frac{\Delta L}{L} = (0.001829(\phi t)^{1.035} \tag{2.23}$$

where ϕt is the fast neutron fluence in 10^{22} $\frac{n(>1\text{ MeV})}{\text{cm}^2}$.

Literature studies from references [40] and [41], show that helium bubble swelling is the predominant mechanism resulting in dimensional instability and changes of irradiated beryllium.

The ^{4}He content in beryllium reflectors can be estimated using Equation (2.24) [38]

$$C_{^4\mathrm{He}}(appm) = 4880 \ \pm \ 90 \ \times \ \phi t \ \times \ 10^{-22} \tag{2.24}$$

with ϕt defined as before.

Beryllium reflector damage, mentioned in the previous paragraphs regarding swelling and embrittlement, does not form the scope of this study; it will not be discussed further. The few points discussed above will be useful when the lifespan of SAFARI–1 reactor beryllium reflector needs to be predicted.

This study shall focus on the beryllium reflector poisoning as indicated before.

Chapter 3

Calculational methods

3.1 Introduction

This chapter describes the numerical codes used to perform the neutronic calculations in this study. The codes of interest are the nodal diffusion codes, OSCAR–3, the latest release OSCAR–4, the Monte Carlo codes, MCNP5.51, MCNPX2.6.0 and the nuclide inventory code FISPACT–2005.1.

3.2 The OSCAR code system

The OSCAR code system [42], [43], [44] is developed and maintained by the Radiation and Reactor Theory group of Necsa. The current production version of the OSCAR code system, is the OSCAR–3 code, which is still extensively used to provide calculational support to the SAFARI–1 reactor in terms of core–follow and reload calculations, as well as safety analysis. The code system is also used by the reactor calculational groups at NRG Petten and the Delft University in the Netherlands. The new release, OSCAR–4 [45], is currently in the final validation stages before it completely replaces the OSCAR–3 code system.

The OSCAR code modules are based on modern reactor physics methods and use response–matrix neutron transport solutions to tabulate few–group neutron cross–sections. Neutronic calculations are performed in a fine–group structure (172 WIMS XMAS group structure) to produce few group cross sections, for use in a 3D global neutron nodal diffusion equation solver, MGRAC (**M**ulti–**G**roup **R**eactor **A**nalysis **C**ode).

The major difference between the OSCAR–3 and OSCAR–4 code systems may be found in the global diffusion simulator (MGRAC), with a large number of improved methods and models centred around control rod depletion, burnable poison and detector modelling approaches. The OSCAR code system takes neutron leakage spectra, important in the modelling of reactor cores, into account.

This is done by allowing calculations in multiple energy groups – typically six or more broad–energy groups. The modules of the OSCAR code system are discussed in detail below.

3.2.1 The cross section generation module of OSCAR

The OSCAR cross section generation package encompasses a whole range of codes used in the production of few–group constants. The code packages that are currently used for cross section generation are, HEADE (**HE**terogeneous **A**ssembly **DE**pletion), a two–dimensional transport code based on a lower–order interface current method and STYX – a two–dimensional collision probability code [42], [43], [44].

HEADE performs heterogeneous transport assembly depletion and off–base calculations, that is the calculation that takes changes in fuel temperature, moderator density, boron concentration, etc. into consideration. The assembly problem is described in terms of rectangular nodes or cells, which can contain either cylindrical pins or plates. The basic nuclear data for the HEADE code is derived from the 172–group WIMS7 nuclear data library [46]. The cross sections are usually collapsed to six energy groups and in case STYX calculation is needed, the cross sections are first collapsed to 24 energy groups in HEADE as required by STYX calculations, then STYX collapses the cross sections to the six energy groups required for core calculations. HEADE incorporates all of the functions required for generating few–group homogenized assembly cross sections, flux or power form functions and interface flux discontinuity factors as functions of exposure, water density, water temperature, fuel temperature, control rod status, etc. The homogenized assembly cross sections and other data can be written to a so–called HEADE file.

The use of HEADE is limited by a lack of geometric flexibility and restrictions in the theoretical capabilities. Where HEADE cannot be used, the STYX collision probability code is used. It is used for special purposes such as the determination of few–group cross sections for irradiation rigs and the control of the SAFARI–1 control element which consists of an upper control section and a bottom fuel follower section. It also plays an important role in determining the heterogeneous flux form functions for irradiation rigs which are used in conjunction with nodal reactor calculation results to estimate specific reaction rates.

3.2.2 The cross section linking module in OSCAR

The cross section linker provides a link between the cross section generation module discussed in Subsection 3.2.1 and MGRAC. There are two code packages used here, namely POLX and LINX [42].

POLX reads a single HEADE file containing few–group cross sections and other data tabulated as a function of several state parameters to perform a least–square quadratic polynomial fit on

data for a given assembly, for example, a fuel assembly or reflector assembly. For fuel assemblies the exposure range is usually partitioned into a few user–specified ranges to enhance the accuracy of the fit. The polynomial coefficients as well as burn–up chain data are written to an assembly specific POLX file and stored for repeated later use.

LINX is used to merge several POLX files into a single run–time library (LINX file) for direct use by the MGRAC nodal code.

3.2.3 The core analysis module in OSCAR

In the OSCAR–3 code system the two main codes are the MGRAC nodal diffusion code and the fuel shuffling code, SHUFFLE. The EXPOSURE file is the main interface between the two codes and it contains core loading information, nodal exposure and isotopic number densities.

In the OSCAR–4 code system, the EXPOSURE file is replaced by a number of files, that is the BASE file, basically defining the design of the component (e.g. fuel element, reflector element, etc), the LOAD file, containing the component loading history (e.g. fuel location, etc) and the HISTORY file containing the irradiation history of the component. The SHUFFLE code is still retained for core reload purposes. Further description and applications of the OSCAR code system is found in reference [47].

3.3 The Monte Carlo N–Particle Codes MCNP and MCNPX

Particle transport analysis is usually performed using Monte Carlo techniques which constitute the tracking of each particle, for example neutron, gamma, electron, etc., from birth, throughout its lifetime and ultimately to its loss by either absorption or escaping from the system. A widely used and proven code to perform these analyses or calculations is the MCNP code – Monte Carlo N–Particle code. The Monte Carlo codes, that is the MCNP 5.1.51 [48] and MCNPX 2.6.0 codes [49], [50] are briefly discussed in Subsections 3.3.1 and 3.3.2.

3.3.1 MCNP5 code system

MCNP5 is a 3D general–purpose Monte Carlo N–Particle code that can be used for neutron, photon, electron, or coupled neutron/photon/electron transport, including the capability to calculate *k–effective* eigenvalues for systems containing fissile and fissionable materials. The neutron energy regime is from 10^{-11} MeV to 20 MeV for all isotopes and up to 150 MeV for some isotopes; the photon energy regime is from 1 keV to 100 GeV, while the electron energy regime is from 1 keV to 1 GeV.

Important standard features that make MCNP very versatile and easy to use include a powerful general source, criticality source and surface source, both geometry and output tally plotters, a rich collection of variance reduction techniques, a flexible tally structure, and an extensive collection of cross–section data. Version 5 (MCNP 5.1.51) is the latest release of the MCNP code system, some of the improvements in the code include improved photon physics, neutral particle radiography, enhancements and additions to variance reduction methods, new source options and improved parallelism support (PVM, MPI, OpenMP).

3.3.2 MCNPX code system

The MCNPX code is an extension of the MCNP code with capabilities of following exotic charged particles, α–particles and ions in addition to neutrons, protons and electrons. It is capable of tracking nearly all particles at nearly all energies. It is a superset of MCNP4C3 and has many capabilities beyond MCNP4C3. The code uses standard evaluated cross section libraries, of which many extend to 150 MeV, along with physics models where libraries are not available. The code's latest version is MCNPX 2.6.0. Amongst the new capabilities of MCNPX 2.6.0 (i.e. beyond MCNPX 2.5.0) is that it can perform burn–up calculations, i.e. neutron–driven isotopic transmutation reactions. The burn–up calculation is based on the CINDER90 [51] activation code and this capability (i.e. burn–up) is currently limited to criticality (KCODE) problems.

MCNPX burn–up calculation capabilities are usually limited by the size of the problem, for example, simulating the entire reactor cycle burn–up or core–follow calculations is usually expensive in computational time, that is an extremely slow execution time. Generally, the Monte Carlo codes execute many orders of magnitude slower than neutron diffusion codes and are not suitable for use in routine core–follow calculations. Nevertheless, the burn–up capability of MCNPX will be used in this study whenever the need arises.

At the Radiation and Reactor Theory group (RRT), the reactor analysis group of Necsa, the MCNP code system is mainly used for the benchmarking of OSCAR and to perform calculations in more complex geometries where OSCAR cannot be used. Nodal diffusion codes are inaccurate in predicting a detailed neutron flux spectrum (and absolute flux level) within certain complicated geometric structures, as is often found in certain irradiation rigs inserted into an MTR core. Furthermore, diffusion methods do not perform well in regions with large flux gradients, for example in and close to control rods.

On the other hand, codes such as OSCAR, are ideal for routine core reload design and core–follow calculations, due to the speed of nodal diffusion methods.

In order to utilize the advantages of both MCNP and OSCAR, an OSCAR–MCNP link, namely OSMINT [52], [53] has been developed for use in the RRT group of Necsa. OSMINT reads the isotopic content of the SAFARI–1 reactor core from an OSCAR EXPOSURE file and then

automatically generates surface, cell and material cards for an MCNP run. The advantage of this is that the correct core isotopics can be included in the detailed 3D MCNP model for the entire core. OSMINT takes a "snapshot" of the SAFARI–1 core at a selected point in time and automatically generates an MCNP input data file, which can then be used to determine the desired steady state parameters.

3.4 Transmutation nuclide inventory codes

The main task of an inventory code is to solve a set of differential equations which describe the amount of various nuclides present, following the irradiation of a given material (fuel and non–fuel) in a neutron field.

Burn–up of non–fuel material, for example, beryllium reflector, is not accounted for in the OSCAR code system. Consequently, the transmutation nuclide inventory codes are usually used to account for this purpose, as in MCNPX 2.6.0 with CINDER90 integrated to specifically perform burn–up calculations.

To account for this limitation in the OSCAR code system, that is the lack of burn–up capabilities for non–fuel materials, a transmutation nuclide inventory code is employed, namely FISPACT–2005.1 [54]. The code is briefly described in Subsection 3.4.1.

3.4.1 FISPACT–2005.1

FISPACT [54] is the inventory code included in the EASY (**E**uropean **A**ctivation **S**ystem) code package. It is a nuclide inventory code that has been developed for neutron–induced activation calculations. The main difference between FISPACT–2005.1 and the previous versions, is that the upper energy limit has been increased from 20 to 60 MeV. It uses external libraries of reaction cross sections and radioactive decay data for many nuclides to calculate an inventory of nuclides produced as a result of irradiation. The absolute total neutron flux, as well as a detailed neutron energy spectrum within the target material, is used together with data such as the target material specifications and irradiation and decay times to determine the activities of the desired isotope as well as all other isotopes produced.

FISPACT uses seven standard energy structures, namely WIMS, GAM–II, XMAS, VITAMIN–J, VITAMIN–J+, TRIPOLI and TRIPOLI+.

The code system is designed for both fusion devices and accelerator based material test facilities. Nonetheless, the general nature of the calculational method and the data libraries makes it applicable to most situations, for example fission reactors or neutron sources, where materials are exposed to neutrons below 60 MeV.

In FISPACT the recommendation about a non–steady irradiation, for example a in reactor where there is operation and shut–down periods, is to model the rest of the irradiation or operational history by continuous irradiation (fluence is conserved) and only model in detail the last few days, weeks or months of the irradiation, as precisely as possible. This ensures that the short lived activation properties are correct.

The core task of FISPACT is the solution of a set of differential equations that describe the amount of atoms of various nuclides present following the irradiation of a given material in a neutron field. The set of differential equations is given in Equation (3.1):

$$\frac{\mathrm{d}N_i}{\mathrm{d}t} = -N_i(\lambda_i + \sigma_i\phi) + \sum_{i \neq j} N_j(\lambda_{ij} + \sigma_{ij}\phi) + S_i \tag{3.1}$$
$$S_i = \sum_k N_k \sigma_k^f \phi Y_{ik}$$

where, N_i is the amount of nuclide i at time t, λ_i is the decay constant of nuclide i (s^{-1}), λ_{ij} is the decay constant of nuclide j producing i (s^{-1}), σ_i is the total cross section for reactions on i (cm^2), σ_{ij} is the reaction cross section for reactions on j producing i (cm^2), σ_k^f is the fission cross section for reactions on actinide k (cm^2), ϕ is the neutron flux (n cm^{-2} s^{-1}), S_i is the source of nuclide i from fission and Y_{ik} is the yield of nuclide i from the fission of nuclide k.

The final term is only required if actinides are included in the initial material.

FISPACT uses a different method to the ones discussed in Chapter 2, Section 2.4 to solve a system of differential equations developed from the reactions of Equations (2.1) to (2.5) in Chapter 2 using Equation (3.1). It uses the Sidell method – an extension of the Euler (first order Taylor series) which uses an exponential function of the step length. An example of the Sidell solution for a time step h is given in Equation (3.2) [54]:

$$N_i(t+h) = N_i(t) + \frac{\left(e^{\Lambda_i h} - 1\right)}{\Lambda_i} \frac{\mathrm{d}N_i}{\mathrm{d}t} \mid_t \tag{3.2}$$
$$\text{where } \Lambda_i = (\lambda_i + \sigma_i\phi)$$

The values of nuclides, assumed to be in equilibrium, is written as follows:

$$N_i^{equil} = \frac{\{\sum_j N_j(\lambda_{ij} + \sigma_{ij}\phi) + S_i\}}{(\lambda_i + \sigma_i\phi)} \tag{3.3}$$

For the MARIA reactor beryllium reflector, the BERYL program [30] is used, instead of the

activation codes, to account for the transmutation (or burn–up) of the reflector over the reactor operational history.

In this study both MCNPX and the BERYL program will be used to a limited extend, i.e. to benchmark FISPACT models for the SAFARI–1 reactor beryllium reflector burn–up. FISPACT will be the primary code used for activation calculations.

Chapter 4

Methodology

4.1 Introduction

This chapter discusses models that were set–up to perform calculations for the SAFARI–1 research reactor. The models were set–up in OSCAR, MCNP, and FISPACT. MCNP and FISPACT calculations were based on a 172–group energy structure, while OSCAR calculations were based on a 6–groups energy structure. Since MCNP can model in full 3D geometric detail, the MCNP base model briefly described herein reflects the detailed configuration of the reactor, except for the ex–core components such as beam tubes, poolside facility and the pneumatic rabbit. The ex–core components were not modelled in both the OSCAR and MCNP SAFARI–1 reactor models; however, the neutron fluxes in the water where these component are located is calculated.

The first section of this chapter, that is Subsection 4.1.1, highlights assumptions employed in this study. Section 4.2 is dedicated to the OSCAR models. The MCNP and FISPACT models are discussed in Sections 4.3 and 4.4 respectively. The MCNPX burn–up calculations and BERYL program models are discussed very briefly under the latter sections, since they are only used to benchmark the FISPACT models and the results of the benchmark are presented in Section 4.4.

SAFARI–1 reactor cycle *C0508-1* (fully HEU core) was defined as a starting point to conduct the initial analysis of this study. The MCNP input model for this cycle that is *C0508-1*, has been extensively used during the verification and validation processes of the MCNP–SAFARI–1 reactor models. It is for this reason that the cycle is considered an appropriate starting point. Furthermore, cycle *C01101-1* (fully LEU) is used to evaluate the impact of beryllium depletion on core parameters as well as for code–to–experimental data comparisons.

The OSMINT program based on the OSCAR–4 model of the SAFARI–1 reactor is still under development, thus all the MCNP inputs used were based on the OSCAR–3 models.

Take note that all the models and calculations of this study are focused on the beryllium reflector

elements, that is its burn–up effects and its influence on core parameters. The spectrum changes from core–to–core over the entire reactor operational history, however, variations spectrum in intermediate SAFARI–1 reactor cycles was only updated when necessary during the calculations, for example, when there is a significant change in the core layout, a long shut–down period, etc.

4.1.1 Assumptions of the study

The following assumptions were necessary due to a lack of specific information:

(a) The assumed beryllium density was 1.85 g/cm^3.

(b) The beryllium composition of Table 2.2 was used; in this case the beryllium was referred to as impure beryllium and the 100% pure beryllium (i.e. element without impurities) was referred to as pure beryllium.

(c) The beryllium reflector has never been rotated, reloaded in a different position or unloaded from the core, that means that the reactor has operated with the same reflector elements from 1965 to date.

(d) Composition of Table 2.2, was uniformly distributed throughout each reflector before irradiation.

4.2 The OSCAR code models

The overall model of the SAFARI–1 reactor problem in the OSCAR code system is depicted in Figure 1.1 of Chapter 1. Models were set–up for all the materials as shown in this figure; the models range from one dimensional to three dimensional problems. The OSCAR calculations discussed herein were performed using a 172–groups WIMS library collapsed to 6–energy groups. The calculations were performed using OSCAR–3.

4.2.1 Cross section generation

Few–group homogenized cross sections were generated by collapsing the WIMS172 fine group structure to six broad energy groups for use in the core calculations. The six–group boundaries are shown in Table 4.1. The two codes used for cross section generation are the two–dimensional OSCAR sub–codes, namely HEADE and STYX. The use of the STYX code in this study is limited to the control rod model, that is the absorber section of the control rod.

As input to the HEADE code, the SAFARI–1 reactor material information and reactor operating conditions were used. This includes material composition (e.g. ^{235}U fuel enrichment, impurities,

Table 4.1: Six energy group boundaries for OSCAR calculations

Group number	**Energy boundaries (eV)**	
	Lower boundaries	**Upper boundaries**
1	8.21E+05	1.96E+07
2	5.53E+03	8.21E+05
3	4.00E+00	5.53E+03
4	6.25E-01	4.00E+00
5	1.40E-01	6.25E-01
6	1.10E-04	1.40E-01

etc.), material geometric details, reactor power level, fuel and moderator temperature and moderator density. The slab geometry representation was employed in HEADE to model all the reactor materials of interest. To built the model in STYX, the geometric details and the 24–group cross section are required as input. All models have been represented as closely as possible to their true environment – within the limitations of HEADE and STYX.

In HEADE, the cross sections for the standard fuel and the fuel follower plates (i.e. LEU and HEU fuel and fuel follower) were generated with a three–region unit cell consisting of meat (fuel), aluminium clad (Al clad) and light water. The aluminium side plate, the extra water region on the edge of the side plate and the non–fuel region of the fuel plate were also treated as individual cells of one or more region. As an example, the subdivision of a 2–D fuel assembly is shown in Figure 4.1(a) with an enlarged one–dimensional three–region unit cell representation in Figure 4.1(b).

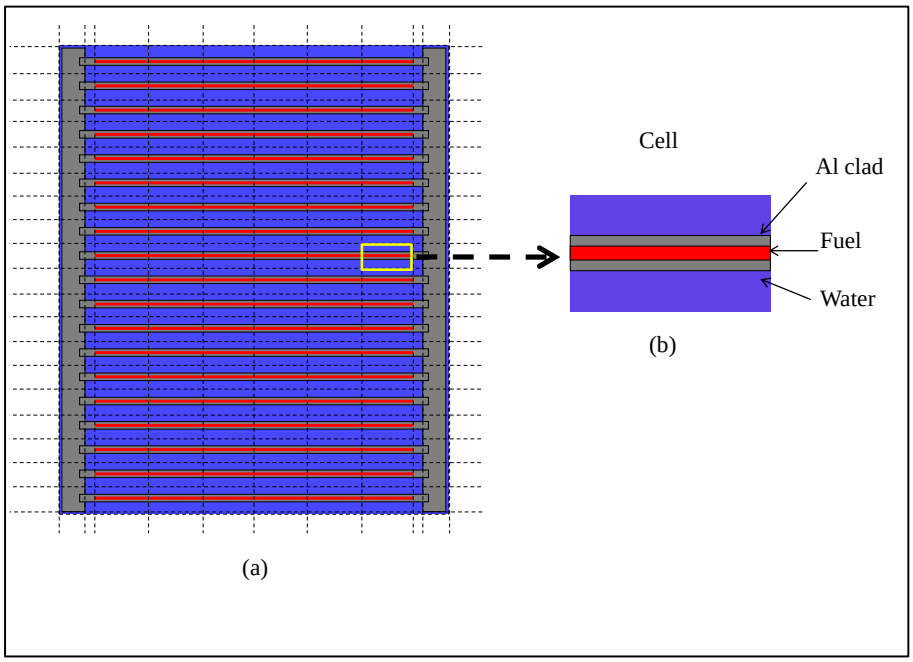

Figure 4.1: HEADE models (a) fuel assembly subdivisions and (b) unit cell representation

Microscopic isotopes were treated explicitly by including every important fission product in the model and the remaining fission products were treated macroscopically. The fuel cross sections were generated as a function of exposure, fuel temperature, moderator density and temperature.

The models of all non–fuel assemblies (i.e. reflector, filler elements, core box, etc.) were also set–up in HEADE using a slab geometry model. As an example, one of the simplified models is shown in Figure 4.2.

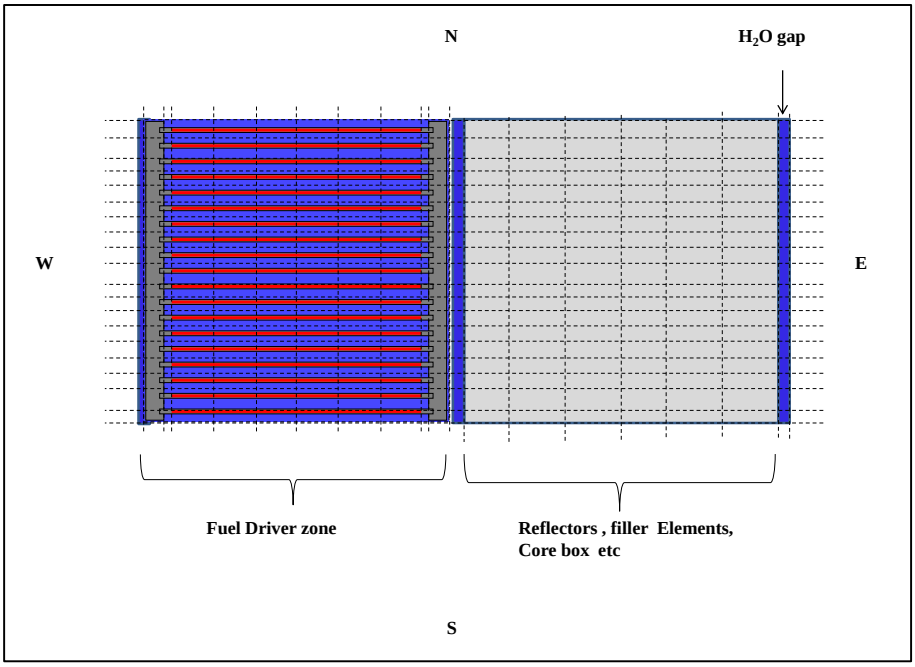

Figure 4.2: Example of HEADE model employed for non-fuel elements

The model shows a fuel driver zone with the non–fuel elements placed next to it. This approach was employed in HEADE to generate cross sections for all the non–fuel assemblies.

All the HEADE models were completed by placing reflective or white boundary conditions on the north, south, west and east side (N, S, W, E) of the model.

For the control rod model, HEADE was used to generate a 24–group cross section library which is written to the STYX input cross section file. A detailed control rod model was set–up in STYX. This model collapses the 24–group cross section to a 6–group control rod cross section as required for core calculations.

A new set of cross sections was generated whenever the material composition of reflector element (e.g. beryllium reflector), filler elements such as aluminium, fuel type, fuel enrichment, fissile loading or assembly geometry changed.

The intermediate codes, POLX and LINX, were used accordingly to prepare the final cross section library for use in reactor core calculations. The 3D full core SAFARI–1 reactor model is discussed in Subsection 4.2.2.

4.2.2 OSCAR–SAFARI–1 reactor core model

Three–dimensional OSCAR model, that is the MGRAC model, was set up for the SAFARI–1 reactor core neutronics and burn–up calculations. The calculations were based on the cross section library as discussed in Subsection 4.2.1.

The core is modelled as a 8 × 9 lattice (see Figure 1.1), with a total of 72 elements, contained in a core box. Each element in the core box is modelled within a pitch of 7.71 × 8.1 cm in the x–y direction. The pitch provides sufficient water passage for cooling the core element's surface, it is also modelled. The radial model of the core is completed by modelling the core box, the 15 cm reflector region (i.e. light water), followed by black boundary conditions. The whole core is modelled using 15 and 14 regions in the x– and y–directions respectively. The generic radial model of the core is shown in Figure 4.3.

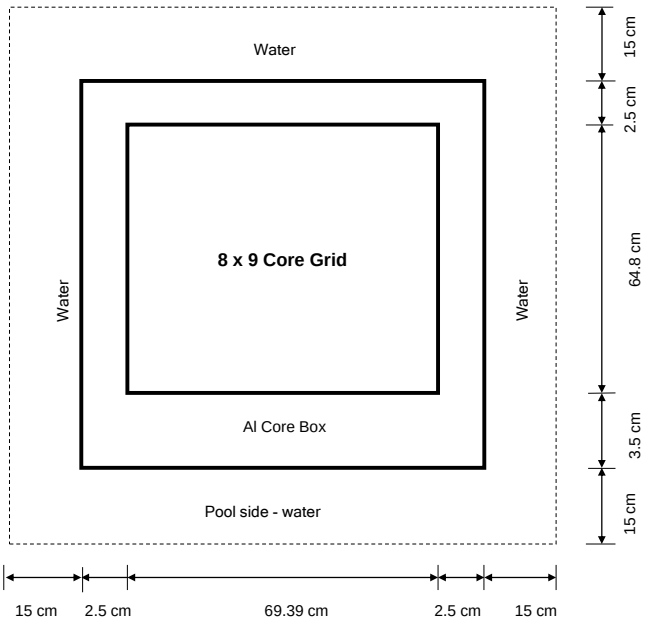

Figure 4.3: Radial schematic of the reactor core

In the axial direction, the core is divided into 17 layers (meshes), of which 13 represent the active core height of 59.37 cm. The remaining 4 meshes represent two lower and two upper reflector regions of 15 cm in total height, containing homogenised mixtures of aluminium and water or beryllium and water. These layers are added for compensation of the non–fuel length of fuel plates, side plates, reflectors and element end adaptors protruding beyond the active core height. The aluminium grid plate, supporting elements from below the core, is also modelled as a homogenised aluminium–water mixture. As an example, the axial core model of one element is represented in

Figure 4.4.

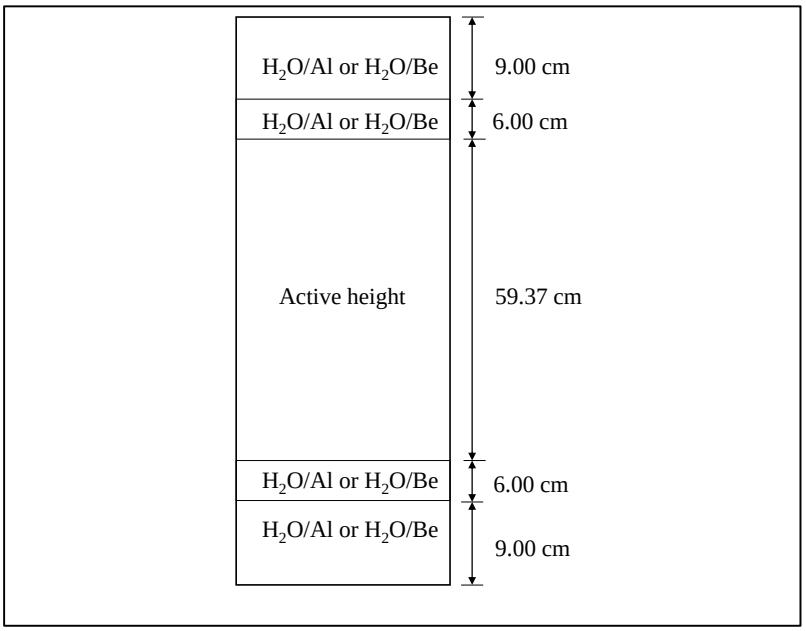

Figure 4.4: Example showing the axial assembly model in MGRAC

To perform the reload and core–follow depletion calculations for each cycle, typical plant data recorded during reactor operation, such as the reactor power level, the reactor cycle megawatt–hours, control bank positions and the regulating rod position were used as input to the 3D full core MGRAC models. Furthermore, the ^{235}U fuel loading, as well as the predicted cycle length were provided and used accordingly. With such information supplied for every cycle, it has been possible to perform the reload and core–follow calculations representing the SAFARI–1 reactor operational history for every reactor cycle to date.

In the OSCAR reload calculations, important safety parameters such as the ones listed below are calculated:

(a) Cycle length;

(b) Excess reactivity;

(c) Control rod worth;

(d) Shut–down margin.

These parameters were calculated for cycles *C0706-1* (see [55]) and *C01101-1*. Furthermore, the experimental data measured at cold and low reactor power, specifically the copper wire measurements, were compared to the calculated results of these cycles.

The OSCAR models matching that of the SAFARI–1 reactor experimental conditions during the actual cold, low power measurements, were represented and modelled as accurately as possible in the MGRAC models.

Most importantly, the effects accompanying the beryllium reflector burn–up, is evaluated for each of the above–mentioned cycles.

4.3 MCNP model of the SAFARI–1 reactor

MCNP calculations were performed using MCNP version 5.1.51 and MCNPX version 2.6.0 was used specifically for burn–up calculations. The MCNP model are a detailed representation of the SAFARI–1 reactor components. The geometric details of the reactor material are treated as explicitly as possible. The model spans 104.39 cm × 100.8 cm × 172.72 cm in the x–y–z directions. The ENDF/B–VII.0 data library, distributed with the software package, was used to perform the required calculations in a 172–group structure. Verification and validation of the MCNP models on various SAFARI–1 reactor core configurations have been performed previously. Readers are referred to references [52] and [53] for further details on the validation and verification of the models.

The whole core configuration and isotopic inventory, as stored in the OSCAR–3 EXPOSURE files are read and manipulated by the OSMINT program to prepare the KCODE MCNP input. Take note that only the KCODE calculations in both MCNP and MCNPX were considered in this study. As an example the MCNP–SAFARI–1 reactor whole core model of cycle *C0508-1* is shown in Figure 4.5.

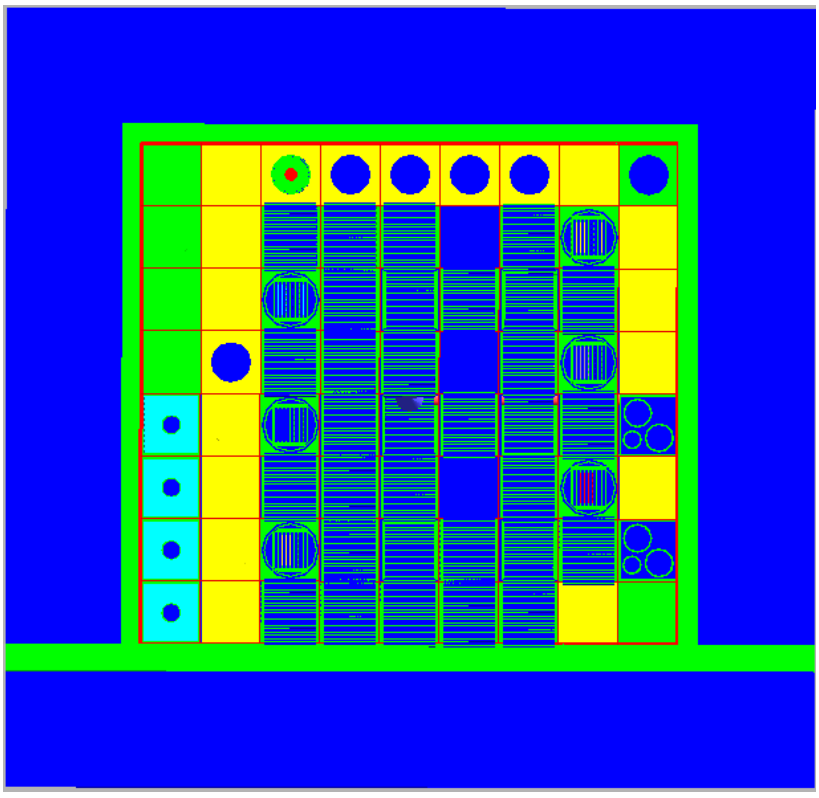

Figure 4.5: MCNP–SAFARI-1 radial model showing beryllium reflectors (in yellow)

As initial calculations, the MCNP input for cycle *C0508-1* (fully HEU core) was modified to include MCNP tallies used in calculating the following parameters:

(a) The effective energy released per fission event w_f; and

(b) The average number of neutrons released per fission ($\bar{\upsilon}$).

These parameters were calculated, for normalisation purposes, in MCNP KCODE mode calculations. This is necessary since the KCODE calculated results need to be properly scaled or normalised in order to get on absolute comparison to the measured quantities (e.g. flux, reaction rate, etc.). Since these parameters may vary for a given core composition, it was necessary to recalculate them for the fully LEU core. The effective energy released per fission event, that is w_f= 180.98 $\frac{\text{MeV}}{\text{fission}}$ and the average number of neutrons released per fission, that is $\bar{\upsilon} = 2.440$ $\frac{\text{neutron}}{\text{fission}}$, for the HEU core. For the LEU core values of $w_f = 181.13$ $\frac{\text{MeV}}{\text{fission}}$ and $\bar{\upsilon} = 2.458$ $\frac{\text{neutron}}{\text{fission}}$ were calculated. The *k-effective* for the fully HEU and LEU core were 0.99121 and 0.99402 respectively. These parameters were calculated at Beginning–Of–Cycle (BOC).

Using the results above and the SAFARI–1 reactor power of 20 MW, the fission neutron source strength or scaling factor, was calculated as follows:

$$\begin{aligned} S &= \frac{P[W] \times \bar{\upsilon}\left[\frac{\text{neutron}}{\text{fission}}\right]}{\left(1.6022 \times 10^{-13}\frac{\text{J}}{\text{MeV}}\right)\cdot w_f\left[\frac{\text{MeV}}{\text{fission}}\right]\cdot k_{eff}} \\ &= 1.69788 \times 10^{18}\ \frac{\text{neutron}}{\text{sec}} \text{ for the } \textbf{HEU} \text{ core} \\ &= 1.70416 \times 10^{18}\ \frac{\text{neutron}}{\text{sec}} \text{ for the } \textbf{LEU} \text{ core.} \end{aligned} \tag{4.1}$$

The source strength calculated in this way is valid for all the systems in KCODE calculations, that is the sub–critical, supercritical and critical systems.

Further modifications were made in the MCNP inputs to calculate the following tallies in all beryllium reflector elements:

(a) The neutron flux tally; and

(b) The reaction rates tally

As an example of how the scaling factor is used, consider an F4 tally, see point (a). In calculating the actual neutron flux, the scaling factor is entered on the MCNP FM card (tally multiplier) and the final result is represented as follows:

$$\phi\left[\frac{\text{neutron}}{\text{cm}^2.\text{s}}\right] = \frac{P[W] \times \bar{\upsilon}\left[\frac{\text{neutron}}{\text{fission}}\right]}{\left(1.6022 \times 10^{-13}\frac{\text{J}}{\text{MeV}}\right)\cdot w_f\left[\frac{\text{MeV}}{\text{fission}}\right]\cdot k_{eff}}\cdot\phi_{F4\ tally}\left[\frac{1}{\text{cm}^2}\right] \tag{4.2}$$

This approach was used in normalising all calculated quantities, see points (a) and (b).

Furthermore, the beryllium reflector composition of Table 2.1 in Chapter 2 was used with an assumed density of beryllium of 1.85 g/cm^3.

The MCNP calculations were run with 1e5 particle histories per cycle, an estimated of *k-effective* of 1.00, 50 inactive cycles before averaging *k-effective* and tallies and a total of 250 cycles. This KCODE card specification ensures that the solution converges and that the statistical errors are acceptable, that is less than 10%, in all the calculated quantities (e.g. fluxes, reaction rates, etc).

The reaction cross sections for reactions (n,2n) and (n,α) on ^{9}Be, (n,α) on ^{6}Li and (n,p) on ^{3}He, as indicated in Chapter 2, reactions of Equations (2.1) to (2.5) were calculated by specifying the MCNP reaction types as indicated Table 4.2 below.

Table 4.2: MCNP reactions type representing beryllium transmutation

MCNP reaction numbers	**Reaction types**	**Materials (ZAID)**	**Isotopes undergoing reaction**	**Product isotopes**
16	(n,2n)	4009	^{9}Be	^{4}He
107	(n,α)	4009	^{9}Be	^{6}Li
103	(n,p)	2003	^{3}He	^{3}H
105	(n,α)	3006	^{6}Li	^{3}H

The above–mentioned quantities, that is the neutron flux, reaction rate and reaction cross sections were computed in all the beryllium reflector elements in the core. In order to accommodate all possible permutations that can provide answers to the motivation of this study, the following beryllium reflector models were employed and the quantities of interest calculated:

(a) Solid and hollow beryllium reflector element

The above–mentioned quantities (i.e. neutron flux, reaction rate and reaction cross sections) were calculated over the entire volume of each beryllium reflector element, thus accounting for the axial and radial average flux distribution. In addition, the quantities were computed for the following cases:

i. The hollow and solid beryllium elements treated individually;

ii. The whole core beryllium, that is solid and hollow beryllium elements treated as one.

These permutations were used to determine a suitable representation of beryllium reflector isotopic concentrations in the OSCAR and MCNP models.

The MCNP5 models were used for MCNPX burn–up calculations, for cycle *C0508-1*. Note that this capability, that is the burn–up capability in MCNPX, is limited by the problem size and the fact that it is extremely slow in execution time for routine whole core burn–up calculations. As a result MCNPX was only used to benchmark FISPACT models for the beryllium reflector burn–up. The model adopted in this regard was burning one beryllium reflector element (i.e. H8) for 45 years and comparing the number densities at the end of 45 years to the FISPACT equivalent model.

The representation of the burn–up card set–up in MCNPX is shown below:

BURN					
TIME	=	16436.3			Incremental time duration (days) for each successive burn step
PFRAC	=	1.0			Fraction of total system power (POWER) applied to burn step
POWER	=	20			Total system power in MWatt
MAT	=	6			Material number of material to be burned = H8 Beryllium
AFMIN	=	1.0×10^{-20}			Irrelevance criterion
		1.0×10^{-10}			Convergence parameter
BOPT	=	1.0	24	1	Q value multiplier, output format, problem runs with models
MATVOL	=	4703.556			Total volume (cm^3) of H8 Be reflector

Using this card it has been possible to calculate number densities of isotopes of interest, that is ^{3}H, ^{3}He, ^{6}Li and ^{9}Be. These results, together with that of the BERYL program, were used to benchmark FISPACT activation models, see Subsection 4.4.1 for the benchmark results.

Typical BERYL program input parameters extracted from the MCNP cycle *C0508-1*, include the 172–group neutron flux, reaction rates and the 172–group microscopic reaction cross sections. The initial number density of beryllium, that is 0.1235 $\left[\frac{\text{atoms}}{\text{b.cm}}\right]$, together with those of ^{6}Li, ^{3}H and ^{3}He initialized to zero, were also required as input.

4.4 FISPACT model and benchmark

The FISPACT code, version 2005.1 was used to perform the time–dependent, nuclide–coupled activation analysis for the beryllium reflectors. The XMAS (172) cross section library was used with important input parameters such as the neutron flux and spectrum, as well as the composition of the irradiated material, that is the beryllium reflector. The 172–group neutron flux and spectrum were obtained from MCNP5 calculations. The assumed beryllium density of 1.85 g/cm^3 and the beryllium reflector composition of Table 2.2 in Chapter 2, input as a number of atoms in FISPACT, were used for all the activation calculations. Other input parameters include the reactor irradiation history given as a quarterly operation and the shut–down time intervals found in Appendix A.

The 172–group MCNP neutron flux and spectrum were used together with the FISPACT 172–group cross section library to produce a 1–group effective cross section library. This library was then used directly in subsequent FISPACT runs. The neutron fluxes were specified at time intervals

corresponding to the operation or irradiation time–step. For the shut–down period, the flux was set to zero, thus corresponding to a decay time–step.

The beryllium reflector FISPACT models, equivalent to that of MCNP discussed in Section 4.3, were set–up. For example, the MCNP models used to calculate neutron fluxes in a beryllium reflector element were represented in the FISPACT input in terms of the element's total mass. The corresponding reflector neutron fluxes obtained from MCNP were then used to irradiate the reflector element – activation calculations. The input mass per solid and hollow beryllium reflector element, is about 8.70 kg and 5.66 kg respectively; therefore, FISPACT models corresponding to the MCNP models discussed in Section 4.3 will have the following masses:

(a) Solid and hollow beryllium reflector element

   i. Each solid and hollow beryllium element with a mass of 8.70 kg and 5.66 kg respectively. There are a total of 13 solid and 6 hollow beryllium reflector elements, and

   ii. Whole core beryllium, that is, solid and hollow beryllium elements treated as one, adding up to a mass of 147.06 kg.

In addition, neutron fluxes and spectra from MCNP calculations, corresponding to the above mentioned permutations were used for activation calculations. Note that the masses mentioned in the previous paragraph were calculated based on the beryllium reflector element configurations of cycle *C0508-1*, that is 13 solid and 6 hollow beryllium reflector elements; otherwise the number of elements and their positions are almost never changed from cycle–to–cycle.

The irradiation history or reactor power was modelled explicitly taking into account the shut–down and operation periods as provided by the reactor management team, that is the quarterly megawatt hours, as in Appendix A.

FISPACT calculations herein were based on models of (i) and (ii) above.

Activation calculations based on 43 and 45 years of beryllium reflector irradiations were divided as follows:

(a) Continuously irradiating the reflectors without spectrum updating using the averaged spectrum over all the beryllium reflectors as calculated from MCNP;

(b) Detailed element specific spectrum (i.e. the spectrum in each element) used for irradiation; and

(c) Finally, the spectrum is updated at suitable intervals (to be determined) for point (i) and (ii) above

It is important to note that the total neutron flux averaged over each reflector element, as well as the spectrum, varies from cycle–to–cycle (discussed in Section 5.3, Subsection 5.3.1) depending on the core configuration. Details on how these variations were accounted for is explained in subsequent paragraphs.

To capture these flux variations in FISPACT calculations, the power history (see Appendix A) was used to normalise the MNCP calculated total neutron flux in each element and the total average over all the beryllium reflectors in a specific core. As an example, fluxes calculated for cycle *C0508-1* at BOC were normalised as follows, before been used in FISPACT input for irradiation:

$$\phi_{\mathrm{Be,i}} = \frac{\text{Quarterly Reactor power}}{20\mathrm{MW}} \times \phi_{\mathrm{MCNP},\textit{C0508-1}} \tag{4.3}$$

where $\phi_{\mathrm{Be,i}}$ is the approximated neutron flux in the beryllium reflector element of the ith time step (e.g. BOC, mid-cycle) within the cycle and $\phi_{\mathrm{MCNP},\textit{C0508-1}}$ is the actual MCNP calculated neutron flux for the beryllium reflector element in cycle *C0508-1*. The quarterly reactor power is given in Appendix A. This approximation takes care of the flux variations within each cycle.

This approximation is necessary because the SAFARI–1 reactor operational history consists of hundreds of cores since 1965. There are more than 100 cycles from 2003 to date. Moreover, details of the core configurations prior to 2003 are lacking, and only the complete detail of the power history is available. Using MCNP to calculate the neutron flux and spectrum for each and every core during this period and for the number of cores involved, would be cumbersome and time consuming, if not impossible.

This approach is applied to approximate the neutron flux $\phi_{Be,i}$ in each beryllium reflector element in all the cycles of interest from 1965 to 2011. It also accounts for variations in reaction rates per cycle during the reactor operational history. Explicit spectrum and neutron flux updating are only applied in the single cycle calculations in this study (i.e. in Section 5.3, Subsection 5.3.4).

The benchmark results of selected FISPACT models are discussed in Subsection 4.4.1.

4.4.1 FISPACT model benchmark

The benchmark results of the FISPACT models, that is (1) the solid beryllium reflector in position H8, are discussed in this section. The benchmark models were based on 45 years of continuous irradiation of the beryllium reflector using constant neutron flux and spectrum.

The 172–group neutron fluxes and spectra of the beryllium reflector were calculated with MCNP5 as discussed before and used accordingly for each model, that is for FISPACT and BERYL models. The FISPACT model corresponding to those of the MCNPX and BERYL program were also set–up and the results of the models are summarised in Table 4.3.

Table 4.3: FISPACT model benchmark results

Isotopes	**Model results**			**Ratio**	
	FISPACT	**MCNPX**	**BERYL**	$\frac{\text{MCNPX}}{\text{FISPACT}}$	$\frac{\text{BERYL}}{\text{FISPACT}}$
^{6}Li	2.335E-06	1.548E-06	2.507E-06	0.7	1.1
^{3}He	1.025E-06	1.833E-07	1.097E-06	0.2	1.1
^{3}H	1.586E-04	5.895E-05	1.694E-04	0.4	1.1
^{9}Be	1.230E-01	1.231E-01	1.237E-01	1.0	1.0

The FISPACT model compares very well to the BERYL model – the two methodologies solve a system of differential equations discussed previously using initial conditions provided by the user. The large difference between FISPACT and MCNPX can be attributed to different methodologies employed by the two codes. In MCNPX, the neutron flux and spectrum updating is internally automated via the predictor-corrector method while in FISPACT and BERYL there are no such updates. MCNPX calculates fluxes using initial conditions at time step t = 0 and passes the calculated fluxes to CINDER to compute new isotopic number densities, then MCNPX uses these new number densities to recalculate the flux which are then used in CINDER for burn–up up to t = 45 years. Amongst other parameters, these updates in MCNPX before depletion in CINDER contribute to the difference observed here. Further details on the MCNPX burn–up can be found in references [49], [50] and [51].

The calculational path used in this study can be found in Appendix B, Figure B.1. The results of this study are discussed in Chapter 5.

Chapter 5

Results and discussions

5.1 Introduction

This chapter discusses results obtained, using the calculational tools described in Chapter 3 and the associated models of Chapter 4. Section 5.2 of this chapter focuses on, (1) the influence of initial impurities on the beryllium reflector effectiveness and on some important core parameter and (2) the evaluation of the burn–up of these impurities as a function of time. The analyses are conducted using both OSCAR–3 and MCNP5 for the core–wide related effects and impurity burn–up analyses are evaluated using FISPACT. The initial calculations are based on cycle *C0508-1* at BOC.

The reminder of this chapter focuses on the main aim of this study, that is the impact of neutron–irradiated beryllium reflectors on the core–wide parameters during SAFARI–1 reactor operational history. The service–life of the beryllium reflector is also evaluated.

5.2 Analyses of beryllium reflector impurities

Nuclear reactions with impurity isotopes can produce additional products of isotopes, some of which may have absorption cross sections much higher than that of pure ^{9}Be; this will impact on core neutronics and the beryllium reflector effectiveness. It is therefore essential that the impact of initial impurities as well as the impact accompanying their transmutation with time, is understood.

Moreover, by understanding the time evolution of impurities, it will be possible to isolate the effects related to impurities from those that are related to poison build–up, (i.e. ^{6}Li and ^{3}He) and swelling (i.e. ^{3}H and ^{4}He) in the reflector.

To capture the effects of impurities explicitly, the elemental composition of Table 2.2 is specified as an isotopic composition in the calculations. Analysis based on pure and impure beryllium reflectors

(i.e. with the impurities of Table 2.2 specified) and the results of this evaluation are discussed in Section 5.2.1. The transmutations of impurities, as well as the product isotopes with irradiation time, are discussed in Subsection 5.2.2.

5.2.1 Impact of initial impurities on beryllium reflector and on core parameters

In OSCAR–3, the analysis was divided into two parts, namely, (1) the influence of initial impurities on group constants such as the absorption cross section using the 2D lattice code, HEADE and (2) the impact on core–wide parameters such as the neutron flux distribution and the multiplication factor (*k-effective*) using a 3D full core model in MGRAC. MCNP calculations were also performed to quantify the OSCAR–3 evaluations.

The results for the solid and hollow beryllium reflector HEADE models are presented in Table 5.1 and the 3D full core results obtained from MGRAC and MCNP models are discussed in subsequent paragraphs. Note that the comparisons in this section were made relative to a pure beryllium reflector model. The %Δ in in Table 5.1 is calculated using Equation 5.1:

$$\%\Delta = \frac{\Sigma_a^{\text{impure}} - \Sigma_a^{\text{pure}}}{\Sigma_a^{\text{pure}}} \times 100 \tag{5.1}$$

Table 5.1: Absorption cross sections of pure and impure beryllium reflector calculated in HEADE

Energy group	**Hollow beryllium**			**Solid beryllium**		
	Macroscopic cross section (Σ_a, cm^{-1})		**%Δ**	**Macroscopic cross section** (Σ_a, cm^{-1})		**%Δ**
	Pure	**Impure**		**Pure**	**Impure**	
1	4.745E-03	4.734E-03	-0.23	6.273E-03	6.104E-03	-2.69
2	1.203E-05	1.225E-05	1.83	1.260E-05	1.289E-05	2.30
3	2.658E-04	2.695E-04	1.39	3.666E-05	4.205E-05	14.70
4	1.644E-03	1.662E-03	1.09	2.086E-04	2.271E-04	8.87
5	4.570E-03	4.621E-03	1.12	5.099E-04	5.992E-04	17.51
6	1.210E-02	1.221E-02	0.91	1.326E-03	1.492E-03	12.52

The presence of impurities increases the absorption cross section of the pure beryllium reflector, as seen in Table 5.1. The effects are more marked in the solid beryllium reflector element than in the hollow beryllium reflector. The presence of water in the 52 mm diameter hole of the hollow element overshadowed the effect of impurities in this case, that is the increased absorption cross section.

The cross section library was then generated for all the neutronically important reactor components (including that of the hollow and solid beryllium reflectors) and then introduced to the MGRAC

model of cycle *C0508-1* in order to quantify the impurity effects on core parameters.

The OSCAR–3 results of this model show a decrease in the core reactivity of about 60 pcm and the core–wide changes in thermal neutron fluxes of $\leq 6\%$ were observed in the beryllium reflector and water surrounding the core (mainly in water on the eastern–side of the core). The fluxes in the fuel elements were only reduced by up to 3%.

The MCNP results show a decrease in reactivity of about 44 pcm with a change in the thermal neutron flux of less than 1% in the beryllium reflector.

It is therefore concluded that the initial impurities of Table 2.2 have a negligible effect on the general core parameters and that their impact are insignificant on the effectiveness of the beryllium reflector. Note that all the calculations performed in this study are based on impure beryllium reflectors since it is a true representation of the beryllium reflector in the SAFARI–1 reactor core.

Notwithstanding the conclusions of the above paragraph, it remains imperative to understand and quantify the effect of these impurities with the beryllium reflector burn–up, that is the transmutations of impurities and other products, in the reflector with irradiation time. Further detail on this will be discussed in Subsection 5.2.2.

5.2.2 Burn–up analyses of beryllium reflector impurities and transmutants using FISPACT

To evaluate the transmutation of impurities and variations in the total absorption or thermal neutron poison effect in the beryllium reflector with the operational history, the FISPACT model was employed and activation calculation performed based on impure beryllium. The model was based on the 172–group neutron fluxes and spectrum averaged over all the beryllium reflectors in the core and the impurity composition of Table 2.2 is specified. The total mass, that is 147.07 kg, of the 19 beryllium reflector elements in the core (i.e. cycle *C0508-1*) was also specified in the input. This total beryllium reflector mass was irradiated with the total averaged neutron flux normalized to reactor power, according to Equation (4.3) as explained in Chapter 4, for a period of 43 years. In these analyses, a detailed SAFARI–1 reactor operational schedule was used with shut–down and operation times treated explicitly. In addition that the 43 years were modelled, the spectrum was kept constant.

The results of this analysis are reported in terms of the **E**quivalent **B**oron **C**ontent (EBC), that is a measure of beryllium impurities and transmutation products, relevant to the absorption of thermal neutrons. This will provide a good indication on the magnitude of thermal neutron absorption in the beryllium reflectors over the period of interest.

The EBC of the starting material, that is the starting composition as in 1965, was calculated using Equation (5.2), valid for naturally occurring elements in the beryllium reflector (impurities

of Table 2.2):

$$EBC = \sum_{i}^{n} \frac{\sigma_i \cdot M_B}{\sigma_B \cdot M_i} \cdot w_i \tag{5.2}$$

where σ_B and σ_i are the microscopic thermal absorption cross sections, (at the reference neutron speed of 2200 $\frac{m}{s}$, $E_n = 0.0253$ eV) for naturally occurring boron and the ith element respectively, M_B and M_i are the molar masses of boron and the ith element respectively, and w_i is the weight content of the ith element (in ppm). The sum is for all the elements excluding beryllium.

It is however important to note that the initial composition of the beryllium reflector and the material itself undergo considerable changes during irradiation, in terms of the neutron–induced transmutation products in the material as well as the number of atoms of the product isotopes and that of the beryllium reflector, etc. with time, that is at $t > 0$. As a result Equation (5.2) is not valid to calculate the EBC in this case.

In this study Equations (5.3) and (5.5) were used to account for the variations in the absorption cross section and molar masses, with irradiation time due to isotopic transmutations in the beryllium reflector.

$$\sigma_j = \frac{1}{N_j} \sum_{i}^{n} \sigma_i \cdot N_i \tag{5.3}$$

$$N_j = \sum_{i}^{n} N_i \tag{5.4}$$

$$M_j = \frac{1}{N_j} \sum_{i}^{n} M_i \cdot N_i \tag{5.5}$$

where M_j, σ_j and N_j are the molar mass, cross section and the number of atoms of the element j respectively, M_i, σ_i and N_i are the molar masses, the cross sections and the number of atoms of the ith isotope respectively and n is the number of isotopes i in the element j. The cross section σ_j and molar mass M_j replace that of Equation (5.2) in this case.

The error introduced by using Equation (5.2) at $t > 0$ during the neutron irradiation of the beryllium reflector, is shown in Table 5.2 for dominant elements and isotopes, that is Li, He, ^{6}Li and ^{3}He.

Table 5.2: Error introduced in EBC by expression 5.2 at t>0

Elements		
	Composition after 22 years	**Composition after 43 years**
Definition 5.2	EBC (ppm)	EBC (ppm)
Li	9.64E-01	9.67E-01
He	5.32E-02	1.80E-01
Isotopes		
	Composition after 22 years	**Composition after 43 years**
Definition 5.2, 5.3, 5.5	EBC (ppm)	EBC (ppm)
^{6}Li, ^{7}Li	1.20E+01	1.20E+01
^{3}He, ^{4}He	1.63E+01	1.14E+01

It is clear from Table 5.2 that Equation (5.2) is only valid for the starting materials (i.e. natural element) whereas at t > 0 the changes in material composition with irradiation time become extremely important and have to be accounted for by substituting Equations (5.3) and (5.5) into (5.2). Note that the ^{6}Li concentration does not change much during these periods, since it has already reached equilibrium.

In Tables 5.3 and 5.4 the EBC factor and EBC (in ppm) are reported based on Equation(5.2) for the starting material and at any–time t > 0 (i.e. 22 and 43 years) Equations (5.3) and (5.5) were used.

Note that from this point onward, the word elements will be used with reference to the Equations (5.2), (5.3) and (5.5) unless stated otherwise.

Table 5.3 only considers the transmutation of initial impurities, whereas Table 5.4 summaries the total inventory of the beryllium reflector after 22 and 43 years of reactor operation.

Table 5.3: Evolution of beryllium reflector impurities, prior to irradiation, after 22 years and after 43 years of SAFARI-1 reactor operation

Impurity	**Starting EBC (1965)**		**EBC after 22 years**		**EBC after 43 years**	
	EBC		**EBC**		**EBC**	
Element	**factor**	**ppm**	**factor**	**ppm**	**factor**	**ppm**
Li	1.46E-01	1.46E-01	1.81E+00	1.20E+01	1.81E+00	1.20E+01
B	1.00E+00	1.00E+00	2.06E-04	1.68E-04	1.25E-04	1.03E-04
C	4.15E-06	1.66E-03	4.11E-06	1.65E-03	4.11E-06	1.65E-03
Mg	3.69E-05	3.32E-03	3.69E-05	3.32E-03	3.70E-05	3.33E-03
Al	1.21E-04	4.85E-02	1.21E-04	4.84E-02	1.21E-04	4.81E-02
Si	8.61E-05	3.87E-03	8.41E-05	3.87E-03	8.24E-05	4.00E-03
Mn	3.44E-03	1.72E-01	3.44E-03	1.56E-01	3.44E-03	1.17E-01
Fe	6.52E-04	2.35E-01	6.61E-04	2.44E-01	6.56E-04	2.56E-01
Co	8.98E-03	8.98E-03	1.05E-02	1.15E-02	2.11E-02	3.32E-02
Ni	1.09E-03	1.04E-01	1.13E-03	1.01E-01	1.13E-03	8.84E-02
Cd	3.19E-01	2.23E-01	3.99E-04	2.78E-04	3.15E-04	2.17E-04
Total Beryllium EBC (ppm)		**1.95**		**12.6**		**13.4**

The results of Table 5.3 represent three categories of impurity behaviour (1) the elements that are gradually burnt–out of the reflector but not completely, (2) the ones that are not burnt at all, that is transparent to neutron interactions and lastly (3) those that grow with irradiation time.

Impurities such as B, Mn, Ni and Cd are present at levels lower than that of the starting material, indicating that they are burnt–out of the reflector but not completely. C, Mg, Al, Si, and Fe tend to be transparent to neutrons while Co concentrations seem to grow gradually with time. Table 5.3 suggests that the impurities remain in the beryllium reflector over its service lifetime.

Prior to irradiation, boron is the dominant element and at 22 and 43 years the EBC is completely determined by lithium. Lithium is built–up at first and remains at 12 ppm EBC for the rest of the operational period considered here (i.e. 43 years), suggesting that it has reached equilibrium, this will be quantified in a latter section of this chapter. The behaviour of important isotopes will be quantified by following them over the reactor operational period.

Table 5.4 takes into account the total inventory of the beryllium reflector at 22 and 43 years.

Table 5.4: Total beryllium reflector inventory, prior to irradiation, after 22 years and after 43 years of SAFARI-1 reactor operation

Impurity	Starting EBC (1965) EBC		EBC after 22 years EBC		EBC after 43 years EBC	
Element	**factor**	**ppm**	**factor**	**ppm**	**factor**	**ppm**
H	–	–	2.64E-04	7.31E-03	3.68E-04	4.31E-02
He	–	–	5.75E-02	1.63E+01	1.12E-02	1.14E+01
Li	1.46E-01	1.46E-01	1.81E+00	1.20E+01	1.81E+00	1.20E+01
B	1.00E+00	1.00E+00	2.06E-04	1.68E-04	1.25E-04	1.03E-04
C	4.15E-06	1.66E-03	4.11E-06	1.65E-03	4.11E-06	1.65E-03
N	–	–	1.83E-03	1.84E-10	1.83E-03	8.73E-10
O	–	–	1.73E-07	6.12E-13	1.43E-07	6.29E-12
F	–	–	7.11E-06	6.04E-17	7.11E-06	1.23E-15
Ne	–	–	3.72E-04	2.53E-07	3.68E-04	8.76E-07
Na	–	–	2.68E-04	1.50E-09	2.66E-04	5.40E-09
Mg	3.69E-05	3.32E-03	3.69E-05	3.32E-03	3.70E-05	3.33E-03
Al	1.21E-04	4.85E-02	1.21E-04	4.84E-02	1.21E-04	4.81E-02
Si	8.61E-05	3.87E-03	8.41E-05	3.87E-03	8.24E-05	4.00E-03
P	–	–	7.35E-05	1.67E-07	7.35E-05	5.96E-07
S	–	–	3.27E-06	6.62E-12	3.66E-06	9.39E-11
Cl	–	–	1.63E-04	6.69E-20	7.43E-17	6.60E-29
Ca	–	–	2.56E-04	3.22E-19	2.23E-04	1.95E-17
Sc	–	–	3.80E-03	6.27E-18	3.80E-03	1.11E-16
Ti	–	–	1.16E-03	8.64E-11	8.31E-04	7.31E-10
V	–	–	5.97E-08	2.08E-12	1.37E-03	1.54E-07
Cr	–	–	2.32E-04	1.97E-04	2.68E-04	9.74E-04
Mn	3.44E-03	1.72E-01	3.44E-03	1.56E-01	3.44E-03	1.17E-01
Fe	6.52E-04	2.35E-01	6.61E-04	2.44E-01	6.56E-04	2.56E-01
Co	8.98E-03	8.98E-03	1.05E-02	1.15E-02	2.11E-02	3.32E-02
Ni	1.09E-03	1.04E-01	1.13E-03	1.01E-01	1.13E-03	8.84E-02
Cu	–	–	8.43E-04	4.04E-05	8.29E-04	1.48E-04
Zn	–	–	1.99E-04	6.24E-08	2.03E-04	1.32E-06
Ga	–	–	3.43E-04	8.92E-15	3.47E-04	5.01E-12
Ge	–	–	5.87E-04	6.50E-17	6.10E-04	1.33E-13
Ru	–	–	8.20E-05	3.32E-15	7.89E-05	1.67E-14
Rh	–	–	1.52E-03	9.98E-12	1.52E-03	1.10E-11
Pd	–	–	2.80E-05	3.05E-11	2.36E-05	1.81E-10
Ag	–	–	2.66E-04	4.92E-08	1.90E-04	6.13E-08
Cd	3.19E-01	2.23E-01	3.99E-04	2.78E-04	3.15E-04	2.17E-04
In	–	–	1.09E-02	9.32E-06	1.09E-02	1.00E-05
Sn	–	–	1.81E-04	4.91E-07	1.07E-04	1.29E-06
Te	–	–	–	–	4.16E-04	1.85E-16
Total Beryllium EBC (ppm)	**1.95**		**28.6**		**24.8**	

It is clear from Table 5.4 that the total EBC in the beryllium reflector is largely determined by Li and He; the rest of the elements contribute insignificantly to this value. According to the *"ASTM Standards C 1233 Standard Practice for Determining Equivalent Boron Content of Nuclear Materials"*, the elements with an EBC factor ≤ 0.0001 contribute insignificantly to the total absorption or poison effect on the thermal neutron, therefore they need not be included in the EBC calculations – this is also evident from the results summarized in Tables 5.3 and 5.4. By applying this limit to Table 5.4, it can be seen that the important elements are He, Li, B, N, Sc, Ti, V, Mn, Co, Ni, Rh, Cd and In. Some of these elements are present at very low levels, thus their contribution to absorption is negligible. The rest of the elements have an EBC factor ≤ 0.0001 and therefore can be neglected when calculating the EBC.

When lithium EBC reaches a value of 12 ppm, an increase in the total EBC is primarily determined by helium. Variations in the helium concentration with reactor shut–down and operation periods, lead to oscillations in the total EBC above 12 ppm, the lithium saturation value (see Figure 5.7 on page 67). For example, an increase in EBC observed at 22 years is attributed to an increase in the helium concentration due to a reduction in power from 16 to 5 MW during this period, while a reduction at 43 years corresponds to an increase in power to 20 MW during this period.

The results of Tables 5.3 and 5.4 also point out that the reflector becomes less effective over prolonged neutron–irradiation periods. This is mainly due to the build–up of Li and He in the reflector, the rest of the elements remain at negligible levels over this period. The absorption by these elements (i.e. Li and He) is primarily due to the large absorption cross section for the thermal neutrons of ^{3}He and ^{6}Li isotopes – hence they are known as neutron poisons. The poisoning of the reflector by these isotopes forms an integral part of this study and will be discussed further in Section 5.3.

Important conclusions from the above results are that (1) the impurities and their transmutation products do not completely burn–out of the reflector; they remain in the reflector during its service lifetime, (2) the beryllium reflector becomes less effective with irradiation time due to build–up of Li and He (i.e. ^{6}Li and ^{3}He), the rest of the inventory contributes insignificantly to the total thermal neutron absorption, compared to this elements (or rather isotopes).

The above results do not account for variation of the impurities and transmutation products at any given time over the 43 year period considered here as a result, the detailed variations of the important elements, for example He, Li, Cd, B, Co, etc. are not well represented and accounted for in earlier discussions. Detailed analyses of the behaviour of these elements (isotopes), as a function of time, will be quantified in subsequent sections of this chapter. It is also imperative to quantify the variations in the He concentration with reactor shut–down and operation periods as well as the saturation value of Li, as reported in Tables 5.3 and 5.4. Other elements are also considered in this analysis for better understanding of their behaviour during irradiation.

In addressing the above cases, the elements were treated and followed explicitly, i.e. individually,

as a function of the reactor operational history, by considering their individual isotopic content as well as the way they evolve over a period of 43 years. It is also necessary to refer to the SAFARI–1 reactor power history, discussed in Chapter 2, at this point; this will enable better understanding of the isotopic behaviour in the beryllium reflector element with the reactor operational history. In this way, the build–up, burn–up as well as the constant behaviour of the isotopes and hence the elements, will be understood and will be well accounted for in this study. The SAFARI–1 reactor power history is presented in Figure 5.1.

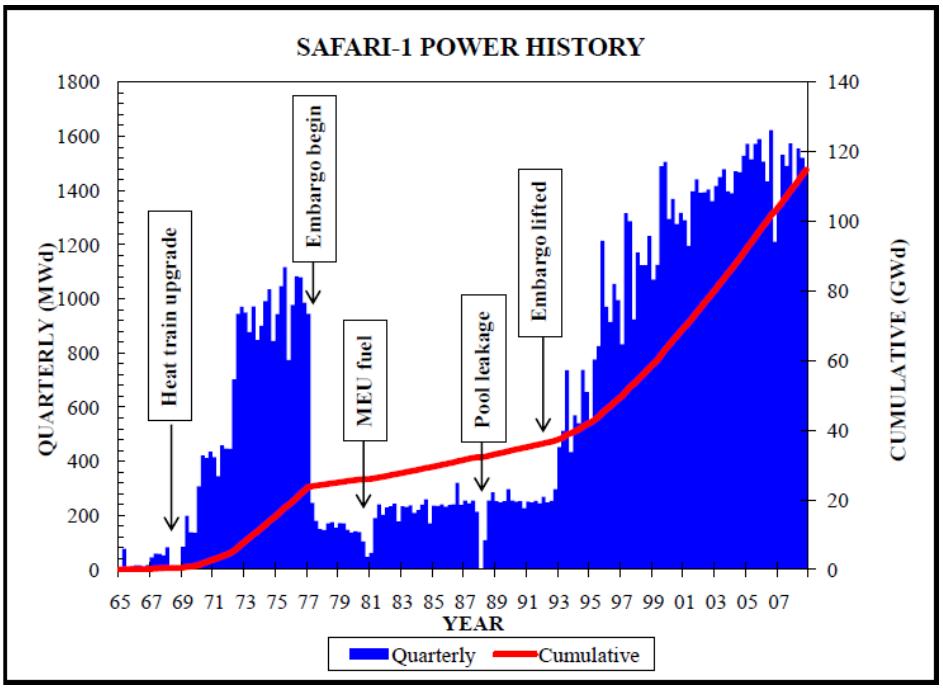

Figure 5.1: The SAFARI-1 reactor power history

The following discussion is focused on the isotopes that are important with regard to thermal neutron absorption or poisoning in the beryllium reflector. The transmutations of the initial impurities and some important product isotopes are shown in Figures 5.2 to 5.6. The variation of isotopic content in the beryllium reflector is reported as a weight content in ppm (w_i). Note that the elements or isotopes discussed here are selected from Tables 5.3 and 5.4, based on their importance, that is those that are present in large amounts and at the same time have an EBC factor >0.0001, i.e. those that contribute significantly to the total absorption in the beryllium reflector. The elements that satisfy this EBC criterion, but are present in the lowest levels in the reflector, are not covered here, for example Sc has an EBC of 3.8×10^{-3}, but is present in very low levels, that is in the order of 10^{-15} ppm.

The contributions of ^{3}H and ^{4}He are considered despite their essentially zero absorption cross sections, because they induce swelling and embrittlement of the reflector, thus playing a vital role in determining when the reflector is to be replaced.

The ^{6}Li, ^{3}He, ^{4}He and ^{3}H isotopes are treated separately, since they form an integral part of this study. Furthermore, these isotopes build–up in large amounts with neutron–irradiation as compared to most of the isotopes present in the reflector.

Figure 5.2 accounts for impurities, i.e. isotopes and thus elements that are transparent to neutron interactions; the rest of the important impurities is accounted for in subsequent paragraphs.

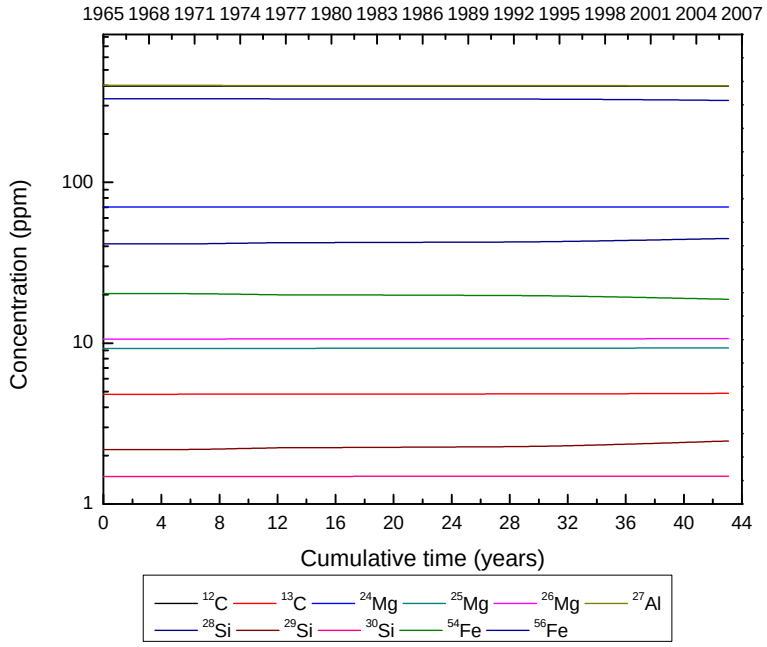

Figure 5.2: Transparent isotopes in the beryllium reflector as a function of reactor power history

Figure 5.2 further confirms the results of Tables 5.3 and 5.4, that the impurities remain in the reflector during its lifetime.

Except for Li, B, Mn, Co, Ni and Cd, all the impurity elements in Table 2.2 are transparent to neutron interactions in the beryllium reflector. The transparent nature of elements such as C, Mg, Al, Si and Fe as observed in Tables 5.3 and 5.4, is explained by the isotopic behavior shown in Figure 5.2. The isotopes are burnt extremely slowly or are not burnt at all; they remain below 400 ppm over a period of 43 years. The transmutations of these impurities proceed in a more or less linear fashion and do not lead to any rapid increase or decrease in concentrations. Most importantly, the isotopes (Figure 5.2) or elements (Tables 5.3 and 5.4) contribute insignificantly to the total poison effect (i.e. EBC factor ≤ 0.0001) in the reflector, thus are not require to be included in the EBC calculation. The transmutations of the ^{6}Li and ^{7}Li isotopes are shown in Figure 5.3 and a discussion follow below.

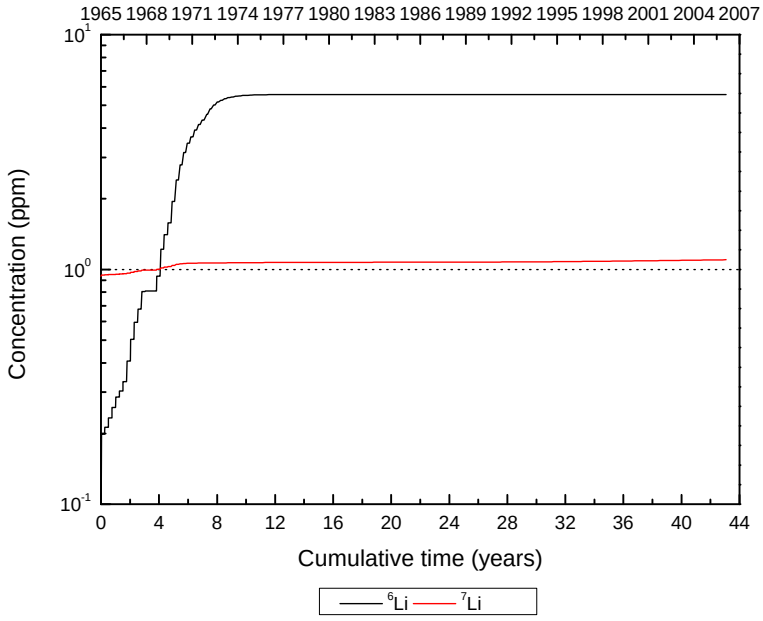

Figure 5.3: Transmutation of the ^{6}Li and ^{7}Li isotopes in the beryllium reflector

Beryllium–9 is transmuted into ^{6}Li by the ^{9}Be(n,α)^{6}Li reaction (see reaction of Equation (2.1) in Chapter 2) and reaches the asymptotic value of 6 ppm in about $t = 12$ years according to Equation (2.11) (i.e. spectrum assumed constant), while ^{7}Li saturates at about 1 ppm as seen in Figure 5.3. The formation of ^{6}Li via β^{-} decay of ^{6}He, is balanced out by its burn–up via the (n,α) reaction forming ^{3}H. Lithium–7, produced via an (n,α) reaction of ^{10}B and an (n,γ) reaction of ^{6}Li, is increased slightly within the first 5 years and thereafter saturates below the ^{6}Li curve.

Lithium–6 contributes by a large amount towards the EBC due to its large absorption cross section as seen in Tables 5.3 and 5.4, thus its behaviour in the beryllium reflector during the reactor operational history is crucial and will be revisited in Section 5.3.

The build–up of ^{3}H via the ^{6}Li(n,α)^{3}H reaction, burn–up of ^{3}He via the ^{3}He(n,p)^{3}H reaction, as well as the formation of ^{4}He from all the beryllium nuclear reaction chains (see Figure 2.7) is shown in Figure 5.4.

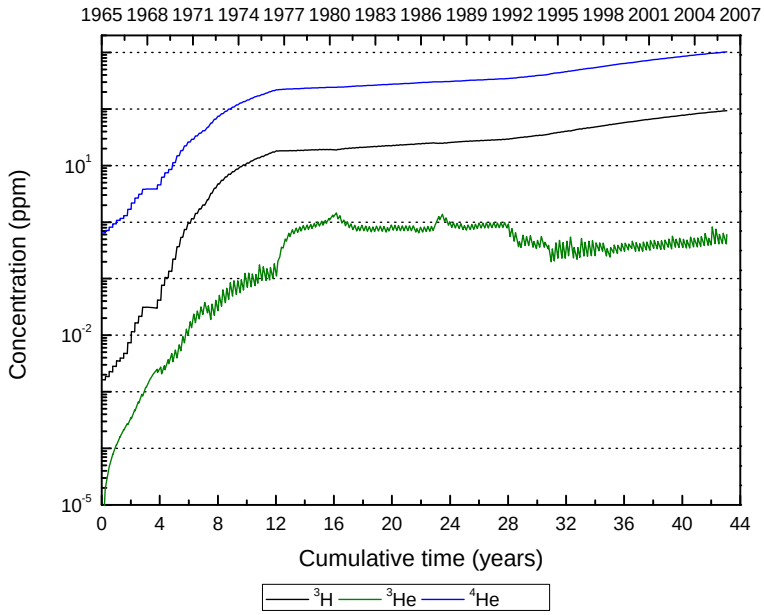

Figure 5.4: Transmutation of ^{3}H, ^{3}He and ^{4}He in the beryllium reflector

There is a steeper growth in the isotopic build–up in the first few years, as depicted in Figure 5.4; thereafter the isotopes tend to grow steadily with ^{4}He been the dominant isotope. This steady build–up behaviour is attributed to ^{6}Li saturation, influencing mainly both ^{3}H and ^{4}He. ^{3}He build–up and burn–up is primarily a function of operation and shut–down periods – it follows the reactor operational schedule as explained before. The two peaks observed in the ^{3}He curve are attributed to a reduction in power of 1976 and a 6 months shut–down in 1988. Its concentration tends to grow steadily from 1996, when the reactor started operating more frequently at 20 MW with a 4 to 5 days shut–down.

It is clear that ^{6}Li, ^{3}He, ^{3}H and ^{4}He are present at high levels in the beryllium reflectors of the SAFARI–1 reactor and that their saturation, except for ^{6}Li, is not achieved in the 43 years of reactor operation. Furthermore, most of the impurities are transparent to neutrons and most importantly, they do not influence the thermal neutron absorption of the reflector.

Further analysis of the poisoning and swelling phenomena will be discussed in Sections 5.3 and 5.5 respectively.

It is necessary to understand why the isotopes of elements such as B, Co and Cd are not burnt–out completely from the reflector, even after a long time of reactor operation (i.e. 43 years), see Tables 5.3 and 5.4. This behaviour was accounted for by evaluating the variation in concentration of isotopes such as ^{10}B, ^{11}B, ^{58}Co, ^{59}Co, ^{60}Co and ^{113}Cd with irradiation time. The results are discussed and presented in Figure 5.5.

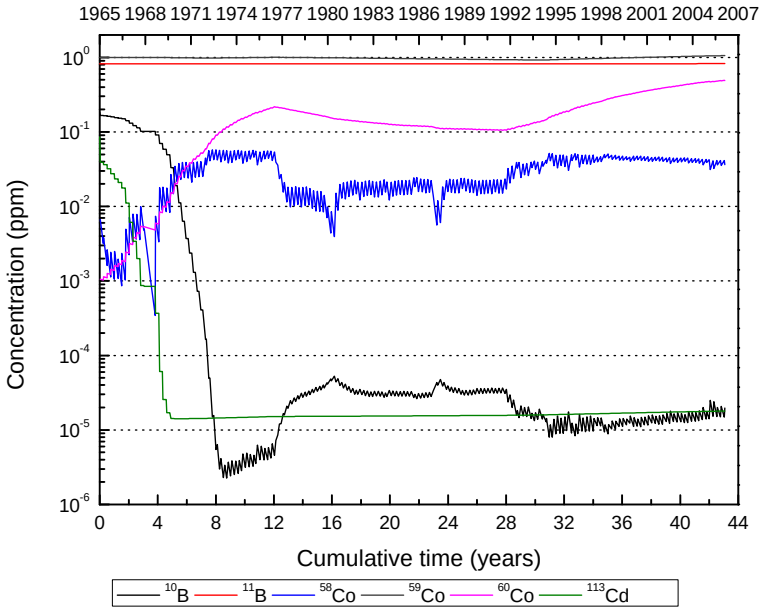

Figure 5.5: Transmutations of other dominant thermal neutron absorbers in the beryllium reflector

^{11}B and ^{59}Co, present at about 1 ppm in the beryllium reflector, burn–up in equilibrium with production. ^{58}Co and ^{10}B isotopes are very sensitive to the reactor power history while ^{60}Co is less sensitive. ^{113}Cd is burnt to below 10^{-4} ppm and thereafter tends to saturate at a value of 2×10^{-5} ppm.

^{60}Co, an isotope of concern in radioprotection, is mainly produced via the ^{59}Co(n,γ)^{60}Co reaction. The ^{60}Co content follows the reactor operational history, in that it is gradually increased and decreased following an increase and decrease in the reactor power. ^{58}Co, produced via the ^{58}Ni(n,p)^{58}Co reaction, is more sensitive to the operational schedule than ^{60}Co, mainly because of its short half–life of 71 days. This is clearly seen during shut–down periods, that is, the 9 and 6 months shut–down periods of 1968 and 1988 respectively, and when the power is reduced, that is the reduction in power in 1976 – see Figure 5.1. Its concentration increases with an increase in power.

Initially, the ^{113}Cd and ^{10}B isotopes were gradually burnt during the first few years (i.e. 2 years for ^{113}Cd and 4 years for ^{10}B) of operation, corresponding to the low reactor power levels during that period, their burn–up rate rapidly increased when the reactor power was increased around 1969.

^{113}Cd is burnt much faster than ^{10}B, before saturation at 2×10^{-5} ppm after 5 years. At this point equilibrium was reached between its burn–up, its formation by an (n,γ) reaction with ^{112}Cd and β^- decay of ^{113}Ag with a half–life of 5.37 hours. As a result the isotope is not completely burn–out of the reflector.

^{10}B is burnt–out to about 3×10^{-6} ppm after about 8 years of operation and thereafter its content is markedly increased with a significant jump at about 12 years (1977) after the reduction of the reactor power to 5 MW. The peak in 1981 (i.e. 16 years) corresponds to the reduction in power and the one in 1988 (i.e. 23 years) is a consequence of a 6 month reactor shut–down period. This interesting behaviour from about 8 years onwards is a result of the β^- decay of ^{10}Be to ^{10}B; see beryllium reaction chains in Figure 2.7. However, the amounts of ^{10}B formed are small due to the low thermal (n,γ) cross section of ^{9}Be and the long half–life of ^{10}Be (i.e. 1.6×10^6 years). As a result, its contribution to the thermal neutron absorption in beryllium is negligible.

At low power and during shut–down the burn–up of ^{10}B is dominated by its production via the β^- decay of ^{10}Be. From 1993 when the power was increased, ^{10}B is burned–up at a rate higher than its production by ^{10}Be decay. Therefore, the burn–up and production rate of ^{10}B after a few years of reactor operation, is predominately determined by the reactor power level and the β^- decay of ^{10}Be.

Some of the major contributors to the EBC are isotopes of Ni and Mn (mainly ^{55}Mn). The behaviour of these isotopes is shown in Figure 5.6.

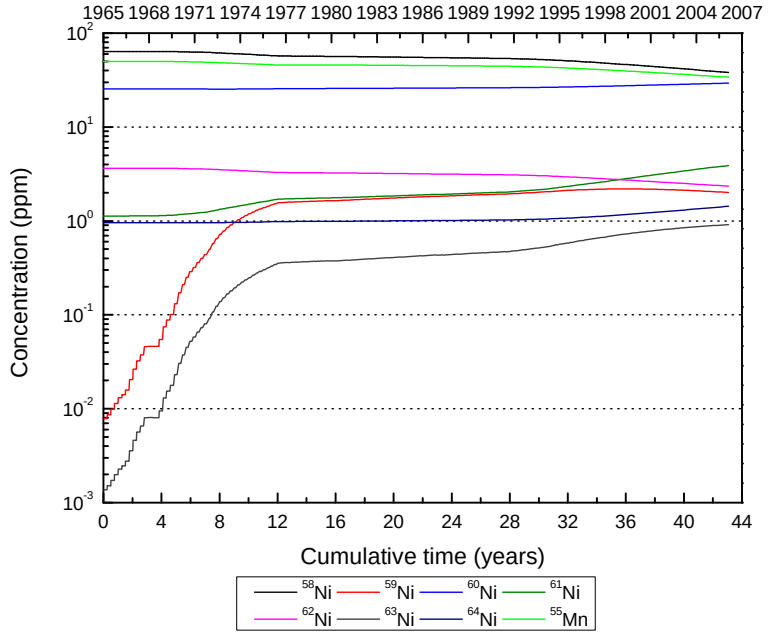

Figure 5.6: Transmutations of other important neutron absorbers in the beryllium reflector

In Figure 5.6 ^{59}Ni, ^{60}Ni, ^{61}Ni, ^{63}Ni and ^{64}Ni grow with time while ^{58}Ni and ^{62}Ni as well as ^{55}Mn are burnt. These isotopes contribute significantly to the total EBC factor of both the Ni and Mn elements of Tables 5.3 and 5.4, with ^{58}Ni and ^{55}Mn having concentrations bigger than 50 ppm each. The isotopes are present in amounts larger than that of ^{3}He and ^{6}Li; however, their absorption cross sections are small compared to those of ^{3}He and ^{6}Li, as a result their EBC factor is small

and thus contribute less to the total absorption in the reflector. Notwithstanding, it is important to consider them, when calculating the total EBC of the beryllium reflector.

The total EBC in the beryllium reflector as a function of time is shown in Figure 5.7 and the percentage contribution of the dominant isotopes is shown in Figure 5.8. 67

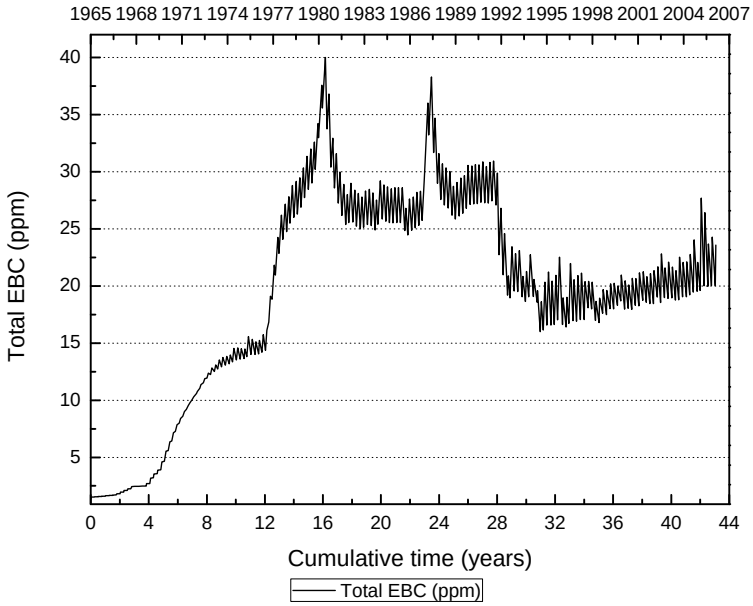

Figure 5.7: Total EBC in the beryllium reflector as a function of time

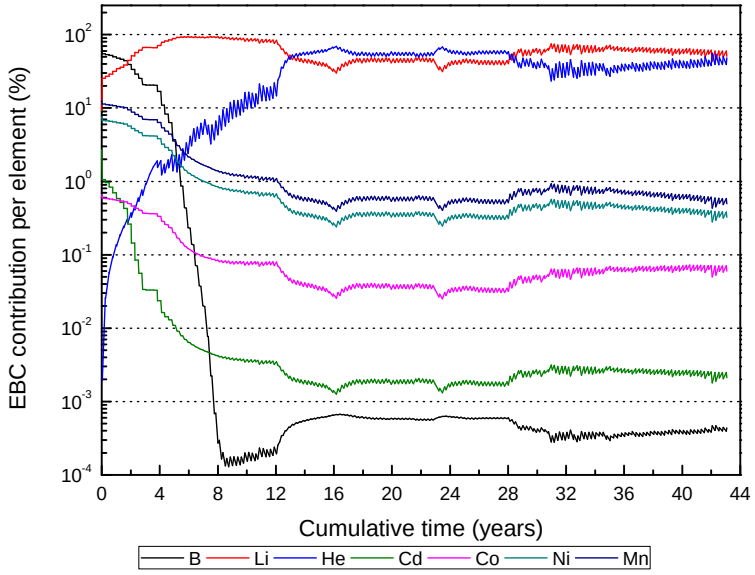

Figure 5.8: Percentage EBC contributions of important elements in the beryllium reflector

The total EBC curve (i.e. Figure 5.7) follows the behaviour of ^{6}Li and ^{3}He (Figures 5.3 and 5.4), signifying their major contribution towards the total EBC during the reflector's lifetime. Figure 5.8 shows the contribution of individual elements to the total EBC. Elemental contributions towards the total EBC shows that He and Li elements are the main contributors. Note that Equations (5.2) to (5.5) are used in this case to account for the total contribution of elements at $t > 0$.

In Figure 5.8 it can be seen that within the first 2 years, the total EBC is mainly determined by Boron (^{10}B), followed by Lithium (^{6}Li) from 2 years up to about 12 years where helium (^{3}He) starts to compete with Lithium (^{6}Li). This confirms the observation made before, that the total EBC in the beryllium reflector over a long period of reactor operation, is largely determined by lithium and helium, that is ^{3}He and ^{6}Li isotopes, each contributing up to about 50% of the total EBC.

It is therefore concluded that the impurities, except for ^{6}Li do not influence the effectiveness of the beryllium reflector and that they are not burnt–out of the reflector. Moreover, the reflector becomes ineffective (i.e. becomes an absorber) with irradiation time due to the build–up of ^{3}He and ^{6}Li isotopes and might swell due to the accumulation of ^{4}He and ^{3}H.

The impact of these isotopes on the SAFARI–1 reactor core parameters is analysed in Section 5.3. Additional analyses are conducted to predict swelling of the reflector – thus providing an indication if the reflectors should be replaced.

5.3 Poisoning of the SAFARI–1 beryllium reflector by ^{6}Li and ^{3}He

It is important to note that the reactor power and spectrum in any core arrangement, are irregular and might result in a large non–uniformity of the neutron spectrum for any core. Therefore, the accumulation rate of ^{3}He and ^{6}Li, in an individual beryllium reflector, placed in different positions in the core, may vary significantly in time. It is therefore important to understand the magnitude of the variations in spectrum from cycle–to–cycle, since the spectrum has a direct influence on the build–up of ^{3}He and ^{6}Li isotopes. The spectrum and hence the accumulation of these isotopes is evaluated by adopting two approaches:

(a) Assuming an averaged spectrum over all the beryllium reflector elements; and

(b) A detailed neutron spectrum in the individual beryllium reflector elements.

Note that the spectrum in (a) and (b) is assumed constant over the period considered here. The effect of updating the spectrum is investigated at a later stage.

In Subsection 5.3.1 comparisons are drawn between the spectra of cycles *C0313-1*, *C0508-1*, *C0706-1* (all HEU cores) and *C01101-1* (a fully LEU core) based on (a) above. The detailed element spectrum, that is (b) is also compared to that of (a) for selected elements. The difference in the core configurations of the above–mentioned cores are shown and briefly explained in Appendix C.

These cycles were chosen such that all the worst possible spectrum changes that could occur in any SAFARI–1 reactor core during its operational history are considered.

The influence of the spectrum on poison accumulations, that is ^{3}He and ^{6}Li, follows in Subsections 5.3.2 to 5.3.4.

5.3.1 Comparisons of spectrum averaged over all the beryllium reflectors

Variations in the beryllium reflector spectra based on the SAFARI–1 reactor cores of Section 5.3 and Appendix C are shown in Figure 5.9 for (a) in Section 5.3. In point (b) the detailed spectrum of the beryllium reflector elements, that is A2 and H8 for cycles *C0313-1*, *C0508-1* and *C01101-1*, were considered and plotted in Figure 5.10. The difference between (a) and (b) is emphasised by plotting the detailed and averaged spectra of cycle *C01101-1* on the same curve. The results are shown in Figure 5.11.

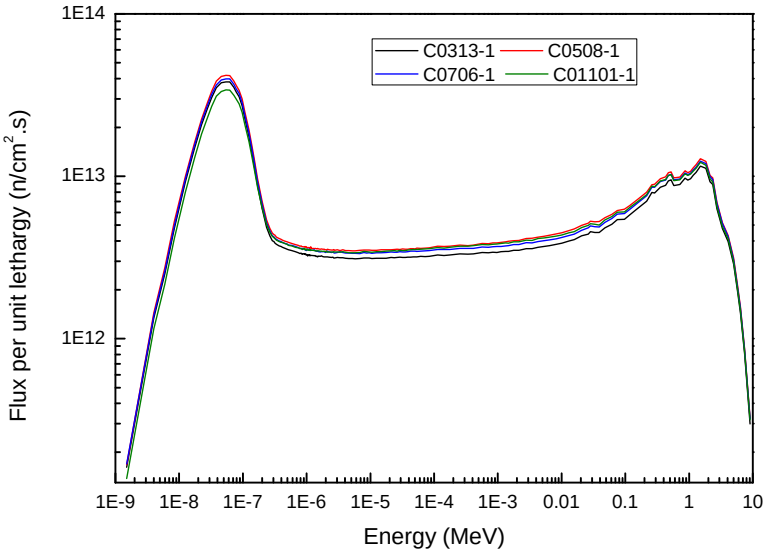

Figure 5.9: Spectrum averaged over all the beryllium reflectors for different cores

The averaged spectrum from cycle–to–cycle or core–to–core varies within a band of 15% in the whole energy range for cycles *C0313-1*, *C0508-1* and *C0706-1*. The spectrum of cycle *C01101-1* only differs in the thermal energy range by up to about 27% (i.e. at about 0.01 eV). This is attributed to the LEU spectrum which is less thermalised than the HEU spectrum. The difference between the HEU and LEU spectra is not clear in this case, since the average values were used.

The presence of a fuel element in position B6 (see Figure 1.1) for the HEU cycle *C0313-1* contributes to a difference of within 10% observed in the epithermal to fast energy range (i.e. < 10 MeV).

In general, the spectra averaged over all the beryllium reflectors in the core do not differ much, as seen in Figure 5.9, thus any of the averaged spectra can be used in computing poison number density by virtue of the small error introduced.

The spectrum in individual beryllium reflector elements, calculated for different cores, is shown in Figure 5.10.

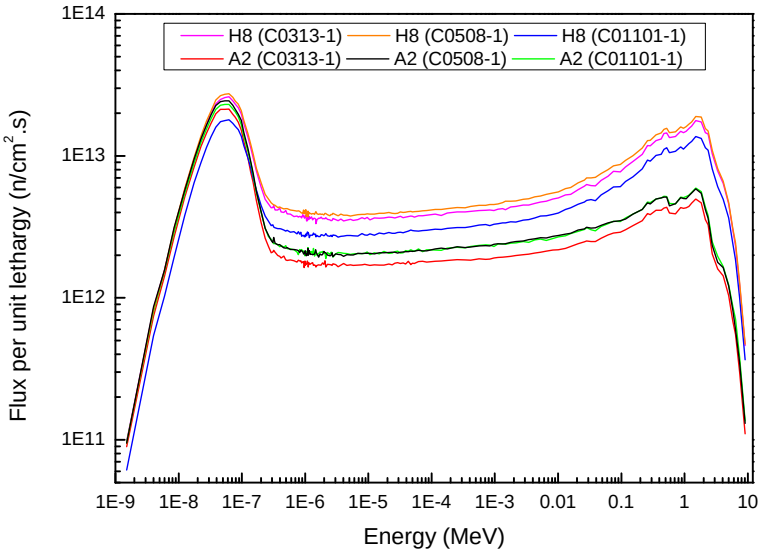

Figure 5.10: Variations of the beryllium reflector element spectra for different cores

The spectrum in individual beryllium reflector elements changes considerably from core–to–core regardless of the core configuration, as seen in Figure 5.10; however, the differences in spectra tends to vary within -40% to +40% for all the reflectors.

To establish how the averaged spectrum represents an individual reflector element in the core, the spectra of elements A2 and H8 (i.e. cycle *C01101-1*) were compared to the averaged spectrum of cycle *C01101-1* and the results are shown in Figure 5.11.

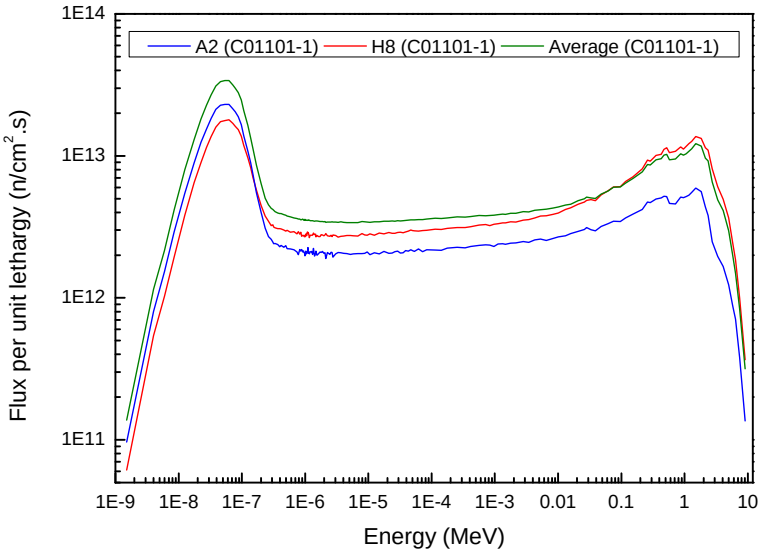

Figure 5.11: Comparison of the averaged and the element specific spectra for core *C01101-1*

It is clear from Figure 5.11 that the averaged spectrum representation underestimates, as well as overestimates, the spectrum in these elements. In this case, H8 is underestimated in the fast energy range (i.e. from about 0.1 MeV – 10 MeV) by up to 24% and overestimated by up to about 55% in the thermal energy range. A2 is consistently overestimated over the entire energy range by up to 30% and 60% in the thermal and fast regions respectively.

Similar observations were made for other reflector elements not shown here. They are either overestimated or underestimated by the average spectrum representation. The variation is within a band of -60% and +60% when individual element spectra is compared to the averaged spectrum in all the cycles considered.

The results above confirm that the spectrum in the beryllium reflector element of the SAFARI–1 reactor, strongly dependent on the reflector's position in the core, as well as its surrounding environment and that it varies strongly from core–to–core regardless of the core configuration.

Therefore, if the poison accumulation in the beryllium reflector is to be accounted for accurately, each element has to be treated separately and its irradiation history should be followed from cycle–to–cycle. However, this approach proves to be impractical, for reasons provided in Section 4.4 of Chapter 4. The specific reflector element spectrum and poison accumulation will be applied only when deemed necessary, for example in single cycle calculations or when only a few cycles are considered. One solution to overcome the problem of updating the spectrum from cycle–to–cycle, will be to determine the intervals as to when spectrum should be updated. This option will be

explored at a later stage in this study.

In the following section, the impact of spectrum variations on poison accumulation, based on the averaged as well as the reflector element specific spectrum as discussed above, is evaluated.

5.3.2 Dependence of the ^{6}Li and ^{3}He build–up on the average neutron spectrum

In Subsection 5.3.1 it was seen that variations in the spectrum averaged over all the beryllium reflector elements in different core configuration, are not important except when the fuel composition in the core differs significantly (e.g. LEU and HEU core).

The impact of these core–to–core spectral changes due to different core configurations, on the poison concentration, is quantified by using the BOC spectrum (averaged over all the beryllium reflectors) calculated from the fully HEU cores of cycles *C0313-1, C0508-1* and *C0706-1* and a fully LEU core of cycle *C0906-1*. The calculated spectrum was used to compute the isotopic number densities in the beryllium reflectors.

The calculations are performed by continuously irradiating the beryllium reflector over a period of 43 years (to the end of 2007). Note that the initial spectrum was not updated during this period.

In the FISPACT input, the irradiation time is modelled as given in Appendix A (quarterly operation and shut–down periods) for the first 40 years of irradiation. In order to improve the accuracy in the estimated poison concentrations, the operational schedule for the last two years (2006 to 2007) comprising of 22 cycles is modelled in detail. This entails modelling irradiation times in finer step size of 30 days operation and 5 days shut–down, as well as a two week annual extended shut–down period, this implies modelling of the reactor operation schedule as is. The irradiation intensity used in FISPACT is in accordance with the approximation discussed in Section 4.4, Equation (4.3).

The results are shown in Figures 5.12, 5.13 and 5.14. The time evolution of ^{3}H is shown for better understanding of the behaviour of ^{6}Li and ^{3}He with reference to reactions of Equations (2.1) to (2.5) in Chapter 2.

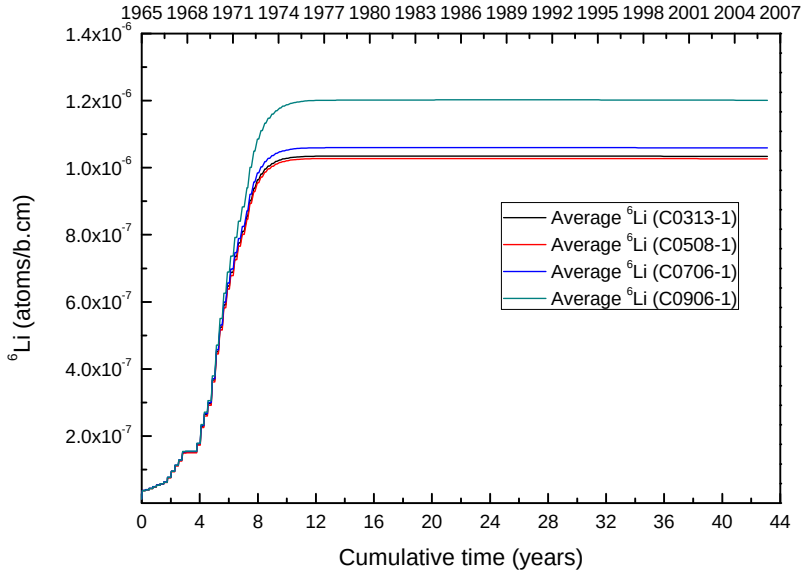

Figure 5.12: Time evolution of the averaged ^{6}Li number density

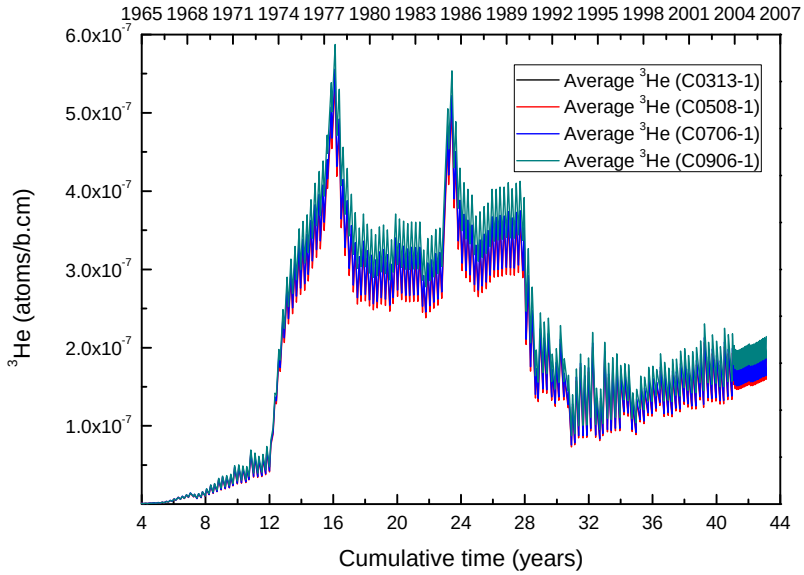

Figure 5.13: Time evolution of the averaged ^{3}He number density

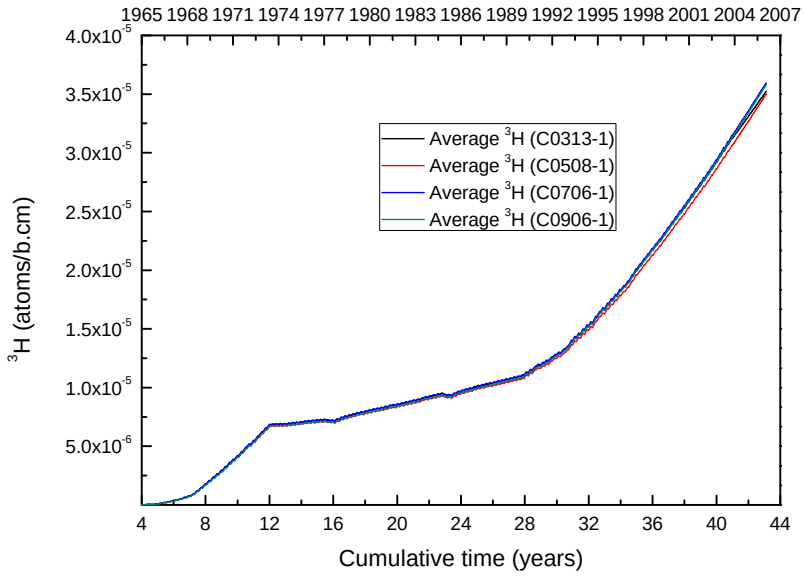

Figure 5.14: Time evolution of the averaged ^{3}H number density

The build–up of ^{6}Li, one of the initial beryllium reflector impurities, starts immediately, while ^{3}He and ^{3}H – initially not present in the reflector, only starts to build–up after 4 years. After about 12 years of operation, all three isotopes change in behaviour. These changes with irradiation are further discussed in subsequent paragraphs.

The isotopic number densities in Figures 5.12, 5.13 and 5.14 differ for all the core configurations and thus for the spectrum considered. The number densities of ^{6}Li, ^{3}He and ^{3}H, computed using the averaged HEU core spectrum, differ to within 3% for cycle–to–cycle comparison. When the number densities computed using the above–mentioned HEU cores, are compared to the number densities computed from the averaged LEU core spectrum, the following differences were observed: 13%, 9% and 3% in number densities of ^{6}Li, ^{3}He and ^{3}H respectively.

Clearly, important changes in isotopic number densities are observed, when the averaged LEU core spectrum is used. The averaged HEU core spectrum for different core configurations, results in negligible changes in number densities for the isotopes of interest. The fully LEU core leads to less thermalised spectra in the core and consequently in the beryllium reflectors, thus resulting in an increased ^{6}Li production from the fast ^{9}Be(n,α)^{6}Li reaction and less burn–up by thermal neutrons in some of the reflector elements via ^{6}Li(n,α)^{3}H reaction (Figure 5.12).

It is important to note that local changes have a negligible effect on the spectrum average over all the beryllium reflector elements, that is the presence of the fuel element in position B6, cycle *C0313-1*, two hydraulic rabbits in cycle *C0508-1* and one in cycle *C0706-1*, compared to the global

changes (i.e. fully LEU core). The presence of the fuel element in B6 and the hydraulic rabbits, only influence the neighbouring reflector elements, for example, B6 influences the spectrum of the reflector elements A6 and A7.

The concentrations of ^{3}He and ^{3}H are least affected by the spectral changes compared to ^{6}Li. The concentration of ^{3}He is mainly sensitive to reactor shut–down periods, as shown in Figure 5.13.

It can be concluded that the local changes in core configurations have a negligible effect on the spectrum averaged over all the beryllium reflectors and thus the isotopic number density in the beryllium reflector; on the other hand, global changes result in an important effect and should be treated explicitly, if accuracy in an isotopic concentration is desired. The behaviour of ^{6}Li, ^{3}He and ^{3}H with an irradiation history as depicted in Figures 5.12, 5.13 and 5.14, is further discussed in subsequent paragraphs.

In Figure 5.12, it can be seen that the rate of ^{6}Li build–up increases with a steeper gradient from 4 years due to its accelerated production from the ^{9}Be(n,α)^{6}Li reaction. During this period, the formation of ^{6}Li is dominant over its burn–up, by thermal neutrons via the ^{6}Li(n,α)^{3}H reaction. The 100% equilibrium level between these two reactions is reached after about 12 years of reactor operation in almost all of the ^{6}Li curves. These equilibrium values are determined by formation and burn–up, as indicated above, or simply by the fast–to–thermal flux ratio in accordance with Equation (3.3) of Subsection 3.4.1 in Chapter 3. The ^{6}Li saturation value is given by the constant below:

$$N_{^{6}\mathrm{Li}}^{equil} = N_{Be} \cdot \frac{\phi_f \, \sigma_{(n,\alpha)}^{^{9}Be}}{\phi_{th} \, \sigma_{(n,\alpha)}^{^{6}Li}} \tag{5.6}$$

In this case, the saturation values determined from the averaged spectrum of cycles *C0313-1, C0508-1, C0706-1* and *C0906-1* were determined to be 10.35×10^{-7} $\left[\frac{\text{atoms}}{\text{b}-\text{cm}}\right]$, 10.27×10^{-7} $\left[\frac{\text{atoms}}{\text{b}-\text{cm}}\right]$, 10.59×10^{-7} $\left[\frac{\text{atoms}}{\text{b}-\text{cm}}\right]$ and 12.76×10^{-7} $\left[\frac{\text{atoms}}{\text{b}-\text{cm}}\right]$ respectively. It can be seen that with an assumption of a constant averaged spectrum over all the reflector elements, the asymptotic value of ^{6}Li number densities is reached after about 12 years. These values can therefore be used to represent the ^{6}Li number density at any given time after 12 years of operation.

During the reactor operation, ^{3}He is burned according to reaction of Equation (2.5) and after shut–down the concentration increases due to the decay of ^{3}H, refer to reaction of Equation (2.4). It is clear from Figure 5.13 that the ^{3}He build–up and burn–up are much more sensitive to reactor operating conditions (i.e. operation and shut–down periods) than ^{3}H and ^{6}Li. The small peaks in the ^{3}He curve depict short shut–down periods or a small reduction in power, while the large ones indicate long shut–down periods or a significant reduction in reactor power.

The time evolution of ^{3}He, depicted above is further elaborated on with reference to Figure 5.1,

that is the reactor power history, in subsequent paragraphs.

Within the first 4 years (i.e. 1965 to 1969) when the reactor was operated at low power, the concentrations of ^{3}H and ^{3}He were present at relatively lower levels in the reflector, as a result the 9 months shut–down in 1968, had no significant influence on the build–up of these isotopes. The concentration started increasing linearly in time, from 1969 when the power was increased to between 5–10 MW. The reduction of power in 1977 (i.e. at 12 years) resulted in a rapid increase in the ^{3}He concentration between 12 and 13 years due to ^{3}H decay (see Figure 5.13). The first peak observed in this graph corresponds to a further reduction in power in 1981 and the second peak is due to the a 6 months shut–down in 1988. The concentration of ^{3}H is reduced by exactly the same amount, for every increase in the ^{3}He concentration, that is the two ^{3}He peaks correspond to the two small dips in Figure 5.14 at 16 (1981) and 23 years (1988).

In 1993 (at about 28 years) when the power was increased to 10 MW, the ^{3}He concentration decreased, due to its burn–up via the ^{3}He(n,p)^{3}H reaction. The decrease in ^{3}He concentration lasted up until about 1997 when the stable reactor operation started, that is operated for about 30 days, interrupted by 4–5 days shut–down, at an average power of 20 MW for 305 days per year. During this period, the ^{3}He concentration increased gradually due to a continuous supply from ^{3}H.

The behaviour of ^{3}H and ^{3}He is related to the general solutions discussed in Chapter 2. At $t \gg 0$, the exponential terms of the general solutions of Equations (2.12) and (2.13) vanishes and the concentrations of ^{3}H and ^{3}He can thus be approximated by the following equations deduced from the general solutions:

$$N_{^{3}\mathrm{H}}(t) = a_1 + \frac{AC}{\lambda_{^{3}H} + C} \cdot t \tag{5.7}$$

$$N_{^{3}\mathrm{He}}(t) = \frac{\lambda_{^{3}H}}{C} \cdot a_1 + \frac{\lambda_{^{3}H} A}{\lambda_{^{3}H} + C} \cdot (t - \frac{1}{C}) \tag{5.8}$$

Note that these equations are only valid for continuous operation. However, Equation 5.7 can be used to approximate ^{3}H concentrations for the SAFARI–1 reactor, since the shut–down periods are very short and have negligible effects on the ^{3}H concentration (see Figure 5.14), that is 4–5 days plus a further annual 12 days extended refuelling and maintenance shut–down periods. The solution for ^{3}He (Equation (5.8)) is strictly valid for continuous operations since ^{3}He behaviour is very sensitive to shut–down periods.

The concentrations of ^{3}H and ^{3}He increase linearly in time with slopes $\frac{AC}{\lambda_{^{3}H}+C}$ and $\frac{\lambda_{^{3}H} A}{\lambda_{^{3}H}+C}$ respectively. This behaviour is clearly illustrated by the ^{3}H curve (Figure 5.14) from about 32 years (i.e. 1997) onwards. During this period, the rate of ^{3}H build–up increased linearly with slopes of 1.889×10^{-6} $\left[\frac{\text{atoms}}{\text{b}-\text{cm}\cdot\ \text{year}}\right]$ and thus its number density at any given time $t \geq 32$ years (Equation 5.7) can be predicted by using the following equation:

$$N_{^3\mathrm{H}}(t) = 1.889 \times 10^{-6} \cdot t - 4.589 \times 10^{-5} \left[\frac{\text{atoms}}{\text{b} - \text{cm}}\right] \tag{5.9}$$

From the discussion above, based on the constant average spectrum applied over 43 years, it can be concluded that the ^{6}Li concentration reaches equilibrium at time $t \approx$12 years and the concentration of ^{3}H can be approximated by Equation 5.9 at time $t \geq$32 years.

The results show that the ^{3}He behaviour is very sensitive to the reactor operation schedule and that it should be treated explicitly, if its behaviour is to be accounted for accurately, in reactor fuel management calculations.

The global change, in a spectrum average over all the reflector elements, have dominant effects on the build–up of poison isotopes, especially ^{6}Li. Local changes are not important when the averaged spectrum is considered, thus any core can be used when calculating the poisons number density (i.e. only for local changes).

The approach based on the averaged spectrum, will be applied when the accuracy in the above–mentioned isotope concentration, is not important. The importance of applying a detailed spectrum or an element specific spectrum is discussed in Subsection 5.3.3.

5.3.3 Dependence of ^{6}Li and ^{3}He build–up on the specific beryllium reflector elements neutron spectrum

In the previous section the accumulation of poisons in beryllium was based on the spectrum averaged over all the reflector elements. In this section, the neutron spectrum in each beryllium reflector element is accounted for and used when calculating the isotopic number densities in each reflector element. Note that over the last 2 years, the spectrum was updated and the reactor operational history modelled in detail.

The importance of updating the spectrum, will be investigated at a later stage in this study.

The calculations are performed, based on the spectrum averaged over each beryllium reflector element (i.e. a total of 19 elements), calculated from the core of cycle *C0508-1*. Note that any cycle could have been chosen for this analysis.

A comparison is drawn between the number densities calculated in the previous section (i.e. spectrum averaged over all the beryllium reflector) and the specific reflector element spectrum, evaluated in this section. The results are summarised in Figures 5.15 and 5.16 for selected reflector elements. This was necessary, due to the large amount of data generated, which could not be presented all at once.

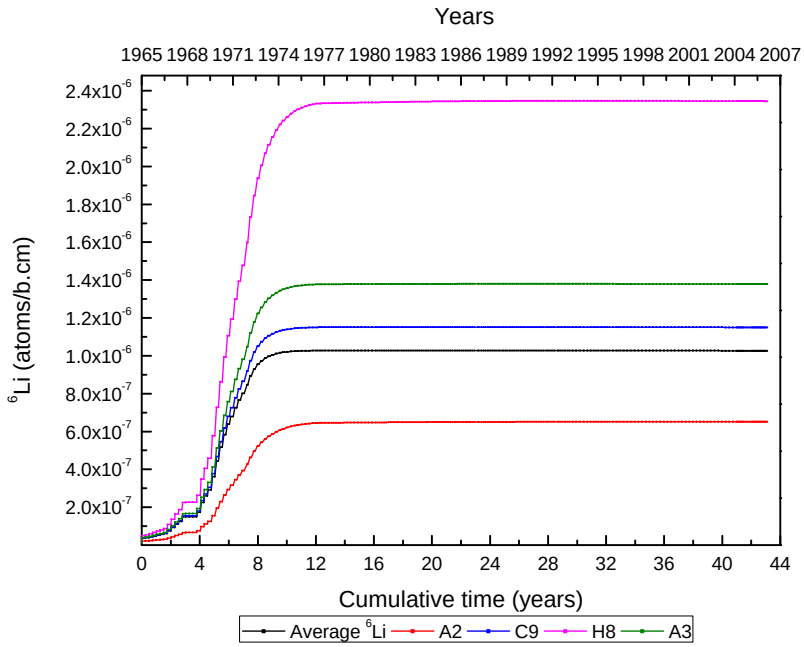

Figure 5.15: Time evolution of ^{6}Li in selected beryllium reflector elements

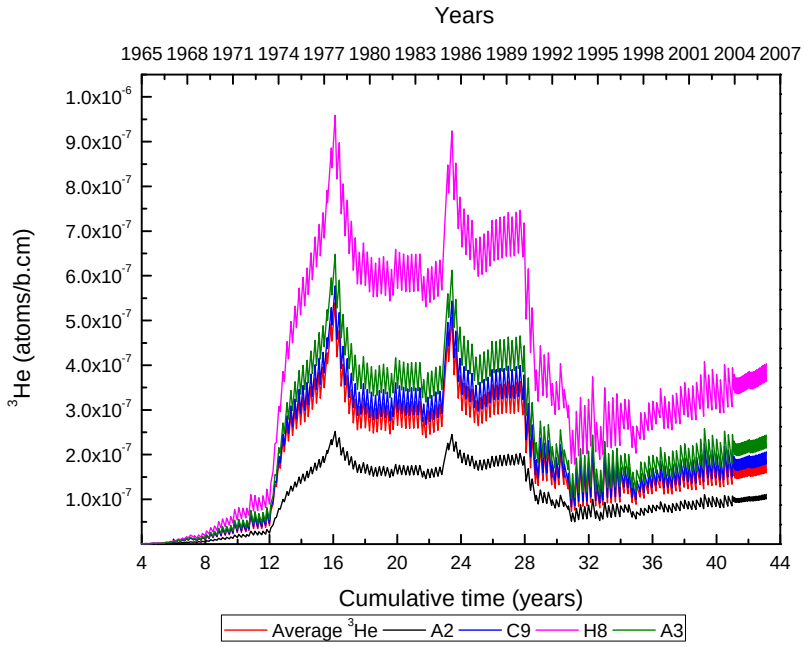

Figure 5.16: Time evolution of ^{3}He in selected beryllium reflector elements

It is clear from Figure 5.15, that assuming the average spectrum over all the reflector elements when calculating the isotopic number density, underestimate and overestimate the poison concentration in the beryllium reflector elements. This is consistent with the spectrum variations discussed in Subsection 5.3.1 and 5.3.2.

The averaged spectrum representation over all the beryllium reflectors, underestimates H8 (the heavily poisoned element) and overestimates A2 (the least poisoned element) by a factor of approximately 2, after about 12 years (after ^{6}Li saturation). All the other elements were represented, to within a band of less than 40% (see Tables 5.5 and 5.6).

The behaviour of the reflector element H8, is mainly due to its surroundings, as the reflector element is surrounded by control rod G7 and two reasonably fresh fuel elements, in positions H7 and G8. This leads to the fast spectrum surroundings and consequently, higher ^{6}Li production from the fast ^{9}Be(n,α)^{6}Li reaction. ^{6}Li production in this position is higher than its burn–up. This observation are consistent with Figures 5.10 and 5.11 in Subsection 5.3.1. Positions A2 and A8 are lower flux positions, as a result, the transmutations of poisons in these positions is extremely slow. The closer the reflector is to the fuel element, the higher the rate of ^{6}Li production will be due the fast spectrum the elements experience.

A higher ^{6}Li burn–up rate is observed in the reflector elements residing in the over–moderated surroundings (e.g. A2). The presence of water softens or thermalizes the spectrum in this reflector element.

The time to reach 99% of ^{6}Li saturation values, differs slightly in all the reflector elements, 100% saturation is reached after about $\approx$12 years in almost all the reflectors elements for both the element specific spectrum and the spectrum averaged over all the reflectors. Note that the time it takes for ^{6}Li to reach equilibrium, is much longer (about 12 years) in the case of the SAFARI–1 reactor than in other reactors, for example, in the MARIA reactor, it was calculated to take about 200 days. This is mainly attributed to the reactor power and the placement of the beryllium reflectors – the core configurations.

Poison distributions in all the beryllium reflectors for cycles *C0313-1, C0508-1, C0706-1* and *C0906-1* are presented in Tables 5.5 and 5.6. The less poisoned reflector elements are found at the top of each table and heavily poisoned elements are at the bottom.

The percentage differences of ^{6}Li distribution in Table 5.5 are calculated relative to the averages 10.35×10^{-7} $\left[\frac{\text{atoms}}{\text{b-cm}}\right]$, 10.27×10^{-7} $\left[\frac{\text{atoms}}{\text{b-cm}}\right]$, 10.59×10^{-7} $\left[\frac{\text{atoms}}{\text{b-cm}}\right]$ and 12.76×10^{-7} $\left[\frac{\text{atoms}}{\text{b-cm}}\right]$ for cycles *C0313-1, C0508-1, C0706-1* and *C0906-1* respectively.

Table 5.5: ^{6}Li distribution in the beryllium reflector due to the spectrum in different cores

Beryllium Reflector Elements	**Cycles**							
	C0313-1		C0508-1		C0706-1		C0906-1	
	^{6}Li$\cdot 10^{-7}$ $\left[\frac{\text{atoms}}{\text{b}\cdot\text{cm}}\right]$	Δ [%]	^{6}Li$\cdot 10^{-7}$ $\left[\frac{\text{atoms}}{\text{b}\cdot\text{cm}}\right]$	Δ [%]	^{6}Li$\cdot 10^{-7}$ $\left[\frac{\text{atoms}}{\text{b}\cdot\text{cm}}\right]$	Δ [%]	^{6}Li$\cdot 10^{-7}$ $\left[\frac{\text{atoms}}{\text{b}\cdot\text{cm}}\right]$	Δ [%]
A2	6.65	35.7	6.51	36.5	6.72	36.5	7.95	37.66
A8	6.85	33.7	8.05	21.6	8.26	22.0	9.48	25.67
B2	6.96	32.7	8.07	21.4	8.36	21.0	9.71	23.89
A7	7.60	26.5	10.90	-6.2	10.83	-2.3	13.50	-5.85
E2	8.02	22.4	8.33	18.9	8.48	19.9	10.78	15.49
D9	8.24	20.2	8.99	12.4	10.56	0.3	12.39	2.85
F9	8.31	19.6	8.82	14.0	10.16	4.1	11.60	9.08
G2	8.36	19.1	8.88	13.4	8.86	16.3	10.79	15.42
C2	8.90	13.9	9.62	6.2	9.90	6.5	11.95	6.30
D2	10.27	0.7	10.90	-6.2	10.75	-1.5	14.06	-10.25
F2	10.28	0.5	9.78	4.7	9.87	6.8	12.69	0.55
C9	10.85	-5.0	11.50	-12.0	11.57	-9.3	13.88	-8.79
A5	11.32	-9.5	10.69	-4.1	11.34	-7.0	13.39	-4.99
A6	11.80	-14.2	6.73	34.5	6.84	35.4	10.31	19.20
H2	11.81	-14.2	12.01	-17.0	12.11	-14.3	13.92	-9.09
B2	12.07	-16.8	12.16	-18.5	12.58	-18.8	14.59	-14.38
A4	12.82	-24.1	13.20	-28.6	13.29	-25.5	14.98	-17.43
A3	13.55	-31.1	13.78	-34.3	13.79	-30.2	15.54	-21.79
H8	23.36	-126.0	23.44	-128.4	23.02	-117.4	26.77	-109.83

In Table 5.6, that is ^{3}He distribution, the percentage differences are calculated relative to the averages 2.04×10^{-7} $\left[\frac{\text{atoms}}{\text{b-cm}}\right]$, 1.86×10^{-7} $\left[\frac{\text{atoms}}{\text{b-cm}}\right]$, 1.92×10^{-7} $\left[\frac{\text{atoms}}{\text{b-cm}}\right]$ and 2.27×10^{-7} $\left[\frac{\text{atoms}}{\text{b-cm}}\right]$ for cycles *C0313-1, C0508-1, C0706-1* and *C0906-1* respectively.

Table 5.6: ^{3}He distribution in the beryllium reflector due to the spectrum in different cores

Beryllium Reflector Elements	**Cycles**							
	C0313-1		C0508-1		C0706-1		C0906-1	
	^{3}He·10^{-7} $\left[\frac{\text{atoms}}{\text{b·cm}}\right]$	Δ [%]	^{3}He·10^{-7} $\left[\frac{\text{atoms}}{\text{b·cm}}\right]$	Δ [%]	^{3}He·10^{-7} $\left[\frac{\text{atoms}}{\text{b·cm}}\right]$	Δ [%]	^{3}He·10^{-7} $\left[\frac{\text{atoms}}{\text{b·cm}}\right]$	Δ [%]
A2	1.28	37.2	1.11	40.4	1.12	41.5	1.31	42.21
A8	1.27	37.6	1.40	24.9	1.61	16.4	1.82	20.07
B9	1.46	28.2	1.41	24.2	1.68	12.3	1.94	14.83
A7	1.29	36.6	1.96	-5.5	2.02	-5.5	2.44	-7.40
E2	1.70	16.7	1.60	14.3	1.66	13.8	2.06	9.63
D9	1.86	8.8	1.66	10.7	2.25	-17.0	2.61	-14.68
F9	1.76	13.4	1.62	12.8	2.14	-11.2	2.42	-6.37
G2	1.68	17.7	1.66	10.9	1.72	10.4	2.06	9.31
C2	1.88	7.8	1.77	4.8	1.79	6.6	2.13	6.58
D2	2.41	-18.2	1.96	-5.5	1.93	-0.7	2.43	-6.96
F2	2.10	-3.1	1.85	0.6	1.93	-0.4	2.43	-6.70
C9	2.38	-16.8	2.06	-10.8	2.39	-24.3	2.83	-24.31
A5	2.01	1.2	2.00	-7.2	2.03	-5.7	2.36	-3.57
A6	1.99	2.3	1.27	31.7	1.29	32.6	1.87	17.98
H2	2.21	-8.7	2.12	-13.7	2.21	-15.4	2.52	-10.75
B2	2.43	-19.5	2.14	-15.1	2.17	-13.1	2.48	-9.22
A4	2.38	-16.7	2.42	-29.9	2.27	-18.5	2.54	-11.57
A3	2.52	-23.5	2.44	-30.9	2.26	-17.8	2.52	-10.96
H8	4.28	-110.1	4.04	-116.8	4.56	-137.6	5.25	-130.67

There is no apparent pattern observed in the poison distribution of Tables 5.5 and 5.6, except that the eastern side reflectors, that is C2, D2, F2 and G2, tends to be approximated better by the averaged poison and hence the averaged spectrum. The slightly large differences in number densities for cycle *C0313-1* are attributed to B6 fuel elements in this cycle.

Furthermore, the hollow elements A3 and A4, tend to be heavily positioned after H8. The spectrum around this region is fast, due to the cadmium ring in A4 and typical fresh fuel elements in position B3 to B5. Hence the higher levels of ^{6}Li production in these reflector elements.

The element–to–element number densities from cycle–to–cycle vary within a band of 40% except for A6 and A7 in cycle *C0313-1* for reasons given below.

The presence of the fuel element in B6 for cycle *C0313-1*, directly impacted on the build–up of poison isotopes for the reflector in position A6. The number densities of ^{6}Li and ^{3}He in this position

for cycle *C0313-1* are higher than in all the other cycles as seen in Tables 5.5 and 5.6. The presence of fuel plates for the ^{99}Mo production in position B6 of cycle *C0906-1* increase poison formation in this position, but to a lesser extend than in *C0313-1*. The configuration of *C0313-1*, specifically B6 fuel element, has local effects on its neighbours, the global effects on other beryllium reflector elements are negligible, as was discussed before.

In general, the LEU core spectrum leads to a harder spectrum and thus higher poison concentration, when compared to the HEU core. Thus, any changes in the core configuration that leads to either local or global spectral variations in the core and thus in the beryllium reflector elements, will directly influence the rate of poison formation and burn–up.

An important conclusion that can be drawn from these discussions is that ^{6}Li concentration saturates at about 12 years in all the reflectors with no spectrum updates. The spectrum in the beryllium reflector elements, varies strongly with position, thus if poison accumulation is to be accounted for accurately, a detailed spectrum for each element has to be used when calculating the poison concentrations. However, this approach can prove cumbersome and time consuming, when implemented from cycle–to–cycle. As an alternative, the spectrum averaged over all the beryllium reflectors will be used and the element specific spectrum will be applied to single cycle calculations.

The changes in poison number densities in individual reflector elements from cycle–to–cycle, are not important, provided that the core configuration and hence the spectrum has not changed.

Detail analysis of spectrum variation and thus poison number density are considered in Subsection 5.3.4.

5.3.4 Dependence of the ^{6}Li and ^{3}He number densities on an updated spectrum

The calculations above, were based on applying a constant spectrum over 43 years. In this section, the impact of spectrum updating on poison transmutations is evaluated.

The evaluation is conducted by updating the spectrum in FISPACT runs. The element specific averaged spectrum, as well as the spectrum averaged over the all reflectors is updated at yearly intervals from 2003 to 2007. Note that due to lack of cycle details from 1965 up until the end of 2002, the spectrum could not be updated. Furthermore, spectrum updating is applied through the fully LEU cycle until the first cycle of 2011, that is *C01101-1*.

Note that the spectral effect on poison concentrations over the average length of the SAFARI–1 reactor cycle, that is 30 days with a 5 day shut–down, were examined by burning with the BOC, mid-cycle and EOC spectra. This showed negligible effects on poison concentrations.

Therefore, the results discussed from here on, are based on updating the spectrum at yearly intervals. The results for the heavily poisoned element, H8 are shown for ^{6}Li in Figure 5.17a

and for ^{3}He in Figure 5.17b.

The poison distribution, based on the updated spectrum, in all the elements as at the end of 2007, as well as for the first cycle of 2011, are summarized in Table 5.7.

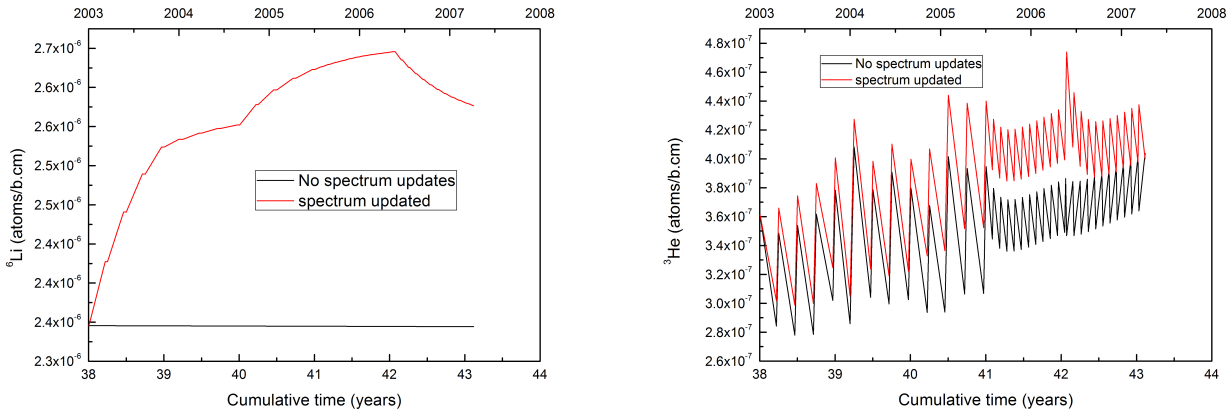

(a) ^{6}Li build-up

(b) ^{3}He build-up

Figure 5.17: Effects of spectrum updating on ^{6}Li and ^{3}He concentration in H8

In Figure 5.17a, it is seen that with variation in spectrum, the ^{6}Li number density increases and does not reach equilibrium; different to the assumption of constant spectrum were the asymptotic value of its number density is reached. The spectral changes lead to a rather weak increase in the ^{3}He number density, see Figure 5.17b. The difference seen from 41 to 43 years in Figure 5.17b, is mainly due to the shut–down periods (i.e. 5 and 12 day annual extended shut–down periods) – ^{3}He is gradually accumulated during these periods.

The poison distribution in each reflector element due to spectrum updating as at end of 2007 (*C0711-1*) and the first cycle of 2011 (*C01101-1*) is summarized in Table 5.7.

Table 5.7: ^{6}Li and ^{3}He number densities as at the end of 2007 and beginning of 2011 based on the updated spectrum

Beryllium Reflector Elements	**Cycles**			
	C0711-1		C01101-1	
	$^{6}\text{Li}\cdot10^{-7}$ $\left[\frac{\text{atoms}}{\text{b}\cdot\text{cm}}\right]$	$^{3}\text{He}\cdot10^{-7}$	$^{6}\text{Li}\cdot10^{-7}$ $\left[\frac{\text{atoms}}{\text{b}\cdot\text{cm}}\right]$	$^{3}\text{He}\cdot10^{-7}$
A2	7.59	0.97	8.04	1.88
A8	9.09	1.31	9.55	2.44
B9	9.37	1.44	9.77	2.63
A6	7.34	1.79	10.38	1.56
G2	10.06	2.66	10.95	2.81
E2	9.50	2.80	11.04	2.61
F9	10.95	2.31	11.75	3.28
C2	11.02	2.65	12.25	2.85
D9	11.58	2.58	12.57	3.41
F2	11.16	3.28	12.95	3.08
A5	12.21	2.93	13.41	2.95
A7	11.86	2.32	13.43	2.02
C9	12.94	2.74	13.90	3.83
H2	13.66	2.56	14.21	3.73
D2	11.69	3.11	14.46	2.61
B2	14.18	2.71	15.04	3.48
A4	14.50	3.42	15.26	3.39
A3	15.41	2.97	16.05	3.63
H8	26.06	5.04	26.92	7.76

Note that the number densities of 2007 are based on the HEU spectrum, while those of 2011 are based on the LEU spectrum. The higher number densities of 2011 are as a result of a 3 year poison build–up and the spectral changes, of the LEU spectrum. The poison number densities of cycle *C01101-1* will be applied when studying their influence on reactor core parameters.

The trends of poison build–up per reflector element in Table 5.7 is similar to that of the results discussed earlier.

5.4 Impact of ^{6}Li and ^{3}He on SAFARI–1 reactor core parameters

The impact of beryllium reflector poisoning on the SAFARI–1 reactor core parameters for cycle *C0706-1* were studied before and published as part of this work, see reference [55]. The paper is also attached in Appendix D. The analysis of this paper was based on the HEU spectrum. Similar calculations are performed in this study for the recent LEU core, that is *C01101-1*, the first cycle of January 2011.

The analysis is based on the reload and core–follow (fuel depletion) of cycle *C01101-1* as in cycle *C0706-1*.

Cycle *C01101-1* has an average cycle length of about 23 days and an average power level of about 20 MW. The poison concentration of Table 5.7 (i.e. *C01101-1*) was applied to this cycle and results were compared to the 100% pure beryllium reflected core (reference core). The effects on core parameters such as reactivity, flux and power redistribution, fuel burn–up, cycle length, as well as important safety parameters, were evaluated and the results are discussed in subsequent sections.

In order to understand the long term effects of the poisoned beryllium reflected core, primarily on ^{235}U burn–up and reactivity, the actual multi–cycle core–follow analysis based on 12 fully LEU cycles and the equilibrium core analyses of 23 cycles, based on cycle *C01101-1*, were conducted. The results of these analyses are compared to the reference case, that is the pure beryllium reflected core. Take note that the poisoned concentration as applied in these analyses is taken from cycle *C01101-1* shown in Table 5.7.

Finally, the single cycle (cycle *C01101-1*) results are compared to experimental measurements.

5.4.1 Single cycle analysis

Single cycle analyses based on the detailed poisoning of each beryllium reflector element show marked negative reactivity effects of about -886 pcm at BOC to about -687 pcm at EOC. The beryllium reflector poisoning has a rather weak influence on the fuel burn–up, this is because the poison build-up has a time–scale of years, while burning of a fuel element is accomplished in months. The poisoned beryllium reflected core results in an insignificant full core ^{235}U mass savings of only 2 grams at EOC when compared to a pure beryllium reflected core. Further analyses on the long term effects related to the ^{235}U burn–up as well as variations in reactivity are discussed at the end of this section.

The impact of poisons on the thermal flux and power redistribution is shown in the core maps of Tables 5.8 and 5.9. The percentage difference in both these tables, relative to the pure reflected core is calculated as follows:

$$\% \text{ Difference } = \left(\frac{\phi_{poison}}{\phi_{pure}} - 1 \right) \times 100$$

Table 5.8: Thermal flux redistribution map due to Be reflector poisoning at 1 day of cycle *C01101-1*

	1	2	3	4	5	6	7	8	9
A	-17.79	-19.88	-14.39	-9.94	-14.12	-12.05	-11.33	-9.68	-8.75
B	-16.87	-17.77	-13.54	-11.27	-8.31	-5.54	-3.94	-4.50	-8.98
C	-16.00	-14.75	-8.85	-5.50	-2.58	-1.04	0.00	-1.71	-8.86
D	-16.31	-15.69	-5.83	-1.69	0.25	1.32	1.69	0.00	-5.72
E	-17.03	-20.51	-4.31	1.04	2.14	3.52	3.99	2.01	-1.57
F	-12.50	-12.27	-1.39	3.30	4.88	5.22	4.58	3.16	0.00
G	-8.13	-6.69	1.78	5.14	5.07	6.46	6.04	3.58	6.91
H	-5.92	-5.12	3.12	6.36	7.21	7.55	5.08	-1.38	4.00

In Table 5.8 it can be seen that beryllium reflector poisoning has significant effects on the thermal flux. The poisoning phenomenon impacts largely on the thermal fluxes of the reflector, fuel elements and their neighbours (e.g. aluminium and lead elements) on the south–eastern corner of the core. Note that both the southern and eastern sides of the core are fully reflected by beryllium reflectors (see Figure 1.1), thus they are the most affected sides around the core and as a result experience a large flux reduction. The net effect of the poisoned beryllium reflector, is a flux tilt to the centre of the core, towards the north–western corner of the core.

Interestingly, A2, the least poisoned element (see Table 5.7), experienced the largest (except for E2) flux reduction of all the reflector elements while the heavily poisoned element H8, experienced

the least reduction in flux. This observation is attributed to the surrounding environment of the reflector elements. A2 is the most thermalised (see Figures 5.10 and 5.11) position in the core than any other reflector element and thus is extremely sensitive to the build–up of thermal neutron absorbers or poisons. On the other hand, H8 is in a fast spectrum environment (see Figures 5.10 and 5.11), it is positioned between two fuel elements and a control rod, therefore the presence of thermal neutron absorbers resulted in a negligible thermal flux reduction. Fuel elements adjacent to the beryllium reflectors on the south–eastern side of the core experienced a flux depression of up to -13.54% (B3), while that towards the northern side increased by up to about 7.55% (H6). The observations above are consistent with a fast flux redistribution in the core.

The power redistribution at 1 day is shown in the core map of Table 5.9.

Table 5.9: Relative power density map due to Be reflector poisoning at 1 day of cycle *C01101-1*

	1	2	3	4	5	6	7	8	9
A									
B			-13.69	-12.11	-7.69	-5.43	-4.14	-4.67	
C			-8.40	-5.21	-1.72	-1.25	0.15	-2.02	
D			-5.58	-1.18	0.32		1.50	0.00	
E			-4.71	1.32	8.79	3.70	3.05	1.82	
F			0.06	4.52	5.20		5.48	2.88	
G			1.52	5.64	15.56	6.92	5.59	2.84	
H			3.04	6.67	7.90	7.64	5.15		

The power and fast fluxes redistribution are consistent with perturbations observed in the thermal fluxes. The power tilt is also to the centre, towards the north–western corner of the core, with the neighbouring fuel element to the poisoned beryllium reflectors, delivering less power (B3) and those distant from the poisoned reflectors, delivering more power than in a case of pure beryllium reflected core. In general, the reduction in power, delivered by fuel assemblies towards the south–eastern corner of the core, in the poisoned beryllium reflected core is balanced out by peaking towards the center and the north–western side of the core.

Most importantly, the above observations tend to correct the historical tilt seen in OSCAR–3 to match that of the experimentally measured SAFARI–1 reactor. The results are quantified by comparison to experimental lower power flux measurement (LPM) discussed later in Subsection 5.4.3.

The local changes, introduced by the beryllium reflector poisoning are also evaluated by considering the most affected reflector element position, E2 as well as the neighbouring position B3 and the irradiation positions C3 and E3. The thermal flux changes in fuel element B3 and beryllium reflector

element E2 are shown in Figure 5.18.

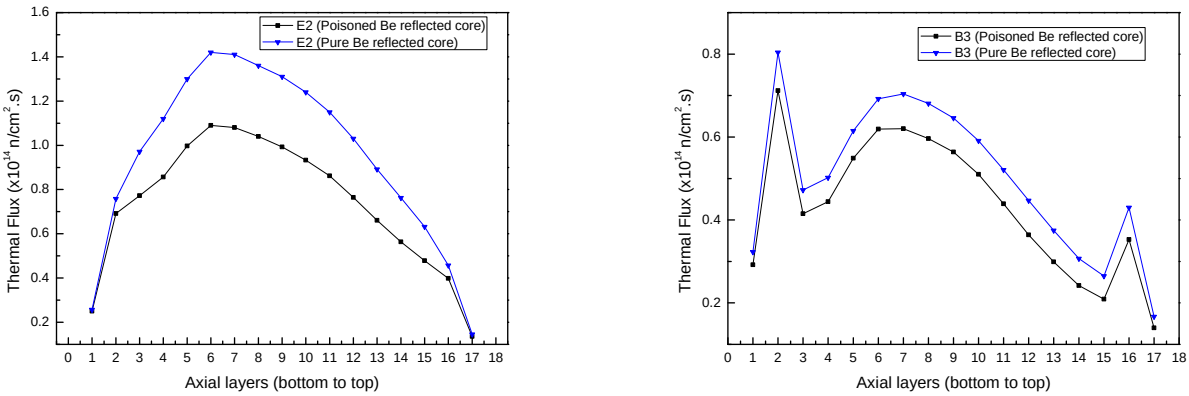

(a) E2 beryllium reflector

(b) B3 fuel element

Figure 5.18: Change in axial thermal flux profile in reflector element E2 and fuel element B3

The flux change in irradiation positions C3 and E3, dedicated to target plate irradiations for ^{99}Mo production, is shown in Figure 5.19.

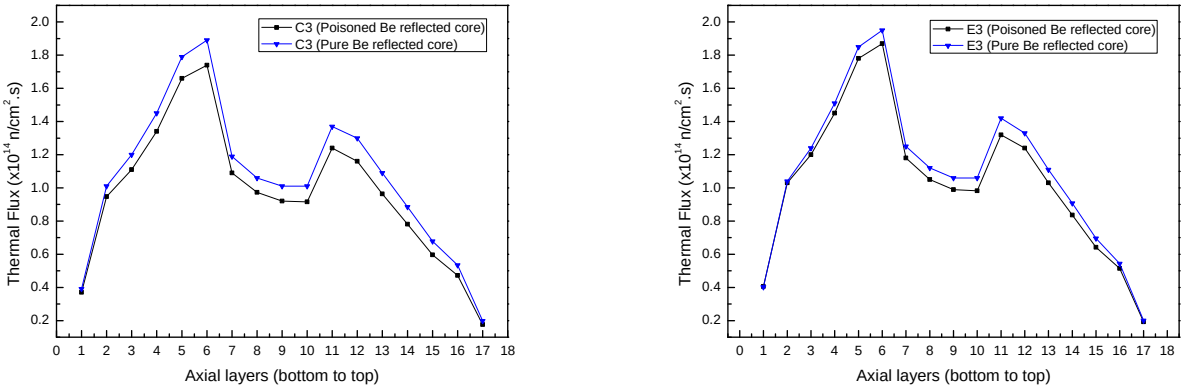

(a) C3 irradiation position

(b) E3 irradiation position

Figure 5.19: Change in axial thermal flux profile in C3 and E3 irradiation positions

The thermal flux peaks observed towards the bottom and top in Figures 5.18 and 5.19 are due to thermalization by water at the top and bottom of these assemblies.

The E2 beryllium reflector and B3 fuel element experienced a flux depression of -20% to -26% and -10% to -21% respectively. The irradiation positions, on the other hand, showed a reduction of 8% to 9% and 5% to 7% in C3 and E3 respectively. Note that for the irradiation position, the flux

reduction is quoted in axial layers 7 to 10, that is the position where the target plates irradiation are modelled in OSCAR–3. The flux is reduced to less than 8% in all the other irradiation positions. This reduction in fluxes, specifically in the target plate irradiation positions, will impact negatively on ^{99}Mo production yields and in general on reactor utilization.

5.4.2 Multi–cycle and equilibrium core analysis

Note that the poisoned number densities were not updated, for the period considered in the equilibrium and multi–cycle analysis calculations, discussed below.

The actual multi–cycle core–follow analysis based on 12 LEU cycles (i.e. corresponding to about a year of the SAFARI–1 reactor operation) showed negligible effects in ^{235}U burn–up of less than 1 gram in full core ^{235}U mass as in the case of a single cycle analysis. The reactivity variations of between -1000 pcm at BOC to -700 pcm at EOC are observed.

The equilibrium core analyses were obtained for both the pure beryllium and poisoned beryllium reflected cores (Table 5.7, cycle *C01101-1*). Note that the changes adopted in cycle *C01101-1* for equilibrium studies, different from that of the single cycle analysis, are only the fuel reload strategy shown below, all the other parameters were left as is (i.e. fix cycle length, etc.) in the pure and poisoned beryllium reflected cores. Note that the reload strategy adopted herein is the most representative but not the actual physical SAFARI–1 reactor reload strategy.

In the adopted reload strategy, three fresh fuel elements H3, B7 and H7 were loaded while ejecting three from the core, i.e. D5, E6, F5, one fresh control, C7, was loaded while G5 was removed from the core. This is done at the BOC of each of the 23 cycles for equilibrium studies.

$$
\begin{aligned}
H3 \rightarrow G8 \rightarrow B3 \rightarrow B4 \rightarrow G4 \rightarrow C4 \rightarrow D4 \rightarrow E4 \rightarrow D5 \rightarrow \text{(out of the core)} \\
B7 \rightarrow C8 \rightarrow H6 \rightarrow E8 \rightarrow B5 \rightarrow C6 \rightarrow D3 \rightarrow G6 \rightarrow E6 \rightarrow \text{(out of the core)} \\
H7 \rightarrow H4 \rightarrow H5 \rightarrow D7 \rightarrow F7 \rightarrow F3 \rightarrow F4 \rightarrow F5 \rightarrow \text{(out of the core)} \\
C7 \rightarrow G7 \rightarrow C5 \rightarrow E7 \rightarrow E5 \rightarrow G5 \rightarrow \text{(out of the core)}
\end{aligned}
$$

The results of the equilibrium core analysis are consistent with that of the single cycle and multi–cycle analysis, in that the difference in ^{235}U burn–up between the pure and poisoned beryllium reflected core is negligible. This is expected since the integrated power or power level and cycle length is defined to be unchanged in the analysis. The small difference seen is due to secondary spectrum effects. Furthermore, the reactivity effects settled at about -895 pcm, as shown in Figure 5.20.

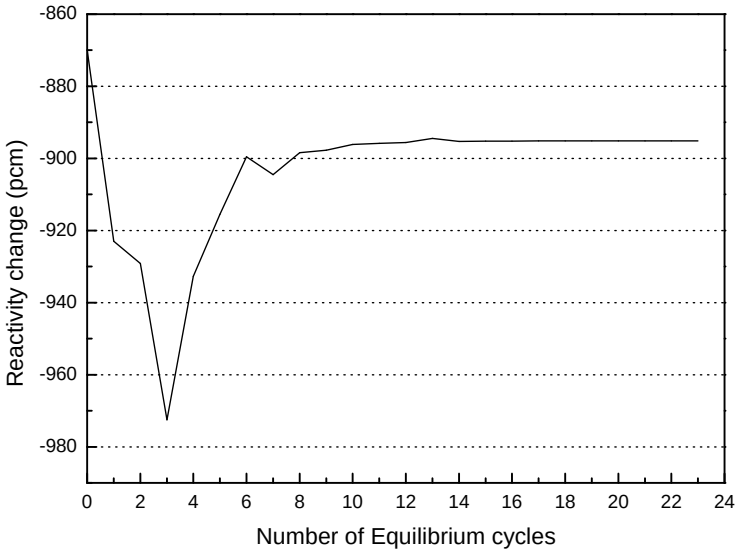

Figure 5.20: Change in reactivity introduced by poisoned beryllium reflector in equilibrium cycle

The results above confirm that the poisoning of the beryllium reflector has no influence on fuel burn–up and the reactivity due to this phenomenon varies between -1000 pcm and -700 pcm.

The impact of the poisoned beryllium reflector on the measured experimental plant data is discussed in Subsection 5.4.3. Due to limited experimental data, the comparisons are limited to the lower power copper wire flux measurements.

5.4.3 Comparison to experimental flux measurements

Low power flux measurements in all the fuel assemblies are performed prior to the reactor start–up of each cycle. The reactor is made critical at very low power and a length of copper wire is inserted into each fuel assembly and control rod follower along its axial centreline and over the full height of the assembly. The axial activity profile of each wire is obtained by a dedicated counting device. The experimental data is then processed for comparison to the OSCAR–3 calculated results. The reactor conditions during this experiment are modelled as accurately as possible in OSCAR–3.

Comparison to low power measurements based on poisoned and 100% pure beryllium reflected cores was conducted using cycle *C01101-1*. The comparison is shown in the core maps of Tables 5.10 and 5.11. The percentage difference is calculated relative to the experimental measurements as follows:

$$\% \text{ Difference } = \left(\frac{\text{Calculated}}{\text{Experiment}} - 1 \right) \times 100$$

The results of the pure beryllium reflected core are shown in the core map of Table 5.10.

Table 5.10: Calculated and measured lower power flux comparison for the pure beryllium reflected core

	1	2	3	4	5	6	7	8	9
A									
B			16.48	11.61	2.57		16.49		
C				7.88		-15.59		16.40	
D			0.37	23.19	-10.73		-1.52		
E				-8.79		2.25		13.54	
F			4.67	-8.95	-18.67		-6.29		
G				-7.36		-4.42		-3.75	
H			-4.54	-11.00	-17.18	-10.19	-10.13		

The results of the poisoned beryllium reflected core are shown in the core map of Table 5.11

Table 5.11: Calculated and measured lower power flux comparison for the poisoned beryllium reflected core

	1	2	3	4	5	6	7	8	9
A									
B			0.99	-1.88	-5.86		12.14		
C				2.04		-16.67		14.49	
D			-4.74	20.98	-10.48		-0.30		
E				-8.12		5.37		15.61	
F			3.35	-6.42	-14.86		-2.75		
G				-3.05		1.25		-1.19	
H			-1.57	-5.65	-11.54	-4.08	-5.81		

Note that the fuel follower results are not shown in both maps of Tables 5.10 and 5.11, this is due to the approximate models of both the control rod and the fuel follower in OSCAR–3 which results in a large error when compared to experimental data. Further explanations and comparisons between the OSCAR–3 and OSCAR–4 control rod and fuel follower models can be found in reference [45].

In general, the comparison of the fuel elements adjacent to the beryllium reflector element (poisoned) and on the northern side of the core (i.e. poolside) show improvements due to the tilt observed in Section 5.4.1. As indicated before, the correction in the OSCAR–3 historical tilt due to the beryllium reflector poisoning tends to improve code–to–experimental data comparisons.

The results look promising and with the envisaged official release of the OSCAR–4 code system, which amongst other improvements, incorporate the correct physical model of the control rod, further improvements are foreseen.

Reload calculations, performed prior to the BOC of each planned cycle using OSCAR–3, serve to evaluate the safety parameters of the planned cycle. Note that in OSCAR–3 the cycle length definition is based on the time it takes for the core to become sub–critical (*k-effective* < 1) whereas the actual SAFARI–1 reactor cycle length is planned and fixed at a specific time (i.e. cycle *C01101-1* has a planned cycle length of 22.96 days), consequently the calculated and planned cycle length might differ.

The results of the calculation performed with pure (reference) and poisoned beryllium reflectors for cycle *C01101-1* are summarized in Table 5.12. The calculations were performed at cold, clean, Xe free core condition except for cycle length predictions, which were modelled with reactor conditions as is for a typical operational cycle.

Table 5.12: Comparison of safety parameters calculated from pure and poisoned beryllium reflected core

Calculated Safety parameters	**Pure Be reflected core**	**Poisoned Be reflected core**	**SAFARI-1 reactor parameters**
Cycle length (days)	32.33	24.00	22.96
Excess reactivity ($)	7.9	6.8	–
Reactivity due to Mo99 target plates	3.07	2.90	–
Control rod worth ($)	26.49	28.55	$\geq$ 20$
Shut-down margin($)	16.62	17.76	$>$ 1/2 rod worth
Absolute power peak (W.cm^{-3})	536.04	474.10	–
Estimated start-up bank (cm) without Mo99 target plates	50.40	52.74	–
Estimated start-up bank with Mo99 target plates (cm)	46.61	47.26	$>$39 cm
Estimated BOC Xe equilibrium bank(cm)	56.22	57.60	–

It is seen in Table 5.12 that beryllium poisoning, influences the safety characteristics of the core significantly. The negative reactivity, introduced by the poisons, reduced the cycle length of the poisoned reflected core to be more compatible with real life scheduling than that predicted by the pure beryllium reflected core. The excess reactivity is reduced while the control rod worth and shut–down margins are increased. That means that the poisoned beryllium reflected core needs more additional reactivity than the pure reflected core. This is compensated for by further control rod withdrawal in the poisoned reflected core. The additional reactivity, due to ^{99}Mo target plates is less since the overall core reactivity is already reduced by beryllium reflector poisoning, moreover, the targets are situated next to the reflectors.

The results above suggest that the corrected beryllium reflector modelling in OSCAR code system (i.e. modelling beryllium depletion) will give a better estimations of the real life SAFARI–1 reactor operational safety parameters. In general, modelling beryllium reflector depletion shows promising results and should be implemented in the soon to be released OSCAR–4 code system for the realisation of improved code–to–experimental data comparisons.

Temporarily, the details of poison build–up in OSCAR–3 will be accounted for by using the calculational approach discussed in this study.

5.5 Swelling of SAFARI–1 beryllium reflectors

The high rate of helium generation in beryllium via ^{9}Be(n,2n)2 ^{4}He, along with the high retention fraction, make He-induced swelling an important design issue. The discussions here, mainly focused on swelling and the fluence experienced by the reflector element, is brief due to a lack of SAFARI–1 reactor irradiated beryllium reflector experimental data, which could be useful in verifying the results calculated in this study. However, the calculated results are compared to the swelling measurements obtained in the Russian and Western experiments at an irradiation temperature of < 100 °C. The fast flux (E $>$ 1 MeV) in individual reflector elements calculated with MCNP is converted to fast fluence.

Swelling, elongation and helium content, are calculated using empirical Equations (2.22), (2.23) and (2.24). The results are summarized in Table 5.13. Note that the calculations were performed using the fluence calculated from cycle *C01101-1* at BOC. The results based on Equation (2.21) (not shown here), shows similar trend as those of Equations (2.22) and (2.23), however, the results are a factor of 10 less.

Table 5.13: Beryllium reflector status at the beginning of 2011

Beryllium Reflector Elements	**Parameters**					
	Fluence	He content	$\frac{\Delta V}{V}$	$\frac{\Delta L}{L}$	ΔL(N-S)	ΔL(E-W)
	10^{22} $\frac{\text{n}}{\text{cm}^2}$	appm	[%]	[%]	[mm]	[mm]
A2	0.963	4785.0	0.528	0.176	0.14	0.13
A8	1.190	5916.0	0.657	0.219	0.18	0.17
B9	1.194	5933.0	0.659	0.220	0.18	0.17
D9	1.400	6956.0	0.777	0.259	0.21	0.20
F9	1.758	8737.0	0.984	0.328	0.26	0.25
H2	1.911	9499.0	1.073	0.358	0.29	0.27
C9	1.995	9913.0	1.121	0.374	0.30	0.28
A7	2.168	10776.0	1.222	0.407	0.33	0.31
B2	2.204	10952.0	1.243	0.414	0.33	0.31
A6	2.210	10983.0	1.247	0.416	0.33	0.32
G2	2.263	11245.0	1.278	0.426	0.34	0.32
H8	2.502	12435.0	1.418	0.473	0.38	0.36
C2	2.511	12479.0	1.423	0.474	0.38	0.36
A3	2.511	12482.0	1.423	0.474	0.38	0.36
E2	2.774	13789.0	1.578	0.526	0.42	0.40
F2	2.966	14742.0	1.691	0.564	0.45	0.43
A5	3.034	15078.0	1.731	0.577	0.46	0.44
D2	3.078	15300.0	1.757	0.586	0.47	0.44
A4	3.199	15899.0	1.828	0.609	0.49	0.46

The elongation in the N–S and E–W radial directions across the reflector element is calculated using the dimensions of beryllium reflectors, that is 75.82 mm in the E–W and 79.91 mm in the N–S directions (see Figure 2.5 in Chapter 2 for dimensions). Note that Table 5.13 assumes uniform elongation in both the E–W and N–S directions.

Table 5.13 suggests that the reflector on the south–eastern side of the core experiences higher fast fluence and hence a higher rate of swelling and elongation, while the reflector elements on the western side of the core are the least affected, since they experience lower fast fluence. These observations are consistent with the SAFARI–1 reactor asymmetric core configuration, that is there are more fuel elements towards the south–eastern side of the core than on the western side.

The most affected element, A4, experiences fast fluence, volumetric swelling and elongation of about $3.199\times10^{22}\ \frac{\text{n}}{\text{cm}^2}$, 1.828% and 0.609% respectively. Elongation in the radial directions, that is E–W and the N–S of Tables 5.13 was defined to be uniform since the size of the sites is nearly the same. In practice they might differ a lot due to the large difference in the fast fluence profile on the two sides.

The dimensions of the beryllium reflector in the x–y directions are 75.82 mm in the E–W and 79.91 mm in the N–S directions and the assembly pitch is 77.1 mm in the E–W and 81.0 mm in the N–S direction. The total coolant gap in the N–S and E–W are 1.09 mm and 1.28 mm respectively.

The estimated elongation reduces the coolant gaps by a maximum of about 35% in the E–W direction between A4 and A5 by about 22% between A2 and B2 in the N–S direction. The reduction in the coolant gap leads to degradation of the cooling ability for the reactor component including that of the reflector element and might lead to the damage of such components.

The elongation and volumetric swelling are further estimated as a function of time and the calculated data plotted in Figures 5.21 and 5.22 at a 3 years interval from 1965 to the beginning of 2011.

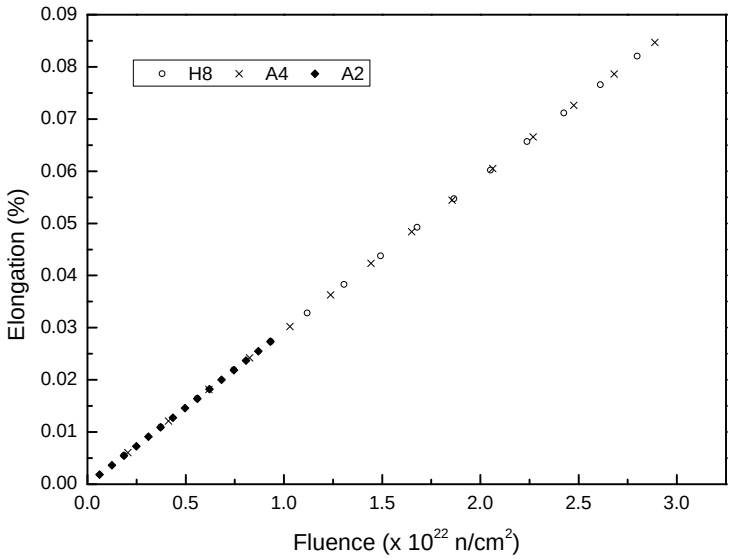

Figure 5.21: Elongation in beryllium irradiated at temperatures of $< 100°C$ as a function of fluence (E > 1 MeV)

In Figure 5.21 it is seen that elongation is proportional to the neutron fluence. The higher the fluence, the faster the rate of elongation in beryllium, this is seen in all the elements experiencing a higher fluence, e.g. A3. The low fluence position, A2, experiences minimal elongation of all the elements as expected. All the elements fall almost on the same trend line but vary in elongation.

In Figure 5.22 comparisons is drawn between the SAFARI–1 reactor calculated data and both the Russian and the Western swelling experimental measurements, published in reference [39].

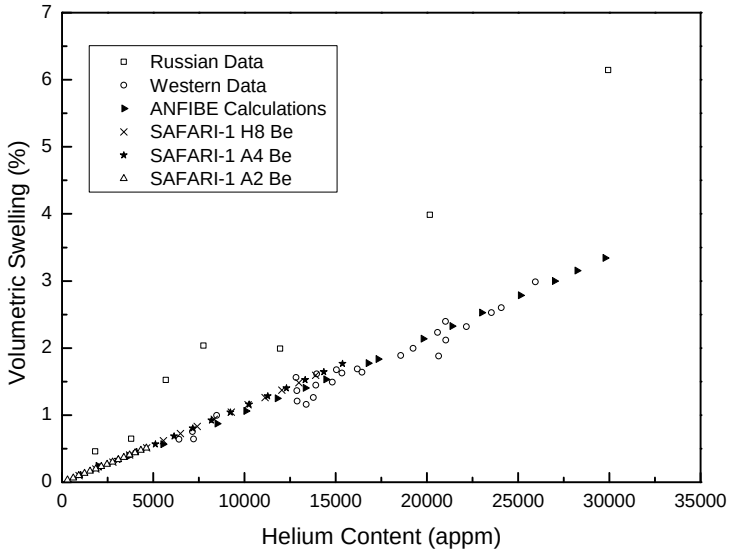

Figure 5.22: Swelling in beryllium irradiated at temperature of $< 100°C$ as a function of He content

It is important to note that the SAFARI–1 reactor data agrees with the Western measurements. The SAFARI–1 reactor beryllium reflector used in this study is assumed to be the hot–pressed beryllium of the Western origin with impurity specification of Table 2.2 as reported by Beeston [17].

Significant differences are observed between the Russian swelling measurements and those obtained in Western experiments. It is reported in reference [39] that the differences are due to the modern beryllium production and processing, that is that the Russian measurements are based on the beryllium irradiated in the 1960's, whereas the Western data are more recent and show a response of modern beryllium production technology. The SAFARI–1 beryllium reflector is of the Western origin, however, there are no records describing its production and processing technology or the suppliers of the reflector elements.

It is therefore important, that experimental measurements are performed, in order to determine the type and possibly the origin of the beryllium reflector. With experimental measurements it would also be possible to quantify the calculated results as well as to understand the graphs of Figures 5.21 and 5.22.

The SAFARI–1 reactor core configuration is almost similar to that of the JMTR of all reactors in Table 1.1 of Chapter 1. The JMTR reactor operating parameter are almost proportional to that of SAFARI–1 reactor, for example the flux ratios are comparable. Based on this argument, the SAFARI–1 reactor beryllium replacement criteria is deduced using the relation below:

$$\phi_f^{\text{SAF}} t_{SAF} \approx \phi_f^{\text{JMTR}} t_{JMTR}$$

where, $\phi_f^{\text{SAF}} t_{SAF}$ is the average fast fluence over the SAFARI–1 reactor beryllium reflectors and $\phi_f^{\text{JMTR}} t_{JMTR} = 1.1 \times 10^{22} \left[\frac{\text{n}}{\text{cm}^2}\right]$ (at E > 1 MeV, given in Table 1.1) is the fast fluence average over the JMTR beryllium reflectors. The time intervals, t_{SAF} and t_{JMTR} are the SAFARI–1 and JMTR replacement intervals in years.

The fast flux average over the SAFARI–1 beryllium reflector is $\phi_f^{\text{SAF}} = 1.63 \times 10^{13} \left[\frac{\text{n}}{\text{cm}^2.\text{s}}\right]$, thus the SAFARI–1 reactor replacement intervals is estimated as follows:

$$\text{Replacement Intervals } t_{SAF} \approx \frac{1.10 \times 10^{22}}{1.63 \times 10^{13}} \approx 21 \text{ years}$$

Therefore, it is estimated that the SAFARI–1 reactor beryllium reflector, operating for about 305 days per year at 20 MW, be replaced at about 21 year intervals with a fluence of about:

$$\text{Fluence}(> 1 \text{ MeV}) \approx 1.63 \times 10^{13} \left[\frac{\text{n}}{\text{cm}^2 \text{ s}}\right] \times 5.53 \times 10^{08}\text{s} \approx 0.90 \times 10^{22} \left[\frac{\text{n}}{\text{cm}^2}\right]$$

This approximation suggest that all the beryllium reflector be replaced, see Tables 5.13. The fluence values of this table are much higher than the estimated value above, since they were calculated over a period of 45 years, taking the reactor's irregular operational history into account.

The estimated fluence value correspond to swelling and helium content of about 0.5% and 4565 appm respectively. These values are similar to that of the ATR reactor for the beryllium reflector replacement, that is 0.5% swelling corresponding to 5000 appm He content (E > 1 MeV).

The summary of Table 1.1, together with the results of this study, justify the beryllium replacement in the SAFARI–1 reactor. However, experimental measurements need to be conducted to quantify the calculated results before undertaking any replacement.

These results, together with the experimental measurements could prove useful for future beryllium reflector replacement.

Chapter 6

Conclusions and recommendations

6.1 Introduction

In this study the general scope of the characteristics of the SAFARI–1 reactor neutron irradiated beryllium reflector, with an emphasis on the impact associated with core parameters such as flux and power distribution, reactivity, general safety parameters and an impact on the the irradiation position, was investigated. The behaviour of the initial beryllium reflector impurities with SAFARI–1 reactor operational history was also evaluated. Furthermore, swelling of the reflector was approximated since it is an important characteristic to justify the reflector's replacement. The conclusions and recommendations of this study are summarised below.

6.2 Analysis of beryllium reflector initial impurity and transmutants

It has been established that the beryllium reflector impurities assumed for calculations in this study, as well as the associated transmutants, do not influence the reflector's effectiveness, except for the ^{6}Li and ^{3}He isotopes, which increase the absorption in the reflector significantly. The impurities remain in the reflector during its entire service life–time.

It still remains important that the assumed impurity content be quantified by conducting experimental measurements on the reflector. The measurements could provide a good indication of the reflector's origin by, amongst other techniques, tracing back some of the current isotopic content to their parent nuclides and comparing them to the beryllium grades of the 1960's.

6.3 Beryllium reflector poisoning by ^{6}Li and ^{3}He

The poisoning of the beryllium reflector by ^{6}Li and ^{3}He has been recognized and its influence on reactor parameters has been established by performing fuel management calculations. That is, it has been shown that the accumulation of these isotopes during the reactor operation history leads to a significant reduction in reactivity and has a direct influence on power and flux distributions. The general safety parameters such as excess reactivity, shut–down margin, control rod worth, power peaking, etc. were also affected by this – thus indicating the importance of understanding and following poisoning phenomena with reactor history as well as with the beryllium reflector history.

The accumulation of these poisons in the beryllium reflector has been shown to strongly depend on the magnitude and spectrum of the neutron flux and hence the position of the reflector element in the core. If the beryllium reflector poison distribution is to be accounted for accurately, and thus the impact on core parameters, the magnitude and spectrum of the neutron flux in each reflector element has to be known and applied in fuel management calculations accordingly. In addition to this detail, the spectrum on the reflectors should be updated – for the SAFARI–1 it is proposed that the spectrum be updated at the beginning of every cycle (BOC) for practical purposes.

The averaged spectrum over all the reflector elements is not a good representation of the individual elements and is thus applied whenever the accuracy in poison distribution in each beryllium reflector elements is not important. For the current SAFARI–1 core configuration it has been established as to which reflectors experience a large amount of poison accumulations.

To improve the accuracy and reliability of the predictive OSCAR code calculations, beryllium burn–up should be incorporated in the next releases of OSCAR. Based on this study, the inclusion of beryllium burn–up chains is planned for implementation in the currently tested OSCAR–4 code system. Temporarily, poison distribution in the OSCAR–3 code system will be accounted for, using the calculational approach discussed herein.

Most importantly, the poisoning phenomena tends to correct the historical tilt seen in OSCAR–3 to match that of the experimentally measured SAFARI–1 reactor.

More experimental measurements are required to further quantify the beryllium poisoning phenomena. It is impossible to predict the reflector's end–of–life, based only on the amount of poison accumulation. Swelling of the reflector plays an important role in determining the end of the reflector's service lifetime, thus it is very important that it is predicted and determined experimentally.

6.4 Swelling of the beryllium reflector

It has been shown through predictive calculations, that the SAFARI–1 reactor beryllium reflector has accumulated large amounts of ^{4}He and thus experienced significant swelling in most reflector elements to date.

The replacement criteria is roughly estimated to be at 21 year intervals, with a maximum swelling of about 0.5%, the helium content of about 4565 appm and the fluence of 0.90×10^{22} $\left[\frac{\text{n}}{\text{cm}^2}\right]$. These values were estimated for reactor operations at 20 MW.

Experimental work need to be conducted in order to quantify these estimated values and before any concrete judgement is made on replacement.

6.5 Recommendations

The most important recommendation is that experimental measurements must be conducted and comparisons to calculated results must be done in order to quantify the results of this study on beryllium reflector poisoning. Furthermore, experimental measurements dedicated to evaluating swelling characteristics of the beryllium reflector should be conducted before undertaking any replacement of the reflector elements currently used.

The results of this study provided a good indication and platform for conducting experimental measurements, that is, determining swelling on the most affected elements and/or the highest fast fluence positions and comparing them to the calculated results – thus quantifying the calculated results.

It is further recommended that some of the beryllium reflectors be shuffled based on their isotopic content and the magnitude of poisoning as calculated and presented in this study, this should be supported by the experimental results. This could be one possibility of prolonging the lifespan of the current used elements that are less affected, saving the new one's for later use and thus saving costs.

Calculations on photo–neutron contribution to the beryllium reflector poisoning need to be performed.

One the future plans is to implement the beryllium reflector depletion chains in OSCAR–4, thus accounting for the isotopic transmutations in the beryllium reflector.

Bibliography

[1] Dorn CK. Products for Nuclear End-Use Applications. Brush Wellman Engineering Materials. Beryllium Products Division, 2009.

[2] Stonehouse JA. Physics and Chemistry of Beryllium. *Journal of Vacuum Science and Technology*, 4(3):1163 – 1170, 1986.

[3] Bretscher MM, Snelgrove JL. The Whole–Core LEU U_3Si_2-AL Fuel Demonstration in the 30-MW Oak Ridge Research Reactor. Technical Report ANL/RERTR/TM–14, Argonne National Laboratory, Illinois, July 1991.

[4] Ma BM. *Nuclear Reactor Materials and Applications*. Van Nostrand Reinhold Co., 1983.

[5] Khattab K, Khamis I. Sensitivity Analysis of Reflector Types and Impurities in 10 MW Type Nuclear Research Reactor. *Indian Journal of Pure and Applied Physics*, 45:491–495, June 2007.

[6] Tranter TJ, Tillotson RD, Mann NR, Longhurst GR. Processing Irradiated Beryllium for Disposal. Proceedings of the 7th IAEA International Workshop on Beryllium Technology, Santa Barbara, CA, November 2005.

[7] Tomberlin TA. Beryllium A Unique Material in Nuclear Applications. 36th International SAMPLE Technical Conference, San Diego, CA, November 2004.

[8] IAEA. Research Reactor Database. http://www.iaea.org/worldatom/rrdb/. Consulted on the 27th April 2010.

[9] Longhurst GR, Rohe RD. Beryllium Use in the Advanced Test Reactor. 8th IEA International Workshop on Beryllium Technology, Lisbon, Portugal, December 2007.

[10] Koonen E. BR2 Research Reactor Modifications: Experience gained from the BR2 Beryllium Matrix Replacement and Second Matrix Surveillance Programme. Technical Report IAEA–SM–310/68, IAEA, October 1989.

[11] Hanawa Y, Tsuboi K, Uchida M, Suzuki K, Takahashi K. Manufacturing of Neutron Reflector Frame for JMTR. 2nd International Symposium on Material Test Reactors, Idaho Falls, USA, 28 September – 1 October 2009.

[12] Primm T. Private Communication. Oak Ridge National Laboratory, USA, May 2010.

[13] Andrzejewski KJ, Kulikowska TA, Marcinkowska ZE. Computations of Fuel Management in MARIA Reactor with Highly Poisoned Beryllium Matrix. *Nukleonika*, 53(4):173–179, 2008.

[14] D'Arcy AJ. Description of the SAFARI-1 Reactor. Safety Analysis Report, Chapter 5 RR–SAR–0005, Necsa, August 2000.

[15] du Bruyn JF. Ad-hoc and Preventative Maintenance System as Part of the SAFARI–1 Management System, Benefits of SAFARI–1 Research Reactor. 13th International Topical Meeting on Research Reactor Fuel Management (RRFM), Vienna, Austria, 22–25 March 2009.

[16] Strydom WJ. Private communication. Necsa, South Africa, March 2010.

[17] Beeston JM. Beryllium Metal as a Neutron Moderator and Reflector Material. *Nuclear Engineering and Design*, 14, 1970.

[18] Verzilov YM, Ochiai K, Klix A, Sato S, Wada M, Yamauchi M, Nishitani T. Non-destructive Analysis of Impurities in Beryllium, affecting Evaluation of the Tritium Breeding Ratio. *Journal of Nuclear Materials*, 329–333:1337–1341, 2004.

[19] Tipton (Ed) CR. *Reactor Handbook*, volume 1, chapter 44, page 897. Inter-Science Publishers,New York, 2nd edition edition, 1960.

[20] Darwin GE, Buddery JH. *Metallurgy of the Rarer Metals-7, Beryllium.* Butterworths Scientific Publications, London, 1960.

[21] Janis 3.0 Software DVD-ROM, ENDF/B-VII.0 nuclear data library.

[22] Xoubi N, Primm RT, Maldonado GI. Loading Beryllium Targets to Extend the High Flux Isotope Reactor's Cycle Length. *Annals of Nuclear Energy*, 33:664–672, 6 March 2006.

[23] Ahmed R, Aslam, Ahmad N, Khan MJ, Tanvir M. Utilization of High-Density Fuel and Beryllium Elements for the Neutron Flux Enhancement in Typical MTR Type Research Reactors. *Progress in Nuclear Energy and Education*, 49:246–252, 2007.

[24] Wolfer WG, McCarville TJ. An Assessment of Radiation Effects in Beryllium. 6th Topical Meeting on the Technology of Fusion Energy, San Francisco, USA, 7 March 1985.

[25] Chakin VP, Ye Ostrovsky Z. Evolution of Beryllium Microstructure under High-Dose Neutron Irradiation. *Journal of Nuclear Materials*, 307–311:657–663, December 2002.

[26] Evans JE. Reaction Products in High nvt Irradiated Beryllium. Technical Report IDO–16364; PTR–119, Phillips Petroleum Co. Atomic Energy Div., Idaho Falls, Idaho, September 1956.

[27] Andrzejewski K, Kulikowska T, Bretscher MM, Matos J. Beryllium Poisoning in the MARIA Reactor. 22nd International Meeting on Reduced Enrichment for Research and Test Reactors (RERTR), Budapest, Hungary, 3–9 October 1999.

[28] Kalcheva S, Koonen E, Ponsard B. Accuracy of Monte Carlo Criticality Calculations During BR2 Operation. *Nuclear Technology*, 151:201–219, August 2005.

[29] Krzysztof J, Andrzejewski K, Kulikowska TA. Isotopic Transmutations in Irradiated Beryllium and their Implications on MARIA Reactor Operation. *Journal of Nuclear Technology*, 146:72–82, 15 April 2004.

[30] Kulikowska T, Andrzejewski K, Bretscher MM. ^{3}He and ^{6}Li Poisoning of the MARIA Reactor Beryllium Matrix. Technical Report IAE-40/A, Institute of Atomic Energy (IAE), Poland, 1999.

[31] Kalygin VV, Malkov AP, Pimenov VV. Effects of ^{3}He and ^{6}Li Accumulation in Beryllium blocks on the Neutron-Physical Characteristics of the MIR Reactor. *Atomic Energy*, 104(2):84–88, February 2008.

[32] Lawrence E, Peters Jr. Thermal Neutron Absorber Buildup in Irradiated Beryllium. Technical Report NASA TM X-2039, National Aeronautics and Space Administration (NASA), Cleveland, Ohio, July 1970.

[33] Kalcheva S, Ponsard B, Koonen E. Reactivity Effects due to Beryllium Poisoning of BR2. International conference on the Physics of Reactors (PHYSOR-2004), Chicago, Illinois, USA, 25–29 April 2004.

[34] Zimin S. A Simple Method to Estimate Beryllium Burn-up in Breeder Blankets of a Fusion Reactor and its Impact on a Tritium Breeding. Technical Report JAERI–M 93–245, Japan Atomic Energy Research Institute (JAERI), December 1993.

[35] Kulikowska T, Andrzejewski K. Parasitic Absorption in Beryllium Blocks of the MARIA Reactor. Proceedings of the International Conference: Nuclear Energy for New Europe 2002, Kranjska Gora, Slovenia, 9–12 September 2002.

[36] Petrov Yu V, Erykalov AN, Onegin MS. Accuracy of WWR-M Criticality Calculations with Code MCU–RFFI. 22nd International Meeting on Reduced Enrichment for Research and Test Reactors (RERTR), Budapest, Hungary, 2–9 October 1999.

[37] Sannen L, De Raedt Ch, Moons F, Yao Y. Helium Content and Induced Swelling of Neutron Irradiated Beryllium. *Fusion Engineering and Design*, 29:470–474, 3 March 2002.

[38] Leenaers A, Verpoucke G, Pellettieri A, Sannen L, Van den Berghe S. Microstructure of Long–Term Annealed Highly Irradiated Beryllium. *Journal of Nuclear Materials*, 372:256–262, 31 January 2007.

[39] Gelles DS, Dalle Donne M, Sernyaev GA, Kawamura H. Radiation Effects in Beryllium used for Plasma Protection. *Journal of Nuclear Materials*, 212–215:29–38, 1994.

[40] Beeston JM. Properties of Irradiated Beryllium Statistical–Evaluation. Technical Report TREE–1063, Idaho, USA, October 1976.

[41] Chakin VP, Kazakov VA, Melder RR, Goncharenko Yu.D, Kupriyanov IB. Effects of Neutron Irradiation at 70–200 °C in Beryllium. *Journal of Nuclear Materials*, 307–311:647–652, 2002.

[42] Müller EZ, Ball G, Joubert WR, Schutte HC, Stoker CC, Reitsma F. Development of a Core Follow Calculational System for Research Reactors. Proceedings of the 9th Pacific Basin Nuclear Conference, Sydney, Australia, 1–6 May 1994.

[43] Reitsma F, Müller EZ. Evaluation of the Use of Nodal Methods for MTR Neutronic Analysis. 17th International Meeting on Reduced Enrichment for Research Reactors (RERTR), Williamsburg, Virginia,USA, 18–23 September 1994.

[44] Reitsma F, Müller EZ. Flexible Exposure and Nodal Mesh Treatment in 3D Nodal Simulator MGRAC: Application to a MTR Case with Axially Movable Assemblies. International Conference on the Physics of Reactors 2002 (PHYSOR–2002), Seoul, Korea, 7–10 October 2002.

[45] Stander G, Prinsloo RH, Müller EZ, Tomašević DI. OSCAR–4 Code System Application to the SAFARI-1 Reactor. International Conference on the Physics of Reactors 2008 (PHYSOR–2008), Interlaken, Switzerland, 14–19 September 2008.

[46] Halsall MJ. A Summary of WIMSD4 Input Options. Technical Report AEEW–M1327, Atomic Energy Establishment, Winfrith, Dorchester, June 1980.

[47] Ball G. Calculational Support provided to SAFARI-1. AFRA Regional Conference on Research reactor Operation, Utilisation and Safety, Algiers, Algeria, 10–11 April 1999.

[48] X-5 Monte Carlo Team. *MCNP – A General N–Particle Transport Code, Version 5, Volume I: Overview and Theory*. Los Alamos National Laboratory, Los Alamos, USA, LA–UR–03–1987 edition, April 2003.

[49] Pelowitz DB (ed). *MCNPX User's Manual, Version 2.6.0*. Los Alamos National Laboratory, Los Alamos, USA, LA-CP-07-1473 edition, April 2008.

[50] Hendricks JS, et al. *MCNPX 2.6.0 Extensions*. Los Alamos National Laboratory, Los Alamos, USA, la–ur–08–2216 edition, April 2008.

[51] Wilson WB, et al. *A Manual for CINDER'90 Version 07.4 Codes and Data*. Los Alamos National Laboratory, Los Alamos, USA, la–ur–07–8412 edition, December 2007.

[52] Belal M, Graham AL, de Villiers D. OSCAR-3 MCNP Interface (OSMINT5) Verification and Validation. 11th International Topical Meeting on Research Reactor Fuel Management (RRFM) and Meeting of the International Group on Reactor Research (IGORR), Lyon, France, 11–15 March 2007.

[53] Strydom WJ, Belal M. SAFARI–1 Spectrum Variations Due to the HEU–to–LEU Core Conversion. Technical Report RRT–SAFA–REP–10003, Necsa, Pretoria, South Africa, January 2010.

[54] Forrest RA. *EASY Documentation Series, FISPACT-2007: User Manual UKAEA FUS534 EURATOM/UKAEA Fusion*, March 2007.

[55] Moloko LE, Korochinsky S, van Rooyen TJ. Impact of Beryllium Reflector Ageing on SAFARI–1 Research Reactor Core Parameters. 15th International Topical Meeting on Research Reactor Fuel Management (RRFM), 20–24 March 2011.

Appendix A

SAFARI-1 reactor operational history

Table A.1: SAFARI-1 reactor quarterly operational history

Years	Operation (Hrs)	Shutdown (Hrs)	Ave. (MW)	Years	Operation (Hrs)	Shutdown (Hrs)	Ave. (MW)
1965	0	0	0	2	520.6	1687.4	5
2	370	1838	5	3	1223.2	984.8	5
3	39	2169	5	4	1367.6	840.4	5
4	57	2151	5	1989	1211.2	996.8	5
1966	72.8	2135.2	5	2	1186.4	1021.6	5
2	78.8	2129.2	5	3	1211.6	996.4	5
3	50.2	2157.8	5	4	1429.2	778.8	5
4	81	2127	5	1990	1224.2	983.8	5
1967	217.4	1990.6	5	2	1202.2	1005.8	5
2	282.8	1925.2	5	3	1212.8	995.2	5
3	278.6	1929.4	5	4	1087.8	1120.2	5
4	251.8	1956.2	5	1991	1206	1002	5
1968	397.4	1810.6	5	2	1187.6	1020.4	5
2	14.6	2193.4	5	3	1216.4	991.6	5
3	0	2208	0	4	1173	1035	5
4	0	2208	0	1992	1287.2	920.8	5
1969	200.4	2007.6	10	2	1188	1020	5
2	478.4	1729.6	10	3	1217.2	990.8	5
3	329.1	1878.9	10	4	1426.8	781.2	5
4	322.7	1885.3	10	1993	1086.8	1121.2	10

Continued on next page

Table A.1 – continued from previous page

Years	Operation (Hrs)	Shutdown (Hrs)	Ave. (MW)	Years	Operation (Hrs)	Shutdown (Hrs)	Ave. (MW)
1970	739.8	1468.2	10	2	1230.5	977.5	10
2	1011.3	1196.7	10	3	1766.7	441.3	10
3	988.1	1219.9	10	4	1041.2	1166.8	10
4	1046	1162	10	1994	1366.9	841.1	10
1971	996.4	1211.6	10	2	1298.2	909.8	10
2	826.9	1381.1	10	3	1769.3	438.7	10
3	1099.8	1108.2	10	4	1573.1	634.9	10
4	1073.1	1134.9	10	1995	1324.2	883.8	10
1972	1069.7	1138.3	10	2	1860.8	347.2	10
2	1686.9	521.1	10	3	1978.8	229.2	10
3	1416.19	791.81	16	4	1619.67	588.33	18
4	1456.63	751.38	16	1996	1294.5	913.5	18
1973	1423.88	784.13	16	2	1219.06	988.94	18
2	1314.63	893.38	16	3	1405.33	802.67	18
3	1457.56	750.44	16	4	1326.61	881.39	18
4	1271.88	936.13	16	1997	1109.67	1098.33	18
1974	1349.56	858.44	16	2	1753.72	454.28	18
2	1487.94	720.06	16	3	1715.39	492.61	18
3	1552.44	655.56	16	4	1230.89	977.11	18
4	1265.06	942.94	16	1998	1560.67	647.33	18
1975	1415.25	792.75	16	2	1498.83	709.17	18
2	1569.5	638.5	16	3	1498.5	709.5	18
3	1675.56	532.44	16	4	1641.11	566.89	18
4	1160.94	1047.06	16	1999	1428.17	779.83	14.5
1976	1466.13	741.88	16	2	1499.56	708.44	14.96
2	1625.63	582.38	16	3	1986.06	221.94	18.42
3	1619.19	588.81	16	4	2007.33	200.67	19.27
4	1478.88	729.13	16	2000	1725.61	482.39	16.63
1977	1416.88	791.13	16	2	1823.94	384.06	17.56
2	1185	1023	5	3	1700.56	507.44	16.17
3	861.2	1346.8	5	4	1756.44	451.56	16.76
4	718.8	1489.2	5	2001	1629.84	578.16	16.08
1978	700	1508	5	2	1509.05	698.95	15.31
2	821.6	1386.4	5	3	1764.79	443.21	17.92
3	843	1365	5	4	1820.11	387.89	17.84

Continued on next page

Table A.1 – continued from previous page

Years	Operation (Hrs)	Shutdown (Hrs)	Ave. (MW)	Years	Operation (Hrs)	Shutdown (Hrs)	Ave. (MW)
4	741.8	1466.2	5	2002	1757.11	450.89	18.47
1979	825	1383	5	2	1759.95	448.05	17.7
2	820.2	1387.8	5	3	1772.53	435.47	18.22
3	706.4	1501.6	5	4	1717.74	490.26	17.17
4	654	1554	5	2003	1788.84	419.16	17.97
1980	675.6	1532.4	5	2	1831.84	376.16	18.59
2	668	1540	5	3	1866.89	341.11	18.95
3	494.4	1713.6	5	4	1764.16	443.84	17.59
4	219.6	1988.4	5	2004	1755.89	452.11	19.54
1981	294.2	1913.8	5	2	1857.37	350.63	18.6
2	911	1297	5	3	1853.32	354.68	18.89
3	1153.4	1054.6	5	4	1929.21	278.79	19.06
4	972.4	1235.6	5	2005	1985.68	222.32	19.94
1982	1100	1108	5	2	1913.63	294.37	20.19
2	1118.2	1089.8	5	3	1986.05	221.95	19.84
3	1165	1043	5	4	2008.42	199.58	20.02
4	852.2	1355.8	5	2006	1903.89	304.11	19.9
1983	1119	1089	5	2	1810.84	397.16	19.74
2	1109.4	1098.6	5	3	2049.47	158.53	19.77
3	1141.4	1066.6	5	4	1529.84	678.16	20.01
4	999.6	1208.4	5	2007	1681.95	526.05	20.37
1984	1053.2	1154.8	5	2	1935.21	272.79	19.89
2	1148.6	1059.4	5	3	1882.47	325.53	19.55
3	1246.8	961.2	5	4	1986.95	221.05	19.93
4	819.4	1388.6	5	2008	1761.5	422.5	19.6
1985	1133.6	1074.4	5	2	1819	364.9	20
2	1129	1079	5	3	1859.4	348.5	19.2
3	1153.2	1054.8	5	4	1794	413.9	19.9
4	1117.4	1090.6	5	2009	1791.2	368.8	19.82
1986	1146	1062	5	2	1815.2	368.8	19.92
2	1153	1055	5	3	1958.6	249.3	20.01
3	1537.8	670.2	5	4	1657.3	550.7	19.77
4	1145	1063	5	2010	1784.6	375.4	19.9
1987	1225.8	982.2	5	2	1826.5	357.48	20
2	1176.6	1031.4	5	3	1967.6	240.39	20

Continued on next page

Table A.1 – continued from previous page

Years	Operation (Hrs)	Shutdown (Hrs)	Ave. (MW)	Years	Operation (Hrs)	Shutdown (Hrs)	Ave. (MW)
3	1224.4	983.6	5	4	1599.3	608.68	20
4	1028.6	1179.4	5	2011	1753.1	454.94	20
1988	0	2208	0	2	–	–	–

Appendix B

Calculational flow path

The calculational path, interfacing the codes employed in this study, is given in Figure B.1 below:

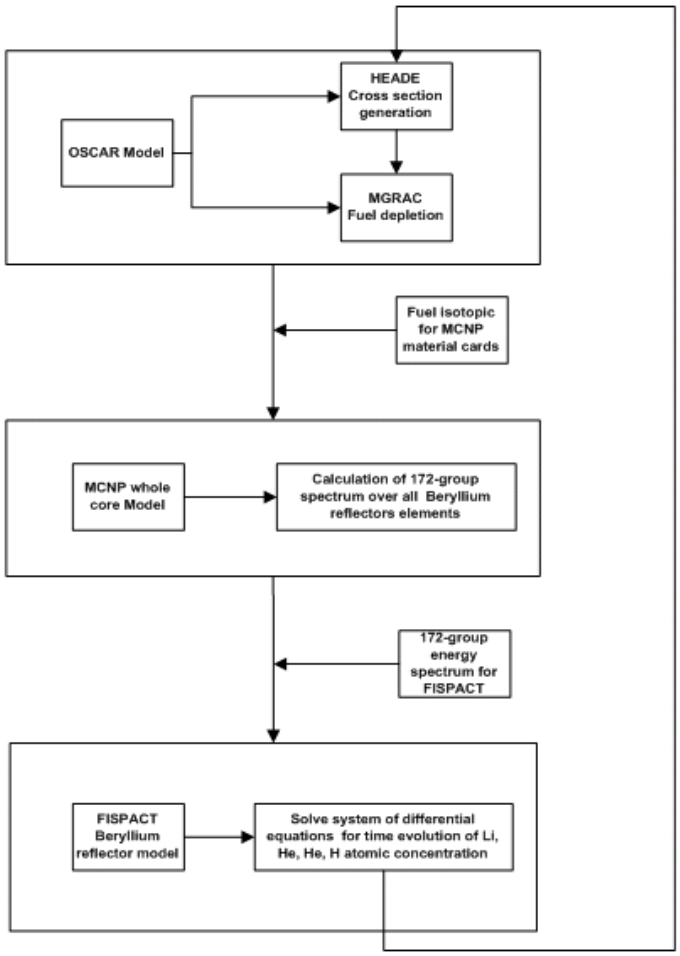

Figure B.1: Calculational path employed in this study

Appendix C

Core maps for beryllium reflector neutron spectrum evaluations

The selected MCNP models of the SAFARI–1 reactor core used to illustrate the influence of a change in core configurations, on the the beryllium reflector spectrum are shown in Figure C.1 on page 113. Note that these core maps resembles (i.e. labels, etc.) that of Figure 1.1 on page 7 in Section 1.2 of Chapter 1.

Some of the differences and similarities in the core maps of Figure C.1 on page 113 are listed below with reference to Figure 1.1:

(a) Core map of cycle *C0313-1* (Fully HEU core):

   i. 5 hollow and 14 solid beryllium reflectors;
   ii. Fuel element in position B6;
   iii. Two hydraulic rabbit systems in E9 and G9;
   iv. Hollow aluminium in A9.

(b) Core map of cycle *C0508-1* (Fully HEU core):

   i. 6 hollow and 13 solid beryllium reflectors;
   ii. Irradiation rig in B6
   iii. Two hydraulic rabbit systems in E9 and G9
   iv. Hollow aluminium in A9.

(c) Core map of cycle *C0706-1* (Fully HEU core):

   i. 6 hollow and 13 solid beryllium reflectors;

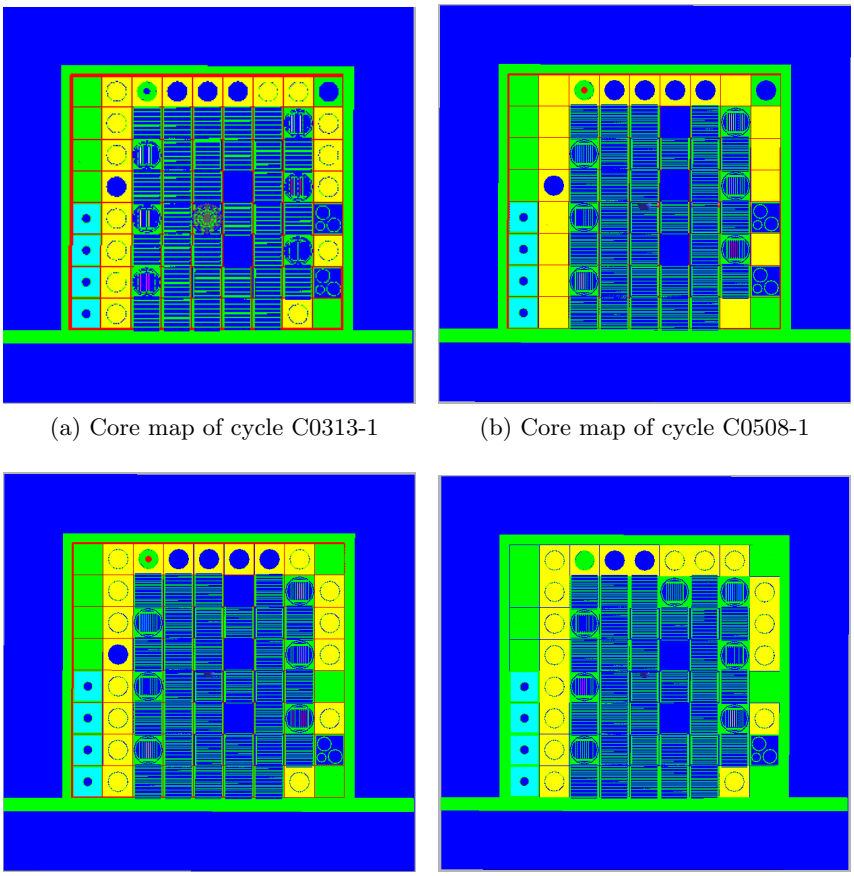

(a) Core map of cycle C0313-1

(b) Core map of cycle C0508-1

(c) Core map of cycle C0706-1

(d) Core map of cycle C01101-1

Figure C.1: MCNP models for different core configuration for beryllium reflector (in yellow) spectrum calculation

ii. Irradiation rig in B6;

iii. One hydraulic rabbit in G9 and hydraulic rabbit in E9 replaced with a solid aluminium;

iv. Solid aluminium in A9.

(d) Core map of cycle *C01101-1* (Fully LEU core):

i. All beryllium reflector elements are solid except for A3, A4 and A5 (hollow elements);

ii. Target plates irradiation rig in B6;

iii. One hydraulic rabbit in G9 and hydraulic rabbit in E9 replaced with a solid aluminium;

iv. Solid aluminium in A9.

Appendix D

RRFM 2011 conference paper

The paper presented at the 15th International Topical Meeting on Research Reactor Fuel Management (RRFM), held in Italy, Rome from the 20–24 March 2011 is attached as a supporting material for this study. The results of this paper were based on cycle *C0706-1* [55].